REPORT DOCUMENTATION PAGE

Form Approved
OMB No. 0704-0188

1. AGENCY USE ONLY (Leave Blank)	2. REPORT DATE	3. REPORT TYPE AND DATES COVERED
	December 1995	Final

4. TITLE AND SUBTITLE
Elastothermodynamic Damping in Composite and Cracked Media

5. FUNDING NUMBERS

6. AUTHORS
Joseph Edward Bishop

AFRL-SR-BL-TR-98-

0024

7. PERFORMING ORGANIZATION NAME(S) AND ADDRESS(ES)
Texas A&M University

9. SPONSORING/MONITORING AGENCY NAME(S) AND ADDRESS(ES)
AFOSR/NI
110 Duncan Avenue, Room B-115
Bolling Air Force Base, DC 20332-8080

10. SPONSORING/MONITORING AGENCY REPORT NUMBER

11. SUPPLEMENTARY NOTES

12a. DISTRIBUTION AVAILABILITY STATEMENT
Approved for Public Release

12b. DISTRIBUTION CODE

13. ABSTRACT *(Maximum 200 words)*
See attached.

14. SUBJECT TERMS

15. NUMBER OF PAGES

16. PRICE CODE

17. SECURITY CLASSIFICATION OF REPORT	18. SECURITY CLASSIFICATION OF THIS PAGE	19. SECURITY CLASSIFICATION OF ABSTRACT	20. LIMITATION OF ABSTRACT
Unclassified	Unclassified	Unclassified	UL

ELASTOTHERMODYNAMIC DAMPING IN COMPOSITE AND CRACKED MEDIA

A Dissertation

by

JOSEPH EDWARD BISHOP

Submitted to the Office of Graduate Studies of
Texas A&M University
in partial fulfillment of the requirements for the degree of

DOCTOR OF PHILOSOPHY

December 1995

Major Subject: Aerospace Engineering

ELASTOTHERMODYNAMIC DAMPING IN COMPOSITE AND CRACKED MEDIA

A Dissertation

by

JOSEPH EDWARD BISHOP

Submitted to Texas A&M University
in partial fulfillment of the requirements
for the degree of

DOCTOR OF PHILOSOPHY

Approved as to style and content by:

Vikram K. Kinra
(Chair of Committee)

Norris Stubbs
(Member)

Thomas C. Pollock
(Member)

Donald T. Ward
(Head of Department)

K Annamalai
(Member)

December 1995

Major Subject: Aerospace Engineering

ABSTRACT

Elastothermodynamic Damping in Composite and Cracked Media.

(December 1995)

Joseph Edward Bishop, B.S., Texas A&M University;

M.S., Texas A&M University

Chair of Advisory Committee: Dr. Vikram K. Kinra

When a composite material is subjected to a stress field, different regions undergo different temperature fluctuations due to the well-known thermoelastic effect. As a result irreversible heat conduction occurs, and entropy is produced which is manifested as a conversion of mechanical energy into heat. Moreover, the changes in temperature produce a thermal strain that is out of phase with the stress, thus converting mechanical energy into heat, i.e. work is lost. We define this process as elastothermodynamic damping.

Herein, using the linear one-way coupled theory of elastothermodynamic relaxation, the elastothermodynamic damping of composite and cracked media is examined. Two equivalent descriptions of elastothermodynamic damping are first established: (1) the mechanical description and (2) the entropic description. An integral-transform technique is then developed to solve for the temperature field of a general composite medium with arbitrary heat generation. With this solution, a general expression for the damping of the composite material is derived. This general solution for the elastothermodynamic damping is then specialized to a solution for a composite material consisting of *N*-isotropic layers in a rectangular,

cylindrical, and spherical coordinate system (i.e. an N-layer slab, cylinder, and sphere, respectively), subjected to any stress field so long as the resulting heat conduction can be described by a single spatial coordinate orthogonal to the layering. With this specialized result the elastothermodynamic damping is examined in laminated, fiber-reinforced, and particulate composites. Finally, the elastothermodynamic damping of cracked media is examined. Specifically, an *approximate* analysis is given for the entropy produced and work lost in the neighborhood of a Griffith crack subjected to a time-harmonic loading in Modes I, II, and III. In all three Modes the temperature at the crack tip remains bounded. In Mode I the entropy produced (per unit volume per cycle) is finite at the crack tip, whereas the work lost (per unit volume per cycle) goes to infinity as $1/\sqrt{r}$. Conversely, in Mode II the entropy produced goes to infinity as $1/r$ as the crack tip is approached, whereas the work lost is finite. In Mode III the thermoelastic effect disappears altogether and, therefore, both the entropy produced and the work lost are zero throughout the plate.

ACKNOWLEDGMENTS

The support given to me by the United States Air Force through a National Defense Science and Engineering Graduate Fellowship is gratefully acknowledged.

TABLE OF CONTENTS

Page

LIST OF FIGURES

Page

Page

Page

Page

Page

Page

Page

LIST OF TABLES

Page

1. INTRODUCTION

Composite materials are increasingly the material of choice for a wide variety of engineering applications. Whereas a considerable amount of research has been performed concerning the stiffness, strength, fracture toughness, fatigue life, coefficient of thermal expansion, etc., of composite materials, their damping properties have been investigated to a much lesser extent. However, damping is a critically important material property from the viewpoint of vibration suppression in a variety of applications: submarines, aircraft structures, automobile bodies, office machines, off-shore structures, and in particular, large and flexible aerospace structures, e.g. a space station. A significant fraction of the body of literature on damping concerns itself with viscoelastic damping in polymeric materials and polymer-matrix composites (PMCs). Even though these materials exhibit high damping, there are many situations where they cannot be used, for example, elevated temperature applications such as the high-speed civil transport, turbine engines, etc. Moreover, they cannot be used in space structures due to the problem of degassing and an attendant degradation of mechanical properties. Therefore, there is a need for developing new materials with high intrinsic material damping without significantly sacrificing other mechanical properties. As a result, there has recently been a considerable activity in designing and characterizing high-damping metal-matrix composites (MMCs) (for example,

---

This dissertation follows the style and format of the *Journal of Applied Mechanics.*

DiCarlo, 1976; DiCarlo and Maisel, 1979; Bhagat, *et al.*, 1989; Kinra, *et al.*, 1991; Kinra and Wren, 1992; Wren and Kinra, 1992; Wong and Holcomb, 1992).

For a given material there are many mechanisms contributing to the total damping of an MMC, e.g. point defect relaxation, dislocation motion, grain boundary sliding, coulomb friction at the inclusion-matrix interface, magnetoelastic effects, and elastothermodynamic relaxation (Nowick and Berry, 1972; De Batist, 1972; Kinra and Wolfenden, 1992). In a recent book-chapter Wolfenden and Wolla (1992) have done an excellent review of damping in MMCs . From the results of these investigations, it has been found that most of the damping mechanisms offer a significant damping only over a small range of frequency, temperature, and stress (or strain). Elastothermodynamic[1] damping (also known as thermoelastic damping) offers an attractive alternative. In this case the damping is due to thermal currents within the material and is not accompanied by any significant loss of stiffness or strength. To first order it is linearly dependent on the absolute temperature, and it is independent of the stress level (i.e. damping is linear). As we shall see, analogous to other sources of damping, elastothermodynamic damping also suffers from the limitation that it is significant only over a finite

---

[1]We propose that *elastothermodynamic* is a more appropriate qualifier for the word damping than *thermoelastic*. Historically (Boley and Weiner, 1960), the word *thermoelastic* has been used to connote a situation where the cause is an externally applied temperature field (*thermo*), and the effect is an elastic stress field (*elastic*), hence *thermoelastic*. In the present context of damping, there is no externally applied temperature field. Instead, the cause is an externally applied traction field and the accompanying stress field (*elasto*), and the effect is a temperature field (*thermo*). Moreover, the dissipation of mechanical energy occurs only if the stress field is time dependent (*dynamic*), hence *elastothermodynamic*

range of frequency. Finally, it is envisioned that the elastothermodynamic damping of composites can be tailored in a manner analogous to that used currently for tailoring stiffness, strength, coefficient of thermal expansion, etc. Of course the tailoring of the former cannot be done independently of the tailoring of the latter.

Whenever a material is stressed adiabatically, there is an accompanying change in temperature, however small. This phenomenon is known as the thermoelastic effect and can easily be deduced from the Maxwell's relations (e.g. Zemansky and Dittman, 1981). For an anisotropic material this effect is given by

$$\left(\frac{\partial T}{\partial \sigma_{lm}}\right)_S = -T\frac{\alpha_{lm}}{C} \tag{1}$$

where T is the absolute temperature, σ_{lm} is the stress tensor, α_{lm} is the linear coefficient of thermal expansion tensor, C is the specific heat per unit volume, and the subscript S denotes an isentropic process. Since the temperature and stress fields are coupled via Eq. (1), inhomogeneities in stress and/or material properties will result in inhomogeneities in temperature. Heat will conduct from the high-temperature regions to the low-temperature regions, and as a consequence of the resulting irreversible heat conduction, entropy will be produced. In a cyclic process such as a vibrating structure, this entropy production will be manifested as a conversion of external work into internal heat energy. *We define this process as elastothermodynamic damping.* This

increase in the internal heat energy over one cycle of vibration will also be referred to as the *work lost.*

The measurement of material damping is a notoriously difficult problem. Any irreversible phenomenon will increase the measured damping, e.g. air damping, inelastic clamping devices, etc. Furthermore, as mentioned previously, there are many mechanisms of material damping, and isolating any one mechanism for study is experimentally demanding. The first experimental research into elastothermodynamic damping was performed by Zener in 1938(b) using a copper beam. He observed that the measured damping agreed with the theory only with respect to the shape of the damping versus frequency curve and with respect to the frequency of peak damping. A precise verification of elastothermodynamic damping as a function of frequency was performed by Berry in 1955 using beams made of α-brass. The comparison between theory and experiment was excellent. Most recently, elastothermodynamic damping has been measured as a function of frequency in 6061-T6 aluminum beams by Wren and Kinra (1988) and Bishop and Kinra (1992) with an excellent comparison between theory and experiment.

Elastothermodynamic damping has been studied analytically by several researchers over the past sixty years. Following Zener's seminal work (1937, 1938a), many authors have studied this damping mechanism in *homogeneous* structures using a variety of solution techniques (Biot, 1956; Lücke, 1956; Deresiewicz, 1957; Alblas, 1961, 1981; Chadwick, 1962; Goodman, *et al.*, 1962; Tasi, 1963; Tasi and Herrmann, 1964; Gillis, 1968; Shieh, 1971, 1975, 1979; Lee, 1985; Landau and Lifshitz, 1986). Budiansky and Sumner (1983)

studied bulk attenuation of composite materials using the self-consistent scheme. Armstrong (1984) analyzed the attenuation of a longitudinal wave passing through either a periodic or a random sequence of slabs. Eshelby (1949) was the first to study the elastothermodynamic damping of an internal defect, namely a quasistatic edge dislocation. Weiner (1958) extended Eshelby's work to high-speed edge dislocations. Savage (1966) studied the elastothermodynamic attenuation of a medium containing elliptical cavities.

The objective of this dissertation is to analytically study the elastothermodynamic[2] damping in composite and cracked media subjected to time-harmonic tractions. The linear one-way coupled theory of elastothermodynamic damping is used for all analysis. In Section 2 the linear one-way coupled theory of elastothermodynamic damping is presented. In Section 3 the elastothermodynamic damping of composite media is examined. In Section 3.1 two descriptions of elastothermodynamic damping are established: (1) the mechanical description and (2) the entropic description. In Section 3.2 the solution of the inhomogeneous heat-conduction problem (the heat-conduction problem including heat generation) by the integral-transform technique, given by Ozisik (1980, pp. 594-610) for a composite medium consisting of *isotropic* subregions with thermally imperfect interfaces, is extended to a composite medium consisting of several subregions, each of which may be *anisotropic*. Using the results of Sections 3.1 and 3.2, a general expression for the damping is derived for the

---

[2]Henceforth, the term damping, when used without qualification, will imply elastothermodynamic damping.

composite material in Section 3.3. In Section 3.4 this general solution for the elastothermodynamic damping is then specialized to a solution for a composite material consisting of *N*-isotropic layers in a rectangular, cylindrical, and spherical coordinate system (i.e. an *N*-layer slab, cylinder, and sphere, respectively), subjected to any stress field so long as the resulting heat conduction can be described by a single spatial coordinate orthogonal to the layering. Many problems of current engineering interest can be modeled as special cases of the *N*-layer solution. (1) *Cartesian coordinate system*: laminated composites in bending and extension; aligned platelet composite; or a periodic array of labs. (2) *Cylindrical coordinate system*: a unidirectional fiber-reinforced composite where each fiber may consist of several concentric cylinders. (3) *Spherical coordinated system*: a particulate composite where each particle may be solid or hollow, or consist of several concentric spheres, for example, an aluminum matrix filled with hollow Al_2O_3 microspheres. Specific results are given for the following problems. (I) A periodic array of isotropic slabs (rectangular symmetry) with a two-layer representative volume element and a thermally imperfect interface subjected to the following mechanical stress states: (a) a time-harmonic uniform stress perpendicular to the layering, and (b) a time-harmonic uniform strain parallel to the layering. (II) A symmetric three-layer plate in pure bending with isotropic layers and with thermally perfect interfaces. (III) A hollow two-layer composite sphere in which each layer is isotropic and has a thermally imperfect interface, subjected to a uniform time-harmonic radial load. In Section 4 the elastothermodynamic damping of cracked media is examined. Specifically, an

approximate analysis is given for the temperature field, the work lost, and the entropy produced in the vicinity of a Griffith crack in Modes I, II, and III.

2. THE LINEAR ONE-WAY COUPLED THEORY OF ELASTOTHERMODYNAMIC DAMPING

Consider a solid subjected to cyclic *forced* vibrations. If the solid is inelastic, a portion of the external work performed by the applied tractions will be converted into heat and other nonrecoverable forms of stored energy. Without reference to any particular physical mechanism of inelasticity (damping), the work lost per unit volume during a cycle of vibration Δw is given by

$$\Delta w = \oint \sigma_{lm} d\varepsilon_{lm} \tag{2}$$

where ε_{lm} is the strain tensor (Nowick and Berry, 1972, pp. 13-14). The work lost per cycle ΔW over the entire material occupying a region R is given by

$$\Delta W = \int_R \Delta w \, dR = \int_R dR \oint \sigma_{lm} d\varepsilon_{lm} \tag{3}$$

This work lost may be interpreted as the work required per cycle to maintain the solid in steady vibration. A normalized measure of the external work lost is given by the specific damping capacity, Ψ, which is defined as

$$\Psi = \frac{\Delta W}{W} \tag{4}$$

where W is the maximum elastic energy during the cycle.

Now consider a particular mechanism of anelasticity, namely, elastothermodynamic damping (The words "inelastic" and "anelastic" are used in the sense defined by Nowick and Berry, (1972, pp. 2-3)). For simplicity only a solid body with adiabatic outer boundaries is considered. The rate of

entropy production per unit volume, $\dot{s}_p$, due to irreversible heat conduction is given by

$$\dot{s}_p = -\frac{q_l T_{,l}}{T^2} \tag{5}$$

where q_l is the heat flux vector and $(\ )_{,l}$ denotes partial differentiation with respect to the components of the position vector x_l (de Groot and Mazur, 1984). Herein, it is assumed that the heat flux vector satisfies the Fourier law of heat conduction

$$q_l = -k_{lm} T_{,m} \tag{6}$$

where k_{lm} is the thermal conductivity tensor (Ozisik, pp. 611-629). The entropy produced per unit volume Δs during a cycle of vibration is given by

$$\Delta s = \oint \dot{s}_p \, dt \tag{7}$$

An additional entropy $\Delta S^{\text{interface}}$ is produced if the medium has any thermally imperfect interfaces at which the temperature is discontinuous. This entropy production will be described in Section 3.1.3.3. The entropy produced per cycle ΔS over the entire body occupying a region R is thus

$$\Delta S = \int_R \Delta s \, dR + \Delta S^{\text{interface}} \tag{8}$$

The temperature field is governed by the two-way coupled heat conduction equation

$$\left(k_{lm} T_{,m}\right)_{,l} - C\frac{\partial T}{\partial t} = T\alpha_{lm}\frac{\partial \sigma_{lm}}{\partial t} \tag{9}$$

(Nowinski, 1978, Ch. 6). The term on the right-hand side is due to the thermoelastic effect, Eq. (1). The qualifier "two-way coupled" implies that the stress field affects the temperature field, and conversely the temperature field

affects the stress field. For most crystalline solids the relative temperature change resulting from the thermoelastic effect is very small. For example, if an unstressed rod of aluminum at an equilibrium temperature of $T_o = 300K$ is subjected to a uniaxial tensile stress of 100 MPa, the decrease in temperature is 0.3 K, i.e. $|\Delta T/T_o| = 10^{-3}$. It is well known that the stresses produced by these small changes in temperature are negligibly small compared to the applied stresses (Boley and Weiner, 1960). Therefore, for our purpose of calculating the small changes in temperature resulting from the thermoelastic effect, we assume that the stress field is independent of the temperature field. Eq. (9) now becomes the *linear one-way* coupled heat-conduction equation. Moreover, without introducing an appreciable error, the algebraic effort can be greatly reduced by replacing T by T_o in the last term (Nowinski, 1978, Ch. 6.1); then Eq. (9) reduces to

$$(k_{lm}T_{,m})_{,l} - C\frac{\partial T}{\partial t} = T_o\alpha_{lm}\frac{\partial \sigma_{lm}}{\partial t} \tag{10}$$

Similarly, T is replaced with T_o in Eq. (5); then, using Eq. (6),

$$\dot{s}_p = \frac{1}{T_o^2}k_{lm}T_{,l}T_{,m} \tag{11}$$

These equations are collectively referred to as the linear one-way coupled theory of elastothermodynamic damping. A simple example illustrating the physics of both the linear and nonlinear theories of elastothermodynamic damping is given in the Appendix.

3. ELASTOTHERMODYNAMIC DAMPING IN COMPOSITE MATERIALS

In this Section the elastothermodynamic damping of composite materials loaded time-harmonically is examined. First, the equivalence of the mechanical and entropic descriptions of elastothermodynamic damping for a general composite medium is established.

3.1 EQUIVALENCY OF THE MECHANICAL AND ENTROPIC DESCRIPTIONS OF ELASTOTHERMODYNAMIC DAMPING FOR A GENERAL COMPOSITE MEDIUM

In 1938 Zener showed that within the linear one-way coupled theory of elastothermodynamic damping, $\Delta W = T_o \Delta S$, where $T_o \Delta S$ is simply the increment of heat per cycle ΔQ in the medium. Thus, the elastothermodynamic damping, characterized by Ψ, may be obtained by calculating either the total external work lost per cycle ΔW or the heat increment per cycle $T_o \Delta S$. The first approach will be referred to as the mechanical description and the second approach as the entropic description. However, Zener's analysis is confined to isotropic homogeneous bodies[3].

The objective of this section is to extend Zener's results to a composite material made up of several subregions, each of which may be anisotropic,

[3]Zener's analysis is slightly more general than what is mentioned here. In his derivation he uses the fact that for an isotropic material, $k_{lm} = k\delta_{lm}$ and $\alpha_{lm} = \alpha\delta_{lm}$, which is also true for a material with cubic symmetry.

and whose interfaces may be thermally imperfect. In the past Kinra and Milligan (1994) have assumed that $\Delta w = T_o \Delta s$, i.e, the local work lost at a point per cycle is equal to the local entropy produced per cycle at that point times the equilibrium temperature. The second objective of this section is to demonstrate that in general this statement is not true. Since Zener's derivation was very terse and extremely difficult to follow, his result is first rederived using a slightly different approach (and hopefully easier to follow). Moreover, the framework developed in this rederivation will allow for the construction of a counterexample to the statement $\Delta w = T_o \Delta s$.

3.1.1 Proof that $\Delta W = T_o \Delta S$ for a Homogeneous Isotropic Solid

The fact that for an isotropic, homogeneous, thermoelastic solid with adiabatic boundaries, subjected to time-harmonic tractions, the *total* work lost per cycle throughout the body, ΔW, is equal to the *total* heat increment per cycle throughout the body, $T_o \Delta S$, will now be proven.

3.1.1.1 Temperature

For an isotropic material, $k_{lm} = k\delta_{lm}$, where k is the thermal conductivity, δ_{lm} is the Kronecker delta, and $\alpha_{lm} = \alpha\delta_{lm}$, where α is the coefficient of linear thermal expansion, Eq. (10) reduces to

$$\left(kT_{,m}\right)_{,m} - C\frac{\partial T}{\partial t} = T_o \alpha \frac{\partial \sigma_{mm}}{\partial t} \tag{12}$$

The stress field may be separated into its spatial and temporal parts,

$$\sigma_{lm}(\mathbf{x},t) = \sigma_{lm}(\mathbf{x})\, e^{i\omega t} \tag{13}$$

where $\mathbf{x}$ is a position vector, ω is the frequency of vibration. Herein, the spatial part of the stress tensor, $\sigma_{lm}(\mathbf{x})$, is taken to be real valued. Since Eq. (12) is a linear partial differential equation, let

$$T(\mathbf{x},t) = T_o^* + V(\mathbf{x},\omega)\, e^{i\omega t} \tag{14}$$

where $T_o^* = (1+i)T_o$, and V is the complex fluctuation of temperature about T_o^*. As usual a physically meaningful stress and temperature is obtained by taking either the real or the imaginary part of $\sigma_{lm}(\mathbf{x},t)$ or $T(\mathbf{x},t)$, respectively. Substituting Eqs. (13) and (14) into Eq. (12), results in

$$\left(kV_{,m}\right)_{,m} - C(i\omega)V = T_o\alpha(i\omega)\sigma_{mm}(\mathbf{x}) \tag{15}$$

Since $\sigma_{mm}(\mathbf{x})$ is given, in principle $V(\mathbf{x},\omega)$ may be calculated using Eq. (15). For convenience V is written as

$$V = \Theta + i\theta \tag{16}$$

where $\Theta = \mathrm{Re}V$ and $\theta = \mathrm{Im}V$. Hence, from Eq. (14),

$$\mathrm{Re}\,T = T_o + \Theta\cos(\omega t) - \theta\sin(\omega t) \tag{17}$$

3.1.1.2 External Work Lost

Using the framework just developed, an expression is now derived for the external work lost in terms of the fluctuating temperature V. The change in temperature produces a thermal strain. The strain tensor ε_{lm} may be decomposed into an elastic part ε_{lm}^{el} and a thermal part ε_{lm}^{th},

$$\varepsilon_{lm} = \varepsilon_{lm}^{el} + \varepsilon_{lm}^{th} \tag{18}$$

Furthermore, the thermal strain may be separated into its spatial and temporal parts,

$$\varepsilon_{lm}^{th}(\mathbf{x},t) = \varepsilon_{lm}^{th}(\mathbf{x},\omega)e^{i\omega t} \tag{19}$$

The following identity derived by Brillouin (1953) will be found quite useful

$$\frac{\omega}{2\pi}\int_0^{2\pi/\omega}\left[\mathrm{Re}(F)\,\mathrm{Re}(f)\right]dt=\frac{1}{2}\mathrm{Re}\left(F\bar{f}\right)=\frac{1}{2}\mathrm{Re}\left(\bar{F}f\right) \tag{20}$$

where F and f represent two time-harmonic complex quantities with frequency ω, and the overbar denotes the complex conjugate. Taking the real values of Eqs. (13) and (19), substituting into Eq. (2), and using Eq. (20) gives for Δw, the local work lost per cycle per unit volume,

$$\Delta w(\mathbf{x},\omega)=-\pi\sigma_{lm}(\mathbf{x})\,\mathrm{Im}\left(\varepsilon_{lm}^{th}(\mathbf{x},\omega)\right) \tag{21}$$

(The elastic part of the strain field does not contribute to the work lost since it is in phase with the stress field). But

$$\varepsilon_{lm}^{th}(\mathbf{x},\omega)=\alpha\delta_{lm}V=\alpha\delta_{lm}(\Theta+i\theta) \tag{22}$$

so that

$$\mathrm{Im}\left(\varepsilon_{lm}^{th}(\mathbf{x},\omega)\right)=\alpha\delta_{lm}\theta \tag{23}$$

Substituting Eq. (23) into (21) gives

$$\Delta w\left(\mathbf{x},\omega\right)=-\pi\alpha\,\theta\,\sigma_{mm}(\mathbf{x}) \tag{24}$$

Using Eq. (3) the total external work lost per cycle is thus

$$\Delta W(\omega)=-\pi\int_R\alpha\,\theta\,\sigma_{mm}(\mathbf{x})\,dR \tag{25}$$

3.1.1.3 Heat Increment per Cycle

Using the framework developed for calculating the temperature field, an expression is now derived for the heat increment per cycle in terms of the fluctuating temperature V. For an isotropic material, Eq. (11) reduces to

$$\dot{s}_p = \frac{k}{T_o^2} T_{,m} T_{,m} \tag{26}$$

Taking the real value of Eq. (14), substituting into Eq. (26) and then using Eqs. (7) and (20) gives the local entropy produced per unit volume during one cycle of vibration,

$$\Delta s(\mathbf{x},\omega) = \frac{\pi}{\omega} \frac{k}{T_o^2} \left(\Theta_{,m} \Theta_{,m} + \theta_{,m} \theta_{,m}\right) \tag{27}$$

Using Eq. (8) the total entropy produced throughout the body per cycle is thus

$$\Delta S(\omega) = \frac{\pi}{\omega} \frac{1}{T_o^2} \int_R k\left(\Theta_{,m} \Theta_{,m} + \theta_{,m} \theta_{,m}\right) dR \tag{28}$$

Since the fluctuations in temperature about T_o are very small (recall that $\Delta T/T_o = O\left(10^{-3}\right)$), the heat increment per cycle ΔQ may be equated to $T_o \Delta S$.

3.1.1.4 Equality of ΔW and $T_o \Delta S$

Using the identity

$$\left(k\Theta_{,m}\right)\Theta_{,m} = \left(k\Theta_{,m}\Theta\right)_{,m} - \left(k\Theta_{,m}\right)_{,m}\Theta \tag{29}$$

and the divergence theorem, Eq. (28) becomes

$$T_o \Delta S = \frac{\pi}{\omega} \frac{1}{T_o} \left[\int_S \left(k\Theta_{,m}\Theta + k\theta_{,m}\theta\right) n_m \, dS - \int_R \left(\left(k\Theta_{,m}\right)_{,m}\Theta + \left(k\theta_{,m}\right)_{,m}\theta\right) dR \right] \tag{30}$$

where S represents the surface of the medium, and n_m are the components of the unit outward normal vector to the surface. Since the boundary of the medium is taken to be adiabatic, $V_{,m} n_m = \Theta_{,m} n_m + i\theta_{,m} n_m = 0$, and therefore

$\Theta_{,m} n_m = \theta_{,m} n_m = 0$. Thus, the surface term vanishes identically, and Eq. (30) reduces to

$$T_o \Delta S = -\frac{\pi}{\omega} \frac{1}{T_o} \int_R \left((k\Theta_{,m})_{,m} \Theta + (k\theta_{,m})_{,m} \theta \right) dR \tag{31}$$

Substituting Eq. (16) into Eq. (15) yields the two real-valued equations,

$$(k\Theta_{,m})_{,m} + C\omega\theta = 0 \tag{32}$$

and

$$(k\theta_{,m})_{,m} - C\omega\Theta = T_o \, \omega \, \alpha \, \sigma_{mm}(\mathbf{x}) \tag{33}$$

Solving these two equations for $(k\Theta_{,m})_{,m}$ and $(k\theta_{,m})_{,m}$ and substituting into Eq. (31), yields

$$T_o \Delta S(\omega) = -\pi \int_R \alpha \, \theta \, \sigma_{mm}(\mathbf{x}) \, dR \tag{34}$$

Comparing Eq. (25) and Eq. (34) gives

$$\Delta W = T_o \Delta S \tag{35}$$

Thus, for an isotropic, homogeneous, thermoelastic solid with adiabatic boundaries, stressed time-harmonically, the *total* work lost per cycle ΔW is equal to the heat increment per cycle $T_o \Delta S$. This result establishes two equivalent approaches to calculating the elastothermodynamic damping: (1) the mechanical approach developed in Section 3.1.1.2, and (2) the entropic approach developed in Section 3.1.1.3.

3.1.2 A Counterexample to Demonstrate that $\Delta w \neq T_o \Delta s$

Using the framework developed in Section 3.1.1, a counterexample is now constructed to demonstrate that the work lost per cycle per unit volume

Δw may not be equal to the local entropy produced per cycle per unit volume Δs times the equilibrium temperature T_o. Consider a homogeneous isotropic Euler-Beroulli beam of rectangular cross-section of thickness h with adiabatic boundaries, subjected to an applied time-harmonic bending moment $M = M_o e^{i\omega t}$, as shown in Figure 1. The only nonzero stress σ_{xx} is given by

$$\sigma_{xx} = -\frac{Mz}{I} \tag{36}$$

where I is the second moment of the cross-sectional area, the z-axis is in the thickness direction, and the x-axis coincides with the centroidal axis. Substituting Eq. (36) into the governing equation for V, Eq. (15), results in

$$\frac{d^2}{dz^2}V - \frac{C}{k}(i\omega)V = -\frac{\alpha}{k}\frac{M_o}{I}T_o(i\omega)z \qquad -\frac{h}{2} \le z \le \frac{h}{2} \tag{37}$$

The adiabatic boundary conditions are

$$\frac{d}{dz}V = 0 \quad \text{at} \quad z = \pm\frac{h}{2} \tag{38}$$

Assuming a solution of the form

$$V = \sum_{\substack{n=1 \\ \text{odd}}}^{\infty} A_n \sin(n\pi z/h) \tag{39}$$

and utilizing the integral transform technique (Ozisik, pp. 594-610) yields

$$A_n = \frac{\alpha T_o}{C}\frac{M_o}{I}\frac{4h}{\pi^2}\frac{(-1)^{\frac{n-1}{2}}}{n^2}\frac{\Omega^2 + i\Omega n^2}{n^4 + \Omega^2} \tag{40}$$

where a nondimensional frequency has been introduced as $\Omega = \omega C h^2/\pi^2 k$.

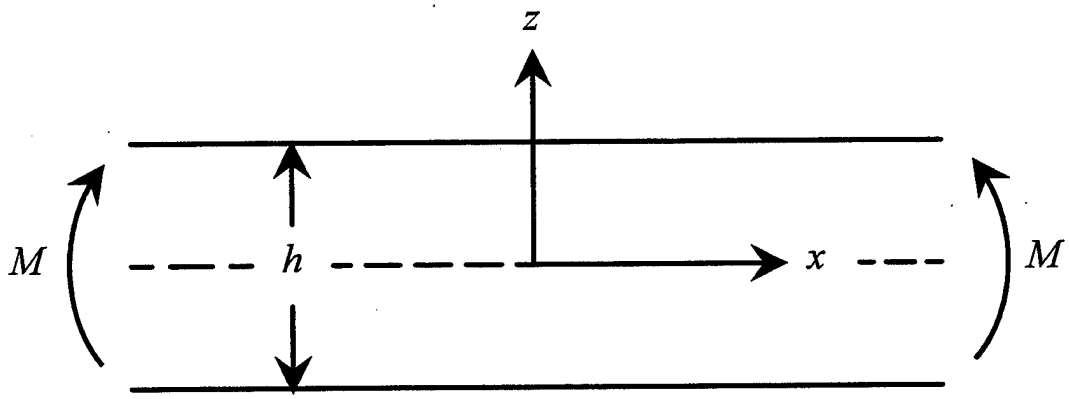

Figure 1. An Euler-Bernoulli beam of thickness h with an applied bending moment M.

To calculate the local work lost per cycle per unit volume, Eqs. (39) and (40) are substituted into Eq. (24) yielding

$$\Delta w = \frac{(\alpha M_o h/I)^2 T_o}{C} \frac{4}{\pi} \sum_{\substack{n=1 \\ \text{odd}}}^{\infty} (-1)^{\frac{n-1}{2}} \frac{\Omega}{n^4 + \Omega^2} \frac{z}{h} \sin(n\pi z/h) \tag{41}$$

To calculate the local entropy produced per cycle per unit volume, Eqs. (39) and (40) are substituted into Eq. (27) resulting in

$$\Delta s = \frac{(\alpha M_o h/I)^2}{C} \frac{16}{\pi^3} \sum_{\substack{n=1 \\ \text{odd}}}^{\infty} \sum_{\substack{m=1 \\ \text{odd}}}^{\infty} \frac{(-1)^{\frac{n+m}{2}-1}}{nm} \frac{\Omega(\Omega^2 + n^2 m^2)}{(n^4 + \Omega^2)(m^4 + \Omega^2)} \cos(n\pi z/h) \cos(m\pi z/h) \tag{42}$$

Motivated by the forms of Eqs. (41) and (42), we now introduce a normalized local work lost,

$$\psi = \frac{\Delta w}{(\alpha M_o h/I)^2 \frac{T_o}{C}} \tag{43}$$

and a normalized entropy produced,

$$\chi = \frac{T_o \Delta s}{(\alpha M_o h/I)^2 \frac{T_o}{C}} \tag{44}$$

ψ and χ are plotted as functions of the normalized position, $\xi = z/h$, in Figures 2 and 3, respectively, for three values of the normalized frequency Ω. For a given frequency, ψ is maximum at the outer surface of the beam, $\xi = 0.5$, whereas χ is maximum at the neutral axis, $\xi = 0$. Thus, in general the

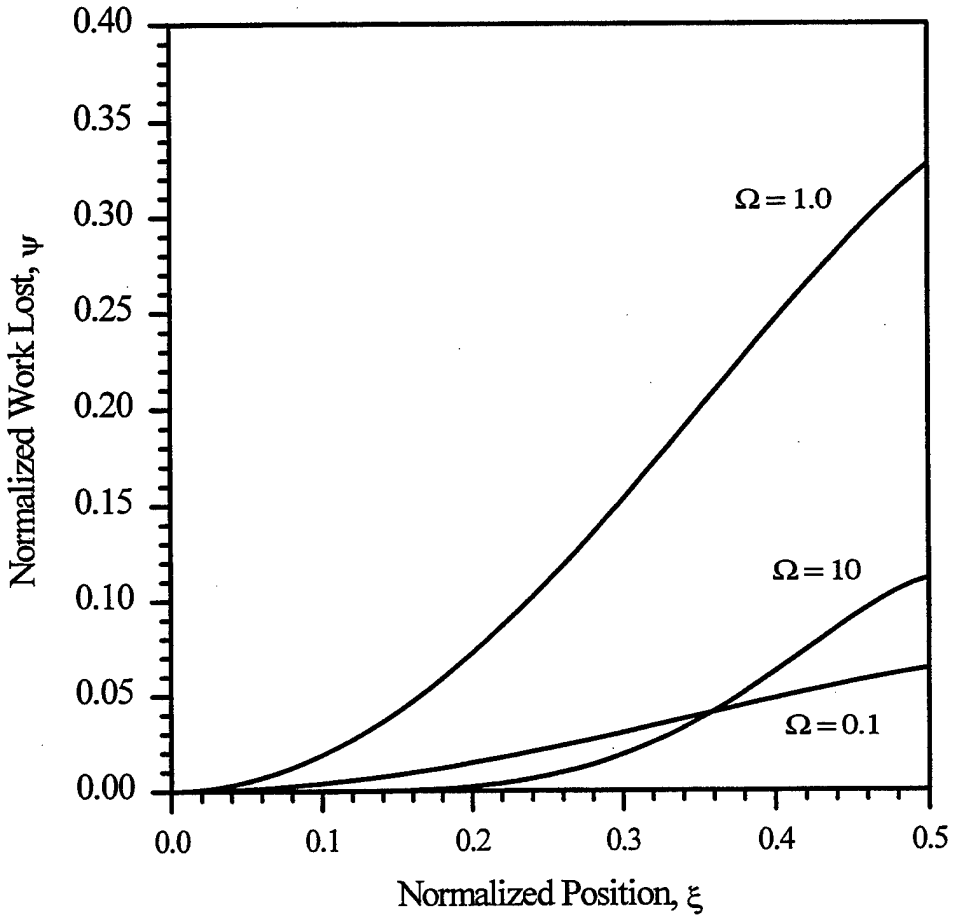

Figure 2. Normalized work lost ψ for an Euler-Bernoulli beam as a function of the normalized thickness coordinate ξ for three normalized frequencies Ω.

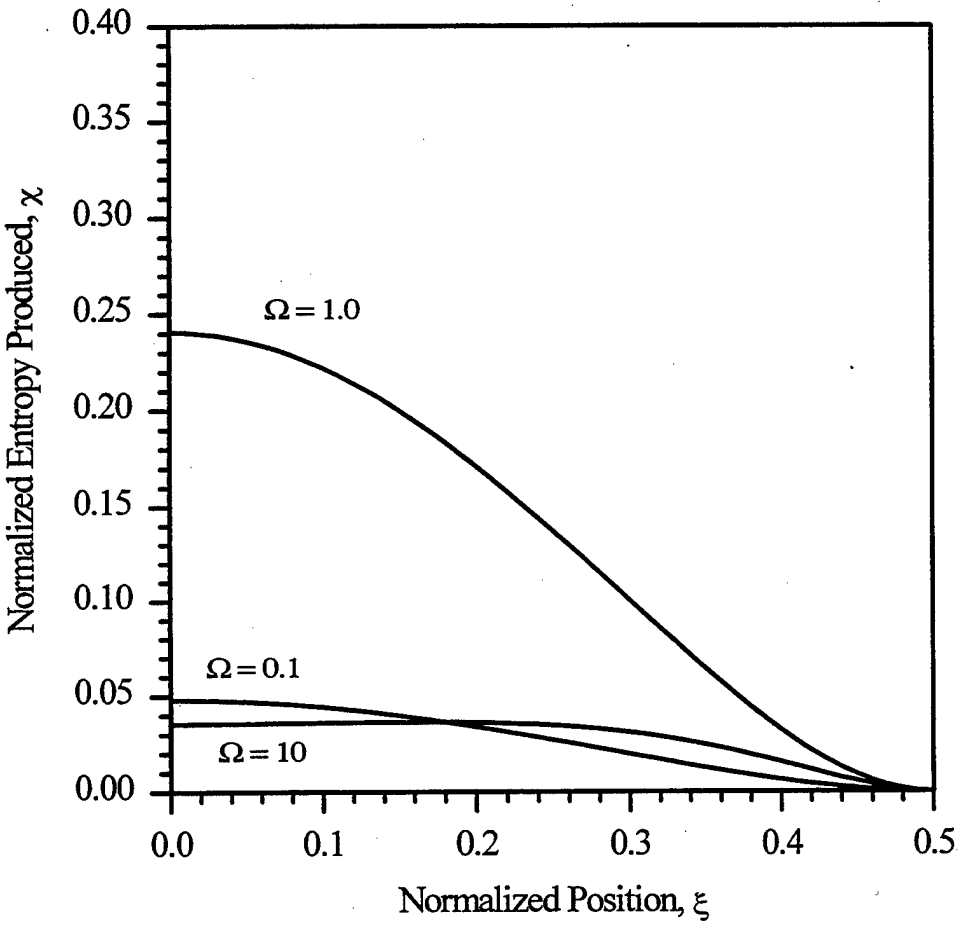

Figure 3. Normalized entropy produced χ for an Euler-Bernoulli beam as a function of the normalized thickness coordinate ξ for three normalized frequencies Ω.

entropy is produced at a different location than where the work is lost, i.e. $\Delta w \neq T_o \Delta s$. As a check on the calculations, the equality $\Delta W = T_o \Delta S$ was verified explicitly using Eqs. (41) and (42).

To further elucidate the results of this counterexample, the following thought experiment is constructed. Given a high-temperature reservoirs (T_H) and a low-temperature reservoir (T_L) as shown in Figure 4, a Carnot heat pump supplied with an amount of work $\Delta W = (1 - T_L/T_H)Q$ per unit time is used to reversibly transfer a quantity of heat $(T_L/T_H)Q$ per unit time from the low temperature reservoir and deliver a quantity of heat Q per unit time to the high temperature reservoir (Callen, 1985). This heat is then transferred irreversibly from the high temperature reservoir to the low temperature reservoir by way of, say, a copper rod. Under steady state conditions, the thermodynamic coordinates of both the high-temperature reservoir and the copper rod do not change. However, an amount of entropy per unit time $S_{IN} = Q/T_H$ enters the copper rod from the high temperature reservoir, whereas an amount of entropy per unit time $S_{OUT} = Q/T_L$ leaves the copper rod and enters the low temperature reservoir. Hence, an amount of entropy per unit time $\Delta S = Q/T_L - Q/T_H$ is produced within the copper rod and transferred to the low-temperature reservoir (Alternatively, this result may be readily obtained by using Eq. (5) and noting that the temperature varies linearly within the copper rod). The result of the entire process is that the low temperature reservoir heats up by an amount $\Delta Q = T_L \Delta S = (1 - (T_L/T_H))Q$ per unit time, which is precisely equal to ΔW. Therefore, an amount of work ΔW has been totally dissipated and turned into heat. Finally, note that even though

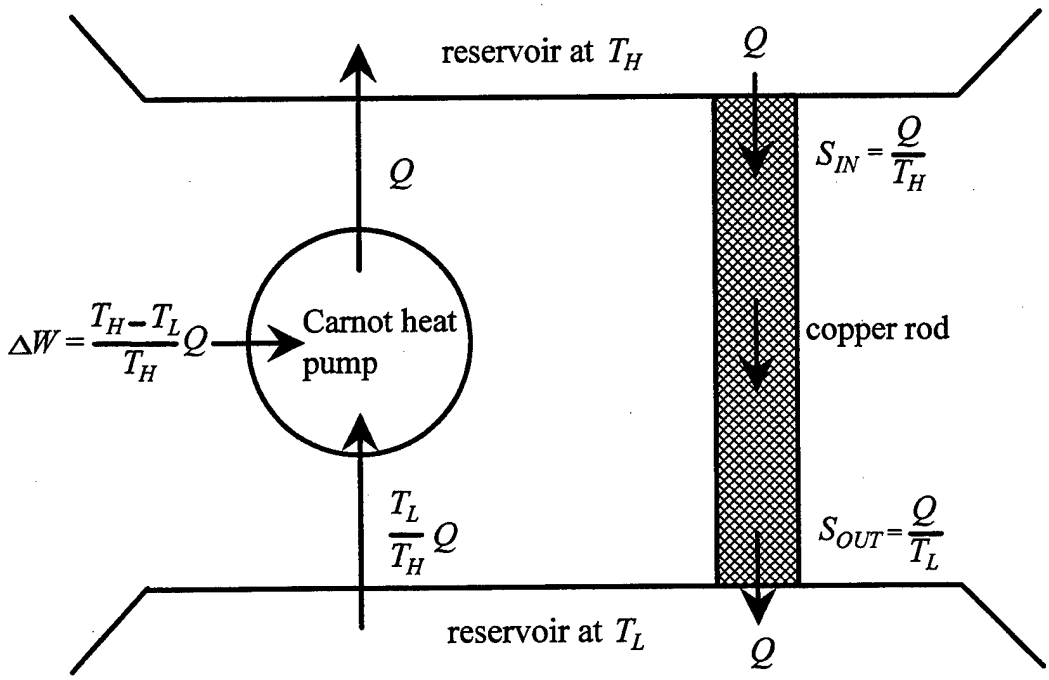

Figure 4. A simple analogy illustrating the fact that the location of work lost may not coincide with the location of entropy production.

the work is supplied to the Carnot heat pump at one spatial location, the entropy is produced in the copper rod, an entirely different spatial location.

3.1.3 Proof that $\Delta W = T_o \Delta S$ for a Composite Material

In Section 3.1.1 it was proven that $\Delta W = T_o \Delta S$ for an isotropic homogeneous material. The equality $\Delta W = T_o \Delta S$ will now be proven for a composite material made up of several subregions, each of which may be anisotropic, and whose interfaces may be thermally imperfect.

3.1.3.1 Temperature

Consider a composite with N-regions where the jth subregion is labeled R^j and has surface S^j as shown in Figure 5. The thermal conductivity and the linear thermal expansion are now described by the tensors, k_{lm}^j and α_{lm}^j, respectively (There is implied summation only on repeated subscripts). The temperature field in each subregion is governed by Eq. (10). Let n_l^j be the unit outward normal vector to subregion R^j. The boundary and interface conditions are as follows (Ozisik, pp. 594-596). The outer boundary of the composite is taken to be adiabatic:

$$(q_l n_l)^j = 0 \tag{45}$$

(only for that part of the jth subregion that constitutes a part of the outer boundary of the composite). The interface conditions are: (1) the continuity of the heat flux vector

$$(q_l n_l)^j + (q_l n_l)^r = 0, \qquad n_l^r = -n_l^j \qquad j \neq r \tag{46}$$

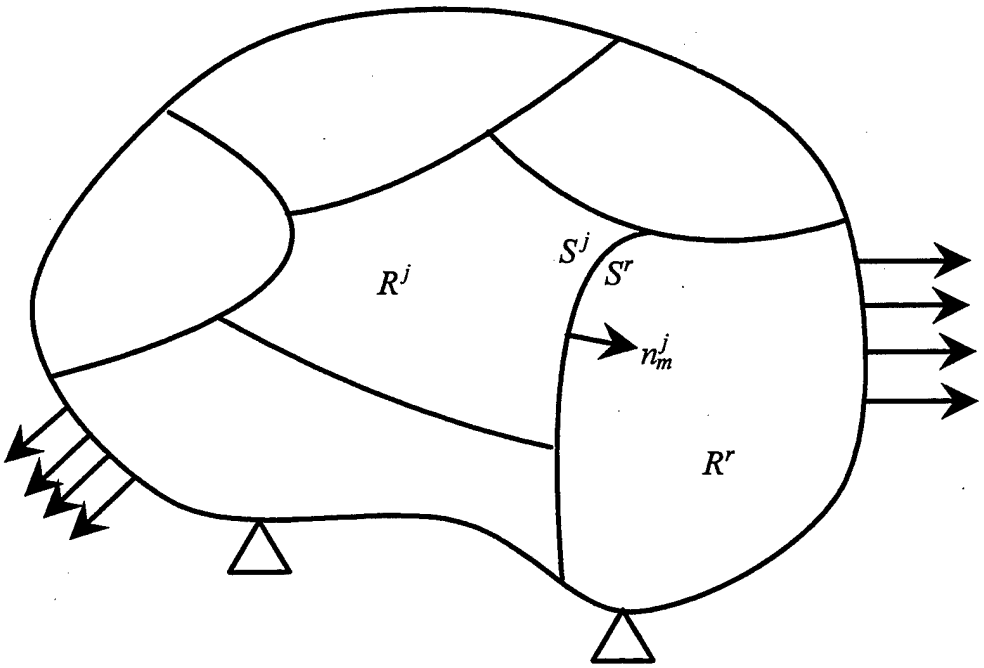

Figure 5. A general composite with anisotopic regions R^j, imperfect thermal interfaces S^j, unit surface normals n_l^j, and applied tractions.

and (2) the condition of imperfect thermal contact

$$(q_l n_l)^j = f^{jr}\left(T^j - T^r\right), \quad j \neq r \tag{47}$$

(only for the common boundary of the subregions R^j and R^r), where $f^{jr} = f^{rj}$ is the thermal contact conductance between adjacent subregions R^j and R^r. Eq. (47) represents the discontinuity of temperature between subregions R^j and R^r. For a perfect thermal interface $f^{jr} \to \infty$, and Eq. (47) reduces to the familiar condition of continuity of temperature, $T^j = T^r$.

As an aside note that the concept of a thermal contact conductance may be used not only to model a distinct imperfect thermal interface but also an interphase layer which is sufficiently thin so that a linear temperature distribution may be assumed. Then f may be thought of as the quotient of two parameters: (1) an effective interphase thickness h, and (2) an effective interphase thermal conductivity κ, such that $f = \kappa/h$. Combining the interface conditions, Eq. (46) and Eq. (47), gives

$$q_l^j n_l^j = -\kappa^{jr}\frac{T^r - T^j}{h^{jr}} = q_l^r n_l^j \tag{48}$$

From this equation it can be clearly seen that the continuity of heat is maintained across an interphase layer whereas the temperature is discontinuous due to the finite distance and finite thermal conductivity of the interphase layer.

Substituting Eqs. (13) and (14) into Eq. (10) results in

$$\left(k_{lm}V^{,j}_{,m}\right)_{,l} - C^j(i\omega)V^j = T_o(i\omega)\alpha^j_{lm}\sigma^j_{lm} \tag{49}$$

3.1.3.2 External Work Lost

The external work lost is calculated using the steps presented in Section 3.1.1.2. Eqs. (18), (19), and (21) remain the same except now each of the quantities is decorated with a superscript $(\ )^j$ for the subregion R^j. Since the coefficient of thermal expansion is now a tensor, in place of Eq. (22)

$$\varepsilon_{lm}^{j\,th}(\mathbf{x},\omega) = \alpha_{lm}^{j} V^{j} = \alpha_{lm}^{j}(\Theta^{j} + i\theta^{j}) \tag{50}$$

so that

$$\mathrm{Im}\left(\varepsilon_{lm}^{j\,th}(\mathbf{x},\omega)\right) = \alpha_{lm}^{j}\theta^{j} \tag{51}$$

In place of Eq. (24)

$$\Delta w^{j}(\mathbf{x},\omega) = -\pi\,\sigma_{lm}^{j}(\mathbf{x})\,\alpha_{lm}^{j}\,\theta^{j} \tag{52}$$

Finally, the total work lost per cycle in the composite is

$$\Delta W(\omega) = -\pi \sum_{j=1}^{N} \int_{R^j} \sigma_{lm}^{j}(\mathbf{x})\,\alpha_{lm}^{j}\theta^{j}\,dR \tag{53}$$

3.1.3.3 Heat Increment per Cycle

Taking the real value of Eq. (14), substituting into Eq. (11) and then using Eqs. (7) and (20) gives

$$\Delta s^{j} = \frac{\pi}{\omega T_o^2}\,k_{lm}^{j}\left(\Theta_{,l}^{j}\,\Theta_{,m}^{j} + \theta_{,l}^{j}\,\theta_{,m}^{j}\right) \tag{54}$$

The entropy produced per unit time at the thermally imperfect interfaces due to a discontinuity in temperature is calculated as follows. The change in entropy per unit time of a subregion R^j by heat flux through a surface S^j is

$-\int_{S^j}\left(q_l^j n_l^j / T^j\right) dS$. Given any two subregions R^j and R^r, the entropy produced per unit time, $\Delta \dot{S}^{jr}$, at their mutual interface, $S^{jr} = S^{rj}$, is thus

$$\Delta \dot{S}^{jr} = -\int_{S^{jr}} \frac{q_l^j n_l^j}{T^j} dS - \int_{S^{rj}} \frac{q_l^r n_l^r}{T^r} dS \tag{55}$$

Therefore, the entropy produced per unit time at all the interfaces is given by the following summation over the subregions

$$\Delta \dot{S}^{\text{interface}} = -\sum_{j=1}^{N} \int_{S^j} \frac{q_l^j n_l^j}{T^j} dS \tag{56}$$

Consistent with the approximations of the linear theory of elastothermodynamic damping, the factor $1/T^j$ is approximated with

$$\frac{1}{T^j} = \frac{1}{T_o + \text{Re}\left(V^j e^{i\omega t}\right)} \cong \frac{1}{T_o}\left[1 - \text{Re}\left(V^j e^{i\omega t}\right)/T_o\right] \tag{57}$$

Substituting Eqs. (6) and (57) into Eq. (56), using Eq. (14) and integrating over one cycle with the aid of Eq. (20) gives the entropy produced per cycle at the thermal interfaces due to a discontinuity in temperature

$$\Delta S^{\text{interface}} = \frac{\pi}{\omega T_o} \sum_{j=1}^{N} \int_{S^j} \text{Re}\left[k_{lm}^j n_l^j \left(V_{,m}^{\ j} e^{i\omega t} - V_{,m}^{\ j} \overline{V}^j / T_o\right)\right] dS \tag{58}$$

The first summation may be rewritten as a sum over the interfaces. Using the continuity of heat flux condition Eq. (46) and the fact that $n_l^j = -n_l^r$ for adjacent subregions, the first summation is identically zero, hence

$$\Delta S^{\text{interface}} = -\frac{\pi}{\omega T_o^2} \sum_{j=1}^{N} \int_{S^j} k_{lm}^j \left(\Theta_{,m}^{\ j} \Theta^j + \theta_{,m}^{\ j} \theta^j\right) n_l^j \, dS \tag{59}$$

Substituting Eqs. (54) and (59) into Eq. (8) gives the total entropy produced per cycle throughout the composite

$$\Delta S = \frac{\pi}{\omega T_o^2}\sum_{j=1}^{N}\int_{R^j} k_{lm}^j\left(\Theta_{,l}^j\,\Theta_{,m}^j + \theta_{,l}^j\,\theta_{,m}^j\right)dR - \frac{\pi}{\omega T_o^2}\sum_{j=1}^{N}\int_{S^j} k_{lm}^j\left(\Theta_{,m}^j\,\Theta^j + \theta_{,m}^j\,\theta^j\right)n_l^j\,dS \tag{60}$$

As in the isotropic case the heat increment per cycle ΔQ may be equated to $T_o\Delta S$.

3.1.3.4 Equality of ΔW and $T_o\Delta S$

Using the identity

$$k_{lm}\Theta_{,l}\,\Theta_{,m} = \left(k_{lm}\Theta_{,m}\,\Theta\right)_{,l} - \left(k_{lm}\Theta_{,m}\right)_{,l}\Theta \tag{61}$$

and the divergence theorem in Eq. (60), the surface terms vanish identically yielding

$$T_o\Delta S = -\frac{\pi}{\omega T_o}\sum_{j=1}^{N}\int_{R^j}\left[\left(k_{lm}^j\Theta_{,m}^j\right)_{,l}\Theta^j + \left(k_{lm}^j\theta_{,m}^j\right)_{,l}\theta^j\right]dR \tag{62}$$

Substituting Eq. (16) into Eq. (49) yields the real-valued equations,

$$\left(k_{lm}^j\Theta_{,m}^j\right)_{,l} + C^j\omega\theta^j = 0 \tag{63}$$

and

$$\left(k_{lm}^j\theta_{,m}^j\right)_{,l} - C^j\omega\Theta^j = T_o\omega\alpha_{lm}^j\sigma_{lm}^j(\mathbf{x}) \tag{64}$$

Solving Eq. (63) for $\left(k_{lm}^j\Theta_{,m}^j\right)_{,l}$ and Eq. (64) for $\left(k_{lm}^j\theta_{,m}^j\right)_{,l}$ and substituting into Eq. (62) yields

$$T_o\Delta S(\omega) = -\pi\sum_{j=1}^{N}\int_{R^j}\sigma_{lm}^j(\mathbf{x})\,\alpha_{lm}^j\theta^j\,dR \tag{65}$$

Comparing Eq. (53) to Eq. (65) gives

$$\Delta W = T_o \Delta S \tag{66}$$

Thus, for a thermoelastic composite material consisting of anisotropic subregions with imperfect thermal interfaces, with an adiabatic outer boundary, and loaded time-harmonically, the *total* work lost per cycle ΔW is equal to the *total* heat increment per cycle $T_o \Delta S$. This result establishes two approaches to calculating the elastothermodynamic damping in composite materials: (1) the mechanical approach developed in Section 3.1.3.2, and (2) the entropic approach developed in Section 3.1.3.3.

3.2 SOLUTION OF THE INHOMOGENEOUS HEAT-CONDUCTION PROBLEM FOR A GENERAL COMPOSITE MEDIUM USING THE INTEGRAL-TRANSFORM TECHNIQUE

In order to use either the mechanical approach or the entropic approach to calculate the elastothermodynamic damping in a composite material, the temperature field, governed by Eq. (10), must first be determined. The first step in this solution is to view the inhomogeneous term in Eq. (10) due to the thermoelastic effect as a heat-generation term. Ozisik (1980, pp. 594-610) has solved the inhomogeneous heat conduction problem (the heat conduction problem including heat generation) for a composite medium consisting of *isotropic* subregions with thermally imperfect interfaces using the integral

transform technique. In this section the solution given by Ozisik is extended to a composite medium consisting of *anisotropic* subregions.

The basic steps in the solution of the inhomogeneous heat-conduction problem using the integral-transform technique are as follows.

(1) The integral transform and inversion formulae are developed using the eigenfunctions of the associated homogeneous problem.

(2) By application of the integral transform, the partial differential heat-conduction equation in space and time is reduced to an ordinary differential equation in time.

(3) The resulting ordinary differential equation is solved subject to the transformed initial condition.

(4) The transform of the temperature is inverted using the inversion formula to obtain the desired solution.

3.2.1 The Time-Dependent Inhomogeneous Heat-Conduction Problem for a Composite Medium

Consider a composite medium consisting of N-anisotropic subregions with heat generation. As in Section 3.1.3 the jth subregion is labeled R^j, has surface S^j, and a unit outward normal vector n_l^j as shown in Figure 5. The temperature field in each subregion is governed by

$$\frac{1}{C^j}\left(k_{lm}^j T_{,m}^j\right)_{,l} + \frac{1}{C^j} g^j(\mathbf{x},t) = \frac{\partial}{\partial t} T^j(\mathbf{x},t) \qquad t > 0 \qquad (67)$$

where $g^j(\mathbf{x},t)$ is the heat generation per unit volume in subregion R^j. The boundary and interface conditions are identical to those described in Section 3.1.3.1. The initial condition is taken to be

$$T^j(\mathbf{x},t) = T_o \quad \text{at} \quad t = 0 \tag{68}$$

3.2.2 Development of the Integral Transform and Inversion Formulae

The first step in solving this inhomogeneous time-dependent heat-conduction problem by the method of integral transform is to develop the integral transform and inversion formulae. At the foundation of this development is the solution of the homogeneous problem. In order to obtain the homogeneous solution, the classical technique of separation of variables is used.

3.2.2.1 Solution of the Homogeneous Heat-Conduction Problem

Assuming a temperature solution of the form $T^j(\mathbf{x},t) = \phi^j(\mathbf{x})\Gamma(t)$, the homogeneous version of Eq. (67) may be separated into spatial and temporal equations,

$$\Gamma(t) = e^{-\beta^2 t} \tag{69}$$

and

$$\frac{1}{C^j}\left(k^j_{lm}\phi^{,j}_{,m}\right)_{,l} + \beta^2\phi^j = 0 \tag{70}$$

where β is the separation constant. The boundary and interface conditions become

$$-k^j_{lm}\phi^{,j}_{,m}\, n^j_l = 0 \tag{71}$$

for the outer boundary, and

$$-k_{lm}^{j}\phi_{,m}^{j}n_{l}^{j}=f^{jr}\left(\phi^{j}-\phi^{r}\right)=-k_{lm}^{r}\phi_{,m}^{r}n_{l}^{j} \tag{72}$$

for the common boundary of the subregions R^j and R^r. Eqs. (70), (71), and (72) constitute an eigenvalue problem for the eigenfunctions $\phi^j(\beta_n,\mathbf{x})$ in terms of the eigenvalues β_n (Unless otherwise stated, only the subscripts l and m are tensorial indices.).

3.2.2.2 Derivation of the Orthogonality Condition

The eigenfunctions obtained by solving the eigenvalue problem have a very special property, a generalized orthogonality. This generalized orthogonality property is the heart of the integral transform technique. In order to derive the orthogonality condition, Eq. (70) is written for two different eigenfunctions $\phi^j(\beta_n,x)\equiv\phi^{j,n}$ and $\phi^j(\beta_p,\mathbf{x})\equiv\phi^{j,p}$ as

$$\left(k_{lm}^{j}\phi_{,m}^{j,n}\right)_{,l}+\beta_{n}^{2}C^{j}\phi^{j,n}=0 \tag{73}$$

and

$$\left(k_{lm}^{j}\phi_{,m}^{j,p}\right)_{,l}+\beta_{p}^{2}C^{j}\phi^{j,p}=0 \tag{74}$$

Eq. (73) is multiplied by $\phi^{j,p}$ and Eq. (74) by $\phi^{j,n}$; the resulting equations are subtracted and integrated over the subregion R^j. Summing over all subregions gives

$$\left(\beta_{n}^{2}-\beta_{p}^{2}\right)\sum_{j=1}^{N}C^{j}\int_{R^{j}}\phi^{j,n}\phi^{j,p}dR=\sum_{j=1}^{N}\int_{R^{j}}\left[\left(k_{lm}^{j}\phi_{,m}^{j,p}\right)_{,l}\phi^{j,n}-\left(k_{lm}^{j}\phi_{,m}^{j,n}\right)_{,l}\phi^{j,p}\right]dR \tag{75}$$

Using the identity of Eq. (61) and the divergence theorem, Eq. (75) becomes

$$\left(\beta_n^2-\beta_p^2\right)\sum_{j=1}^{N}C^j\int_{R^j}\phi^{j,n}\phi^{j,p}dR=\sum_{j=1}^{N}\int_{S^j}\left[\left(k_{lm}^j\phi_{,m}^{j,p}\right)\phi^{j,n}-\left(k_{lm}^j\phi_{,m}^{j,n}\right)\phi^{j,p}\right]n_l^j\,dS \quad (76)$$

where the volume integrals have canceled. Using the outer boundary and interface conditions, Eqs. (71) and (72), and the fact that $n_l^j=-n_l^r$ for adjacent subregions R^j and R^r, the surface integrals in Eq. (76) vanish identically. Thus,

$$\left(\beta_n^2-\beta_p^2\right)\sum_{j=1}^{N}C^j\int_{R^j}\phi^{j,n}\phi^{j,p}dR=0 \quad (77)$$

which yields the orthogonality relation

$$\sum_{j=1}^{N}C^j\int_{R^j}\phi^{j,n}\phi^{j,p}dR=\begin{cases}0 & n\neq p\\ N_n & n=p\end{cases} \quad (78)$$

where

$$N_n=\sum_{j=1}^{N}C^j\int_{R^j}\left(\phi^{j,n}\right)^2dR \quad (79)$$

3.2.2.3 The Integral Transform and Inversion Formulae

Now that the orthogonality relation for the eigenfunctions has been obtained, the integral transform and inversion formulae may be derived. Consider the following representation of a function $T^j(\mathbf{x},t)$, defined in a finite region R^j, in terms of the eigenfunctions $\phi^j(\beta_n,\mathbf{x})$ of the previous eigenvalue problem,

$$T^j(\mathbf{x},t)=\sum_{n=1}^{\infty}A_n(t)\phi^j(\beta_n,\mathbf{x}) \quad (80)$$

where the summation is over all eigenvalues β_n. Multiplying Eq. (80) by $C^j\phi^{j,m}$, integrating over region R^j, and summing over all subregions gives

$$\sum_{j=1}^{N} C^j \int_{R^j} \phi^{j,m} T^j dR = \sum_{n=1}^{\infty} A_n(t) \sum_{j=1}^{N} C^j \int_{R^j} \phi^{j,m} \phi^{j,n} dR \tag{81}$$

Using the orthogonality relation, Eq. (78), and solving for $A_n(t)$ yields

$$A_n(t) = \frac{1}{N_n} \sum_{j=1}^{N} C^j \int_{R^j} \phi^{j,m} T^j dR \tag{82}$$

Eq. (82) is substituted into Eq. (80) and the resulting expression is split into two parts to define the desired integral transform and inversion formulae

$$\text{Integral transform:} \quad \tilde{T}(\beta_n, t) = \sum_{j=1}^{N} C^j \int_{R^j} \phi^j(\beta_n, \mathbf{x}) T^j(\mathbf{x}, t) dR \tag{83}$$

$$\text{Inversion formula:} \quad T^j(\mathbf{x}, t) = \sum_{n=1}^{\infty} \frac{1}{N_n} \phi^j(\beta_n, \mathbf{x}) \tilde{T}(\beta_n, t) \tag{84}$$

3.2.3 Integral Transform of the Inhomogeneous Heat-Conduction Problem

Having established the integral transform and inversion formulae, the inhomogeneous conduction-problem stated in Section 3.2.1 may now be solved. The spatial derivatives in Eq. (67) may be removed with the application of the integral transform. Multiplying Eq. (67) by $C^j\phi^{j,n}$, integrating over subregion R^j, and summing over all subregions gives

$$\sum_{j=1}^{N} \int_{R^j} \phi^{j,n} \left(k_{lm}^j T_{,m}^j \right)_{,l} dR + \sum_{j=1}^{N} \int_{R^j} \phi^{j,n} g^j(\mathbf{x}, t) dR = \frac{d}{dt} \sum_{j=1}^{N} C^j \int_{R^j} \phi^{j,n} T^j dR \tag{85}$$

Using the integral transform formula Eq. (83), the summation on the right is simply $\tilde{T}(t)$. Using the identity given in Eq. (61) and the divergence theorem twice, the first summation in Eq. (85) becomes

$$\sum_{j=1}^{N}\int_{R^j}\phi^{j,n}\left(k_{lm}^{j}T_{,m}^{j}\right)_{,l}\,dR=\sum_{j=1}^{N}\int_{S^j}\phi^{j,n}\left(k_{lm}^{j}T_{,m}^{j}\,n_l^j\right)dS-\sum_{j=1}^{N}\int_{S^j}T^j\left(k_{lm}^{j}\phi_{,l}^{j,n}\,n_m^j\right)dS+\sum_{j=1}^{N}\int_{R^j}T^j\left(k_{lm}^{j}\phi_{,l}^{j,n}\right)_{,m}dR \tag{86}$$

Using the outer boundary and interface conditions, Eqs. (71) and (72), and the fact that $n_l^j=-n_l^r$ for adjacent subregions R^j and R^r, the surface integrals in Eq. (86) vanish identically. Also, from Eq. (70), $\left(k_{lm}^{j}\phi_{,l}^{j,n}\right)_{,m}=-\beta_n^2C^j\phi^{j,n}$, so that Eq. (86) reduces to

$$\sum_{j=1}^{N}\int_{R^j}\phi^{j,n}\left(k_{lm}^{j}T_{,m}^{j}\right)_{,l}\,dR=-\beta_n^2\,\tilde{T}(t) \tag{87}$$

where the integral transform formula Eq. (83) has been used. Substituting Eq. (87) into Eq. (85) yields

$$\frac{d}{dt}\tilde{T}(t)+\beta_n^2\,\tilde{T}(t)=\tilde{g}(t) \tag{88}$$

where an integral transform of $g^j(\mathbf{x},t)$ has been defined as

$$\tilde{g}(\beta_n,t)=\sum_{j=1}^{N}\int_{R^j}\phi^j(\beta_n,\mathbf{x})g^j(\mathbf{x},t)\,dR \tag{89}$$

3.2.4 Solution for the Integral Transform of the Temperature and Inversion

The integral transform of the initial condition Eq. (68) is

$$\tilde{T}_o = T_o \sum_{j=1}^{N} C^j \int_{R^j} \phi^{j,n}\, dR \tag{90}$$

The solution of Eq. (88) subject to this initial condition is

$$\tilde{T}(t) = e^{-\beta_n^2 t}\left[\tilde{T}_o + \int_o^t e^{\beta_n^2 \tau}\tilde{g}(\tau)\, d\tau\right] \tag{91}$$

Using the inversion formula Eq. (84), the temperature field of the composite medium is given by

$$T^j(\mathbf{x},t) = \sum_{n=1}^{\infty} \frac{1}{N_n}\phi^{j,n}(\mathbf{x})\, e^{-\beta_n^2 t}\left[\tilde{T}_o + \int_o^t e^{\beta_n^2 \tau}\tilde{g}(\tau)\, d\tau\right] \tag{92}$$

Since this solution incorporates adiabatic outer boundaries, the first eigenvalue is $\beta_1 = 0$ and the first eigenfunction is $\phi^{j,1} = 1$. With this information it may be shown that

$$\sum_{n=1}^{\infty} \frac{1}{N_n}\phi^{j,n}\, e^{-\beta_n^2 t}\, \tilde{T}_o = T_o \tag{93}$$

Hence, Eq. (92) reduces to

$$T^j(\mathbf{x},t) = T_o + \sum_{n=1}^{\infty} \frac{1}{N_n}\phi^{j,n}(\mathbf{x}) \int_o^t e^{-\beta_n^2 (t-\tau)}\tilde{g}(\tau)\, d\tau \tag{94}$$

This equation represents the temperature field of a composite medium consisting of anisotropic subregions with arbitrary heat generation and whose interfaces may be thermally imperfect.

3.3 ELASTOTHERMODYNAMIC DAMPING IN A GENERAL COMPOSITE MEDIUM

Now that an expression for the temperature field has been obtained for a composite material with arbitrary heat generation, expressions may now be derived for the temperature field, local work lost, local entropy produced, and the elastothermodynamic damping. Comparing Eq. (10) with Eq. (67), it is clear that for the problem of elastothermodynamic damping

$$g^j(\mathbf{x},t) = -T_o \alpha^j_{lm} \frac{\partial \sigma^j_{lm}}{\partial t} \tag{95}$$

Substituting Eq. (13) into Eq. (95) gives

$$g^j(\mathbf{x},t) = -T_o (i\omega) \alpha^j_{lm} \sigma^j_{lm}(\mathbf{x}) e^{i\omega t} \tag{96}$$

Substituting Eq. (96) into Eq. (89) results in

$$\tilde{g}(t) = -T_o (i\omega) L_n e^{i\omega t} \tag{97}$$

where

$$L_n = \sum_{j=1}^{N} \int_{R^j} \phi^{j,n}(\mathbf{x}) \alpha^j_{lm} \sigma^j_{lm}(\mathbf{x}) dR \tag{98}$$

Substituting Eq. (97) into Eq. (94) and carrying out the integration in time yields the following expression for the temperature field of the composite

$$T^j(\mathbf{x},t) = T_o - T_o \sum_{n=1}^{\infty} \frac{i\omega}{i\omega + \beta_n^2} \frac{L_n}{N_n} \phi^{j,n}(\mathbf{x}) \left(e^{i\omega t} - e^{-\beta_n^2 t} \right) \tag{99}$$

The first term in parenthesis represents the time-harmonic solution whereas the second term represents the transient solution. Herein, only the time-

harmonic solution is of interest. Comparing Eq. (99) with Eq. (14), it is clear that the fluctuating temperature is given by

$$V^j(\mathbf{x},\omega) = -T_o \sum_{n=1}^{\infty} \frac{i\omega}{i\omega + \beta_n^2} \frac{L_n}{N_n} \phi^{j,n}(\mathbf{x}) \tag{100}$$

Substituting Eq. (100) into Eq. (52) gives the local work lost per unit volume per cycle,

$$\Delta w^j(\mathbf{x},\omega) = \pi T_o \sum_{n=1}^{\infty} \frac{\omega \beta_n^2}{\omega^2 + \beta_n^4} \frac{L_n}{N_n} \alpha_{lm}^j \sigma_{lm}^j(\mathbf{x}) \phi^{j,n}(\mathbf{x}) \tag{101}$$

Substituting Eq. (100) into Eq. (54) gives the local entropy produced per unit volume per cycle,

$$\Delta s^j(\mathbf{x},\omega) = \pi \sum_{n=1}^{\infty} \sum_{q=1}^{\infty} \frac{\omega\left(\omega^2 + \beta_n^2 \beta_q^2\right)}{\left(\omega^2 + \beta_n^4\right)\left(\omega^2 + \beta_q^4\right)} \frac{L_n}{N_n} \frac{L_q}{N_q} k_{lm}^j \phi_{,l}^{j,n} \phi_{,m}^{j,q} \tag{102}$$

As shown in Section 3.1.3, the total external work lost over the entire composite per cycle may be calculated using either the local work lost or the local entropy produced. From the form of Eqs. (101) and (102) it is mathematically much easier to use the local work lost expressions. Thus, substituting Eq. (100) into Eq. (53), the total external work lost per cycle over the entire composite is given by

$$\Delta W(\omega) = \pi T_o \sum_{n=1}^{\infty} \frac{\omega \beta_n^2}{\beta_n^4 + \omega^2} \frac{L_n^2}{N_n} \tag{103}$$

The elastothermodynamic damping of a composite medium consisting of an arbitrary number of subregions, each of which may be anisotropic and whose

thermal interfaces may be imperfect, subjected to any time-harmonic stress field, may be calculated using Eq. (103).

3.4 ELASTOTHERMODYNAMIC DAMPING IN LAYERED COMPOSITES

The results of Section 3.3 are now specialized to a composite material consisting of N isotropic layers in a rectangular, cylindrical, and spherical coordinate system (i.e. an N-layer slab, cylinder, and sphere, respectively), subjected to any stress field so long as the resulting heat conduction can be described by a single spatial coordinate orthogonal to the layering (see Figure 6). Many problems of current engineering interest can be modeled as special cases of the N-layer solution. (1) *Cartesian coordinate system*: laminated composites in bending and extension; aligned platelet composite; or a periodic array of labs. (2) *Cylindrical coordinate system*: a unidirectional fiber-reinforced composite where each fiber may consist of several concentric cylinders. (3) *Spherical coordinated system*: a particulate composite where each particle may be solid or hollow, or consist of several concentric spheres, for example, an aluminum matrix filled with hollow Al_2O_3 microspheres. Specific results are given for the following problems. (I) A periodic array of slabs (rectangular symmetry) with a two-layer representative volume element subjected to the following mechanical stress states: (a) a time-harmonic uniform stress perpendicular to the layering, and (b) a time-harmonic uniform

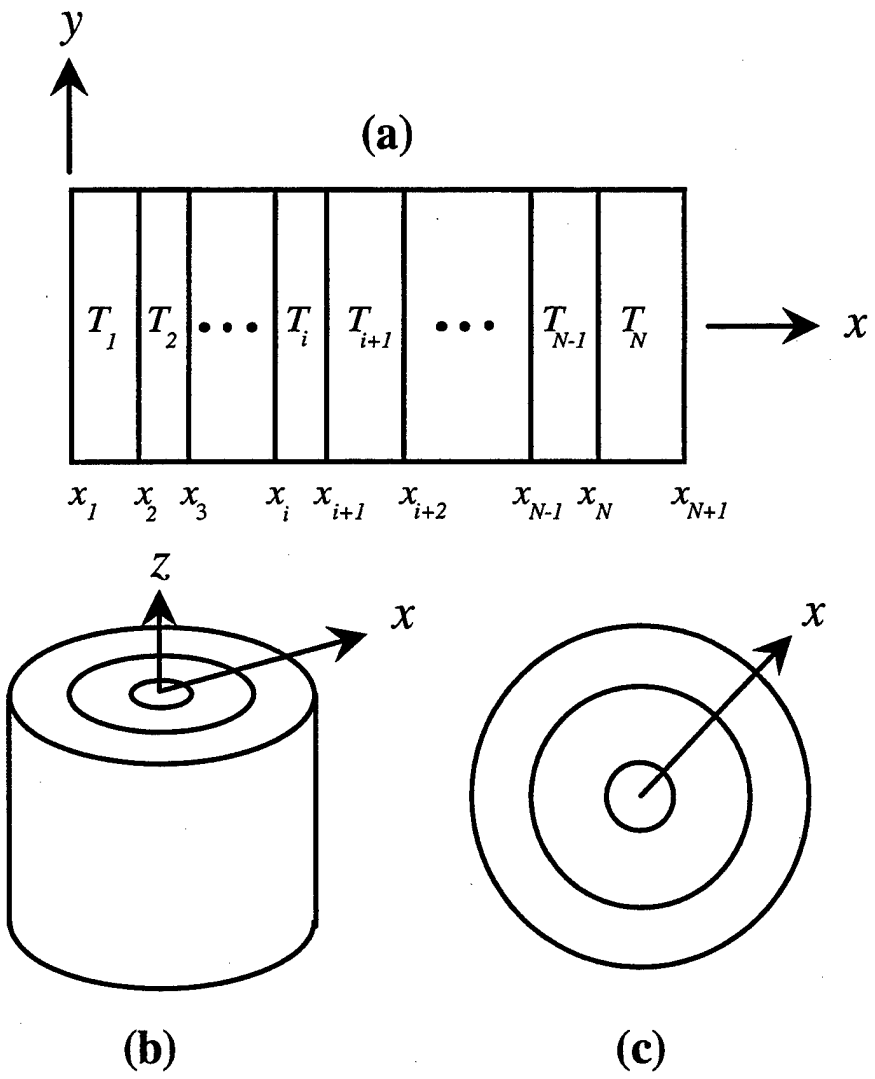

Figure 6. An *N*-layer medium in (a) a rectangular, (b) a cylindrical, and (c) a spherical coordinate system.

strain parallel to the layering. (II) A symmetric three-layer plate in pure bending with a stress field obtained from the classical laminate theory. (III) A hollow two-layer concentric sphere subjected to a uniform time-harmonic radial load.

The fluctuating temperature field of a general composite medium subjected to any time-harmonic loading is given by Eq. (100). For an N-layer composite with isotropic layers, Eq. (100) reduces to

$$V_j(x,\omega) = -T_o \sum_{n=1}^{\infty} \frac{i\omega}{i\omega + \beta_n^2} \frac{L_n}{N_n} \phi_{j,n}(x) \tag{104}$$

where x is the spatial coordinate normal to the layering as shown in Figure 6. (In this section a particular layer will be referenced with a subscript instead of a superscript as in Section 3.3.) But now Eq. (79) reduces to

$$N_n = \sum_{j=1}^{N} C_j \int_{x_j}^{x_{j+1}} \xi^p \phi_{j,n}^2(\xi)\, d\xi \tag{105}$$

where ξ^p is the Sturm-Liouville weight function ($p = 0,1,2$ for rectangular, cylindrical, and spherical symmetry, respectively). Also, Eq. (98) reduces to

$$L_n = \sum_{j=1}^{N} \alpha_j \int_{x_j}^{x_{j+1}} \xi^p \sigma_{kk}(\xi) \phi_{j,n}(\xi)\, d\xi \tag{106}$$

The local work lost per unit volume per cycle in a general composite medium is described by Eq. (101). For an N-layer composite with isotropic layers, this expression reduces to

$$\Delta w_j(x,\omega) = \pi T_o \alpha_j \sigma_{kk}(x) \sum_{n=1}^{\infty} \frac{\omega \beta_n^2}{\omega^2 + \beta_n^4} \frac{L_n}{N_n} \phi_{j,n}(x) \tag{107}$$

The local entropy produced per unit volume per cycle in a general composite is described by Eq. (102). For an N-layer composite this equation reduces to

$$\Delta s_j(x,\omega) = \pi k_j \sum_{n=1}^{\infty}\sum_{q=1}^{\infty} \frac{\omega\left(\omega^2+\beta_n^2\beta_q^2\right)}{\left(\omega^2+\beta_n^4\right)\left(\omega^2+\beta_q^4\right)} \frac{L_n}{N_n}\frac{L_q}{N_q}\frac{d\phi_{j,n}}{dx}\frac{d\phi_{j,q}}{dx} \qquad (108)$$

The total external work lost per cycle for a general composite medium is described by Eq. (103). This expression has the same form for an N-layer composite but now N_n and L_n are given by Eqs. (105) and (106), respectively.

3.4.1 Elastothermodynamic Damping in a Periodic Array of Slabs

Consider a periodic array of slabs of two isotropic materials with imperfect thermal interfaces as shown in Figure 7. A unit cell is shown in an inset in the figure and consists of a layer of material (1) with thickness a and a layer of material (2) with thickness $(b\text{-}a)$. Unless otherwise stated, in the following the subscripts $(\ )_1$ and $(\ )_2$ will refer to materials (1) and (2), respectively. The planes $x=0$ and $x=b$ are adiabatic due to reflection symmetry on these planes. The eigenfunctions for each layer can be determined using the method of Ozisik (1980, pp. 294-334), giving

$$\phi_{1n}(x) = \cos(\gamma_n x/a) \qquad (109)$$

$$\phi_{2n}(x) = A_n\cos(\eta_n x/b) + B_n\sin(\eta_n x/b) \qquad (110)$$

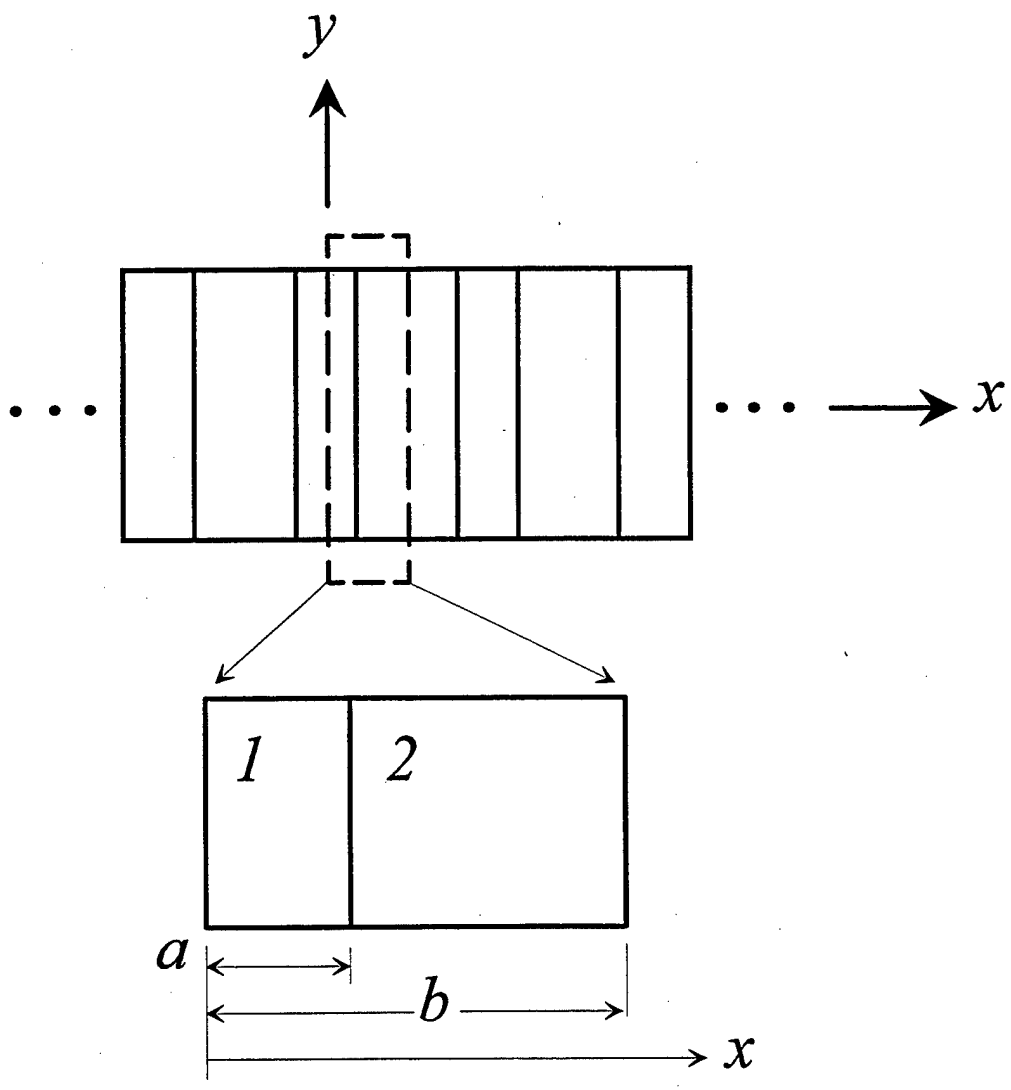

Figure 7. A periodic array of slabs of two materials. The dimensions of a unit cell are shown in the inset.

where

$$A_n = \left[\cos(\gamma_n) - \frac{k_1}{fa}\gamma_n \sin(\gamma_n)\right]\cos(\eta_n a/b) + K\sin(\gamma_n)\sin(\eta_n a/b)$$
$$B_n = \left[\cos(\gamma_n) - \frac{k_1}{fa}\gamma_n \sin(\gamma_n)\right]\sin(\eta_n a/b) - K\sin(\gamma_n)\cos(\eta_n a/b) \tag{111}$$

and

$$\gamma_n = \beta_n\sqrt{\tau_1}, \quad \eta_n = \beta_n\sqrt{\tau_2}\,\frac{b}{b-a},$$
$$\tau_1 = (C/k)_1 a^2, \quad \tau_2 = (C/k)_2 (b-a)^2, \quad K = \sqrt{(kC)_1/(kC)_2} \tag{112}$$

The constant τ is a characteristic time of heat conduction, and f is the thermal contact conductance for the interface. The transcendental equation for the eigenvalues β_n is

$$\begin{vmatrix} \frac{k_1}{fa}\gamma_n \sin(\gamma_n) - \cos(\gamma_n) & \cos(\eta_n a/b) & \sin(\eta_n a/b) \\ K\sin(\gamma_n) & -\sin(\eta_n a/b) & \cos(\eta_n a/b) \\ 0 & -\sin(\eta_n) & \cos(\eta_n) \end{vmatrix} = 0 \tag{113}$$

The following two canonical time-harmonic stress states are considered:

(1) a uniform uniaxial stress perpendicular to the layers

$$\sigma_{xx1} = \sigma_{xx2} = \sigma$$
$$\sigma_{ij_1} = \sigma_{ij_2} = 0 \qquad \text{otherwise} \tag{114}$$

(2) a uniform strain parallel to the layers

$$\varepsilon_{yy_1} = \varepsilon_{yy_2} = \varepsilon$$

so that

$$\begin{aligned} \sigma_{yy_1} &= E_1\varepsilon \quad \text{and} \quad \sigma_{yy_2} = E_2\varepsilon \\ \sigma_{ij_1} &= \sigma_{ij_2} = 0 \quad \text{otherwise} \end{aligned} \tag{115}$$

where σ and ε are constants, E is the Young's modulus, and the time-harmonic factor $e^{i\omega t}$ is implied. These two stress states will be referred to as problem (1) and problem (2), respectively.

Using Eq. (104) the fluctuating temperature in layers 1 and 2 for both problems (1) and (2) is given by

$$V_j(x,\Omega_1) = -T_o(\alpha\sigma_{kk}/C)_1 \sum_{n=1}^{\infty} \frac{\Omega_1^2 + i\Omega_1\gamma_n^2}{\Omega_1^2 + \gamma_n^4} R_n \phi_{j,n}(x), \qquad j = 1,2 \tag{116}$$

where a dimensionless frequency $\Omega_1 = \omega\tau_1$ has been defined, and

$$R_n = \frac{\dfrac{a}{b} I_1 + \dfrac{\alpha_2}{\alpha_1} F I_2}{\dfrac{a}{b} I_3 + \dfrac{C_2}{C_1} I_4} \tag{117}$$

where $F = 1$ for problem (1) and $F = E_2/E_1$ for problem (2), and

$$I_1 = \sin(\gamma_n)/\gamma_n$$

$$I_2 = \frac{1}{\eta_n}\left\{A_n\left[\sin(\eta_n) - \sin(\eta_n a/b)\right] - B_n\left[\cos(\eta_n) - \cos(\eta_n a/b)\right]\right\}$$

$$I_3 = \frac{1}{2} + \frac{1}{4\gamma_n}\sin(2\gamma_n)$$

$$I_4 = \frac{1}{2}\left(1-\frac{a}{b}\right)\left(A_n^2+B_n^2\right)+\frac{1}{4\eta_n}\left(A_n^2-B_n^2\right)\left[\sin(2\eta_n)-\sin(2\eta_n a/b)\right]$$
$$-\frac{1}{2\eta_n}A_nB_n\left[\cos(2\eta_n)-\cos(2\eta_n a/b)\right]$$

(118)

Now intuitively as $\Omega_1 \to 0$ the time period goes to infinity. During each cycle heat has plenty of time to conduct between 'cold' and 'hot' slabs, and essentially isothermal conditions are obtained. In the other extreme as $\Omega_1 \to \infty$ the time period goes to zero, and heat has very little time to conduct. Therefore, with the exception of the interface where there will always be some heat conduction no matter how high the frequency, essentially adiabatic conditions are obtained. These intuitive observations will now be used as a check on Eq. (116).

Suppose the unit cell is initially at rest with equilibrium temperature T_o. At time $t=0$ the stresses σ_{kk1} and σ_{kk2} are suddenly applied to layers (1) and (2), respectively, and held constant thereafter. Within the linear theory of elastothermodynamic damping, from Eq. (1) the instantaneous changes in temperature of the two layers due to the thermoelastic effect are

$$\Delta T_j = -T_o\left(\alpha\sigma_{kk}/C\right)_j \qquad j=1,2 \tag{119}$$

Upon the completion of the heat conduction process, the unit cell will be at a homogeneous equilibrium temperature given by

$$T_o+V_j = T_o - T_o\frac{(a/b)(\alpha\sigma_{kk})_1+(1-a/b)(\alpha\sigma_{kk})_2}{(a/b)C_1+(1-a/b)C_2} \qquad j=1,2 \tag{120}$$

It has been verified that Eq. (116) correctly reduces to this isothermal limit as $\Omega_1 \to 0$. Under strictly adiabatic conditions (i.e. when the thermal conductivity $k = 0$), the temperature in each layer is given merely by the thermoelastic effect, Eq. (119); that is

$$V_j = -T_o(\alpha\sigma_{kk}/C)_j \qquad j = 1,2 \tag{121}$$

Once again, with the exception of the immediate vicinity of the interface, it was shown that Eq. (116) correctly reduces to this adiabatic limit as $\Omega_1 \to \infty$. In passing note that the parameters α/C for problem (1) and $E\alpha/C$ for problem (2) are the most significant factors determining the magnitude of V. The numerical values of these parameters for some pertinent engineering materials are presented in Table 1.

Table 1. Thermoelastic constants and dimensionless parameters

	E (GPa)	k (J/smK)	α (10^{-6}) (1/K)	C (10^{6}) (J/m^3K)	α/C (10^{-12}) (J/m^3)	$E\alpha/C$	Ψ_o
Al	70	222	24	2.43	9.71	0.68	0.0302
Steel	200	52	12	3.82	3.14	0.63	0.0147
Zn	103	113	40	2.73	14.5	1.5	0.1121
Mg	44	154	27	1.79	15.1	0.67	0.0340
Ti	116	39	8.4	2.34	3.59	0.42	0.0066
Al_2O_3	350	29	9	3.19	2.82	0.99	0.0167
SiC	460	90	4.3	4.34	0.99	0.46	0.0037

Numerical results for problem (1) for a SiC-Al periodic layered composite will now be presented. Let layer (1) be SiC and layer (2) be Al. The volume fraction of the SiC "inclusions" is denoted by $V_f = a/b$. A normalized fluctuating temperature Θ is introduced as

$$\Theta = \frac{V}{(T_o \sigma_o \alpha / C)_2} \tag{122}$$

In polar form $\Theta = \|\Theta\| \exp(i\Phi)$, where $\|\Theta\|$ is the magnitude and Φ is the phase of Θ. Consider first a thermally *perfect* interface. In Figures 8 and 9 $\|\Theta\|$ and Φ are plotted, respectively, verses the normalized position $\xi = x/b$ with $\Omega_1 = \Omega_{SiC}$ as a parameter. Note that for $\Omega_{SiC} \approx 1$ the conditions are essentially isothermal and $\Phi \cong \pi$. As Ω_{SiC} increases significant temperature gradients develop and become localized near the interface. At very high frequencies, $\Omega_{SiC} \approx 1000$, the conditions are essentially adiabatic and, once again, $\Phi \cong \pi$ (with the obvious exception of the immediate vicinity of the interface as discussed previously).

Now consider a thermally *imperfect* interface. A normalized thermal contact conductance ζ is introduced as

$$\zeta = \frac{fa}{k_1} \tag{123}$$

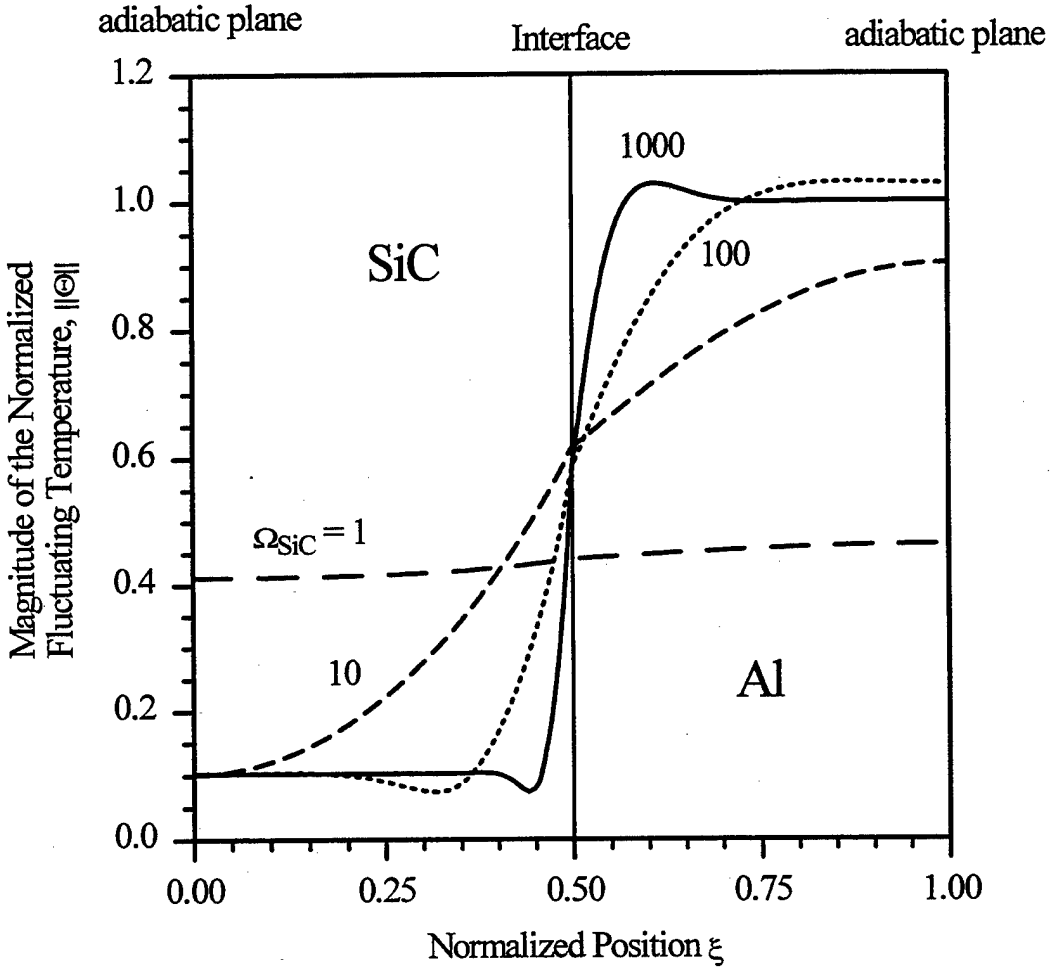

Figure 8. Magnitude of the normalized fluctuating temperature, $\|\Theta\|$, as a function of the normalized position ξ for problem (1) with a *perfect* thermal interface, for the composite SiC-Al, for four normalized frequencies Ω_{SiC}, and for a SiC volume fraction of $V_f = 0.5$.

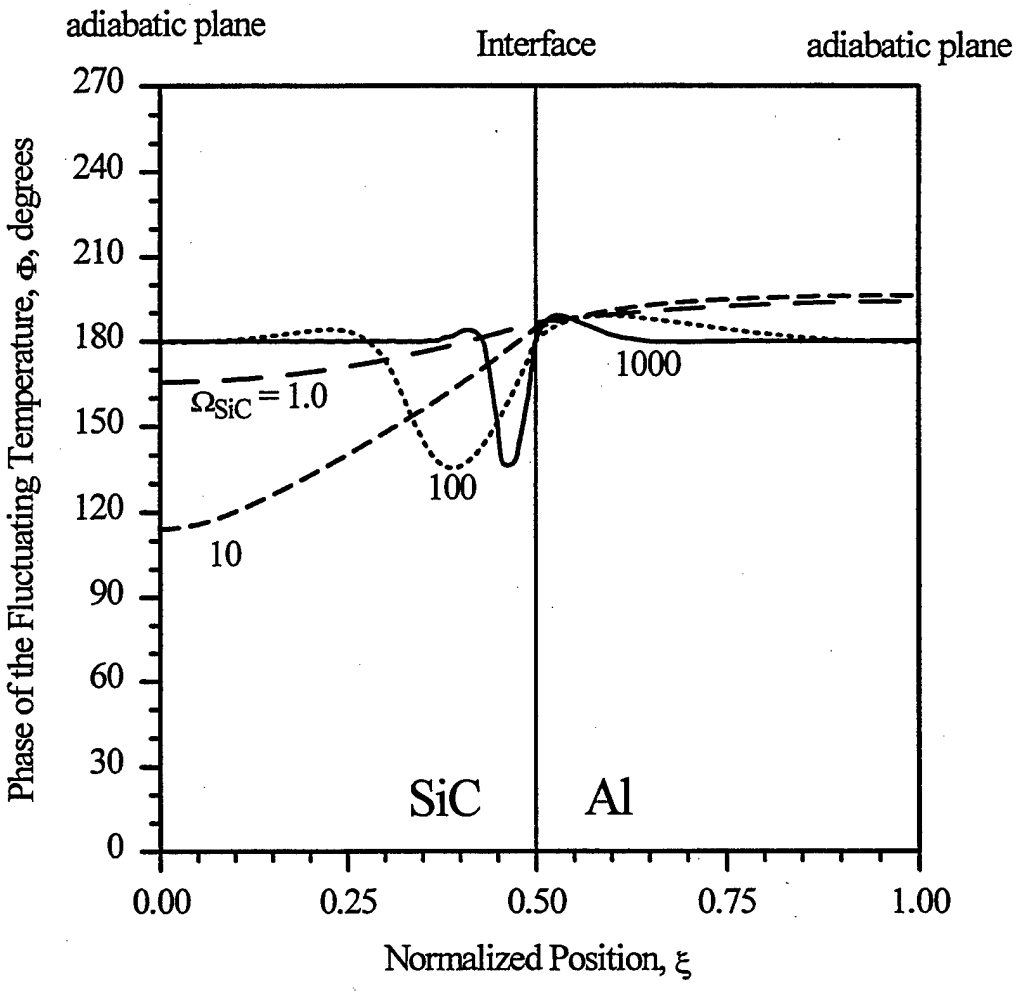

Figure 9. Phase of the fluctuating temperature, Φ, as a function of the normalized position ξ for problem (1) with a *perfect* thermal interface, for the composite SiC-Al, for four normalized frequencies Ω_{SiC}, for a SiC volume fraction of $V_f = 0.5$.

Moreover, if the thermal contact conductance is used to model the presence of an extremely thin interphase layer of thickness h and thermal conductivity κ (so that a linear temperature variation across the thickness may be assumed), then $f = \kappa/h$ and therefore

$$\zeta = \frac{fa}{k_1} = \frac{\kappa}{k_1}\frac{a}{h} \tag{124}$$

In the limit as $h \to 0$ or $\kappa \to \infty$, $f \to \infty$ and the conditions corresponding to a thermally perfect interface are recovered.

In Figure 10 $\|\Theta\|$ is plotted versus the normalized spatial coordinate ξ with ζ as a parameter for a normalized frequency of $\Omega_{SiC} = 10$. (It will be shown later that this particular frequency corresponds to a maximum in the total damping.) A comparison of Figures 8 and 10 reveals that conditions corresponding to a thermally perfect interface are obtained as ζ approaches 100. Conversely, as ζ approaches 0.1 the two layers become thermally isolated. For a typical interphase layer κ is of the order of k_1 and $h/a = O(10^{-2})$. Therefore, from Eq. (124), ζ is of the order of 100, i.e. a condition corresponding to a thermally perfect interface. One may conclude that a typical interphase layer will have little effect on the temperature and thus on the elastothermodynamic damping. This fact will be further elucidated in the following analysis.

Using Eq. (107) the local work lost per cycle in each layer $\Delta w_j(x,\omega)$, $j = 1,2$, is given by

$$\Delta w_j(x,\omega) = \pi T_o(\sigma_{kk}\alpha)_j(\alpha\sigma_{kk}/C)_1 \sum_{n=1}^{\infty} \frac{\Omega_1\gamma_n^2}{\Omega_1^2 + \gamma_n^4} R_n \phi_{j,n} \tag{125}$$

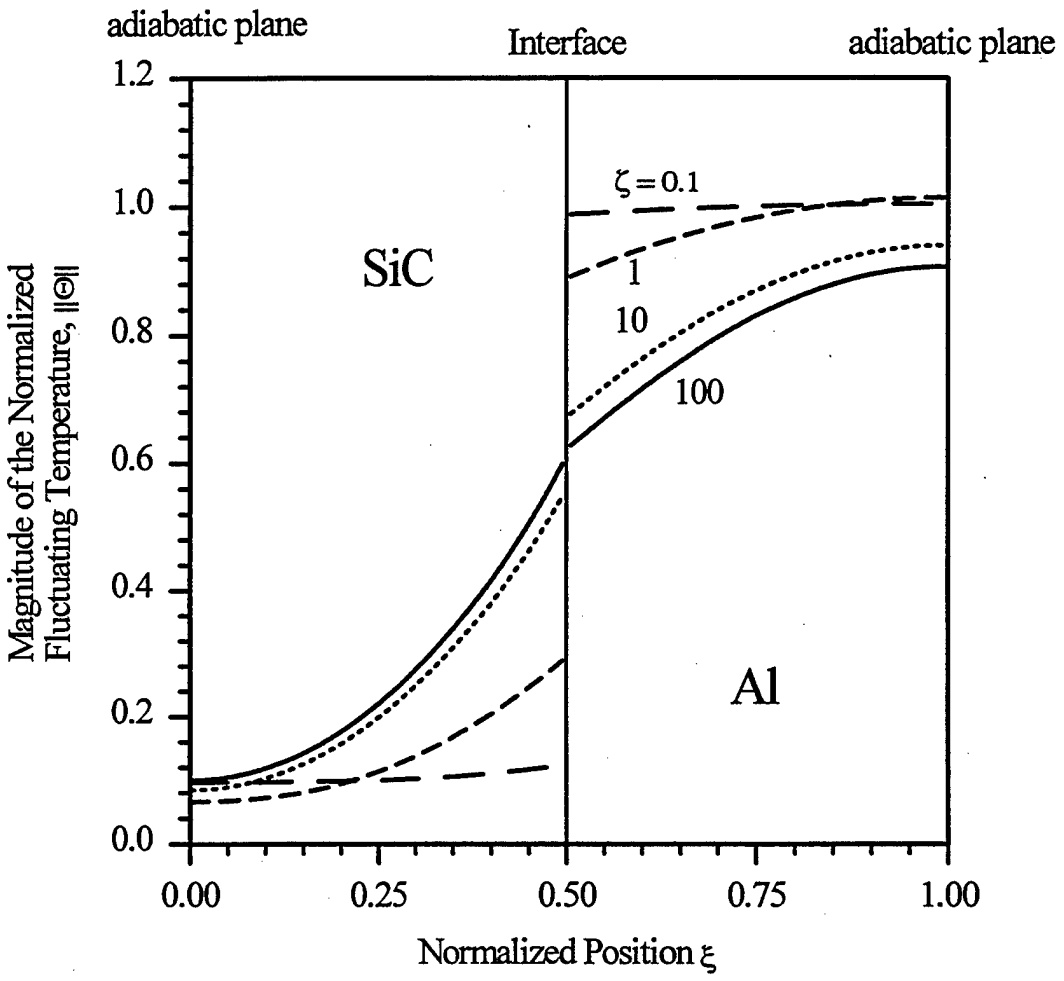

Figure 10. Magnitude of the normalized fluctuating temperature, $\|\Theta\|$, as a function of the normalized position ξ for problem (1) with an *imperfect* thermal interface, for the composite SiC-Al, for four normalized thermal contact conductances ζ, for a normalized frequency $\Omega_{SiC} = 10$, and for a SiC volume fraction of $V_f = 0.5$.

A normalized local work lost ψ is introduced as

$$\psi = \frac{\Delta w}{T_o\left((\alpha\sigma_{kk})^2/C\right)_2} \tag{126}$$

A physical feel for the denominator may be developed as follows. A rod of one unit volume at an equilibrium temperature T_o is subjected to a uniaxial tension of magnitude τ under adiabatic conditions; then $V = -\tau T_o \alpha / C$. While holding τ fixed, the rod is allowed to absorb heat from a reservoir at T_o until it returns to its equilibrium temperature T_o. Next, the rod is unloaded adiabatically; then $V = +\tau T_o \alpha / C$. Once again, the rod is allowed to give up heat to a reservoir at T_o until the rod temperature becomes T_o. The *total* work lost during this cycle is $\tau^2 T_o \alpha^2 / C$. By way of example, for steel, $\alpha = 12\text{x}10^{-6} K^{-1}$ and $C = 3.8\text{x}10^6 J/m^3 K$. If we choose $\tau = 100 MPa$, $T_o = 300K$, and $\kappa = 1$ (plane stress), then $\Delta w = 114 J/m^3$. Interestingly, the temperature increase of the rod due to this conversion of work into internal heat energy is only $\Delta T = 3\text{x}10^{-5} K$. For use in the next section, the *total* entropy produced during this cycle is $\tau^2 \alpha^2 / C$. For the example under consideration, $\Delta s = 0.38 J/m^3 K$.

For the case of a thermally *perfect* interface, ψ is plotted in Figure 11 versus the normalized position ξ with the normalized frequency Ω_{SiC} as a parameter. The maximum local work lost is in the aluminum layer for all the frequencies shown. Note that the local work lost is actually negative in the SiC layer. At first sight this may appear disturbing for it implies that work is being produced rather than converted into heat. However, the only constraint

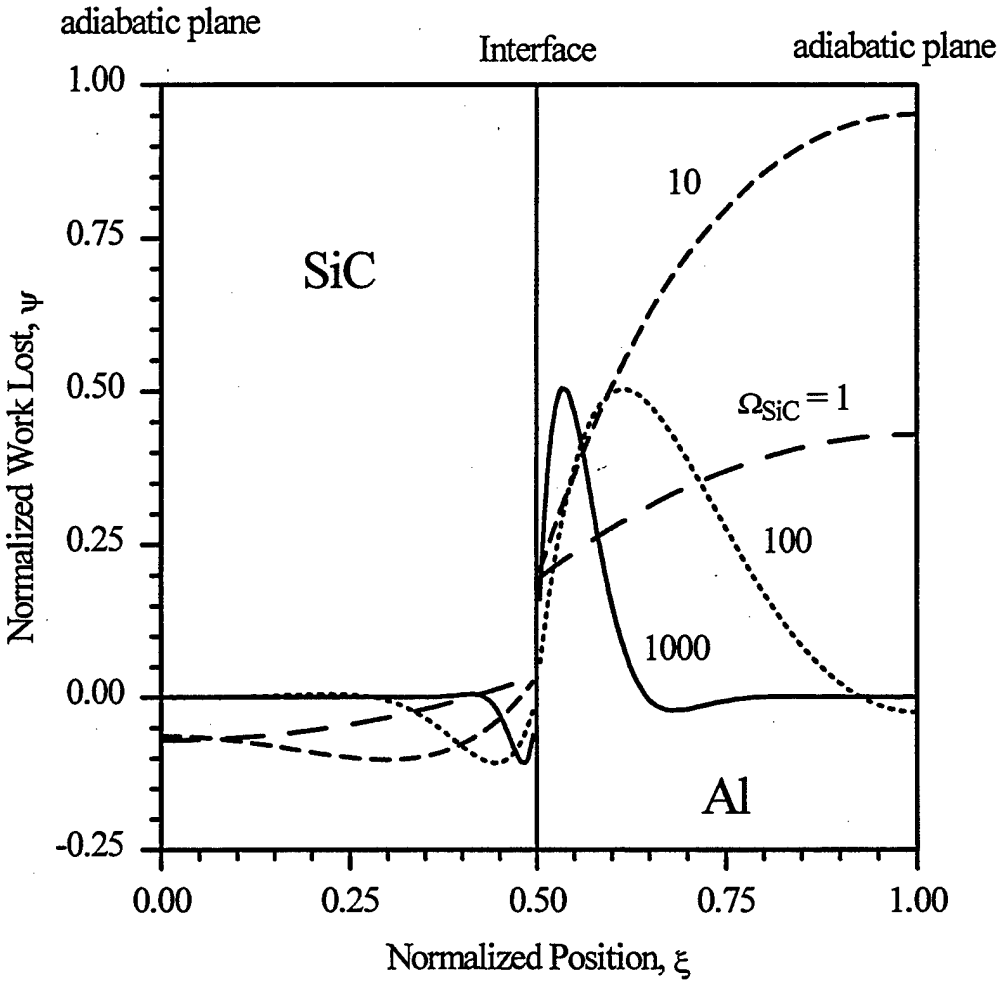

Figure 11. Normalized work lost ψ as a function of the normalized position ξ for problem (1) with a *perfect* thermal interface, for the composite SiC-Al, for four values of the normalized frequency Ω_{SiC}, and for a SiC volume fraction of $V_f = 0.5$.

imposed by the second law of thermodynamics is that the *total* entropy produced throughout the composite (a closed thermodynamic system which does not exchange heat with its surroundings) during one cycle of loading is either zero or positive, i.e. $\Delta S \geq 0$. It follows from Eq. (66) that $T_o \Delta S \equiv \Delta W \geq 0$, i.e., the *total* work lost throughout the composite during one cycle should be zero or positive. It follows that $\Psi \geq 0$. From an examination of Figure 15, it is apparent that this second-law constraint is clearly satisfied. Figure 12 shows the effect of a thermally *imperfect* interface on the local work lost for $\Omega_{SiC} = 10$. As the interface 'degrades', i.e. decreasing ζ, the heat exchange between the slabs decreases, and the work lost decreases as expected.

Using Eq. (108) the local entropy produced per cycle in each layer $\Delta s_j(x,\omega), j = 1,2$, is given by

$$\Delta s_j(x,\omega) = \pi k_j \tau_1 (\alpha \sigma_{kk}/C)_1^2 \sum_{n=1}^{\infty}\sum_{m=1}^{\infty} \frac{\Omega_1\left(\Omega_1^2 + \gamma_n^2\gamma_m^2\right)}{\left(\Omega_1^2 + \gamma_n^4\right)\left(\Omega_1^2 + \gamma_m^4\right)} R_n R_m \frac{d\phi_{j,n}}{dx}\frac{d\phi_{j,m}}{dx} \quad (127)$$

As a check on the calculations, the results of Kinra and Milligan (1994) for two semi-infinite rods in perfect thermal contact were reproduced by letting Ω_{SiC} in Eq. (127) become sufficiently large so that the heat conduction was confined near the interface. A normalized local entropy produced χ is introduced as

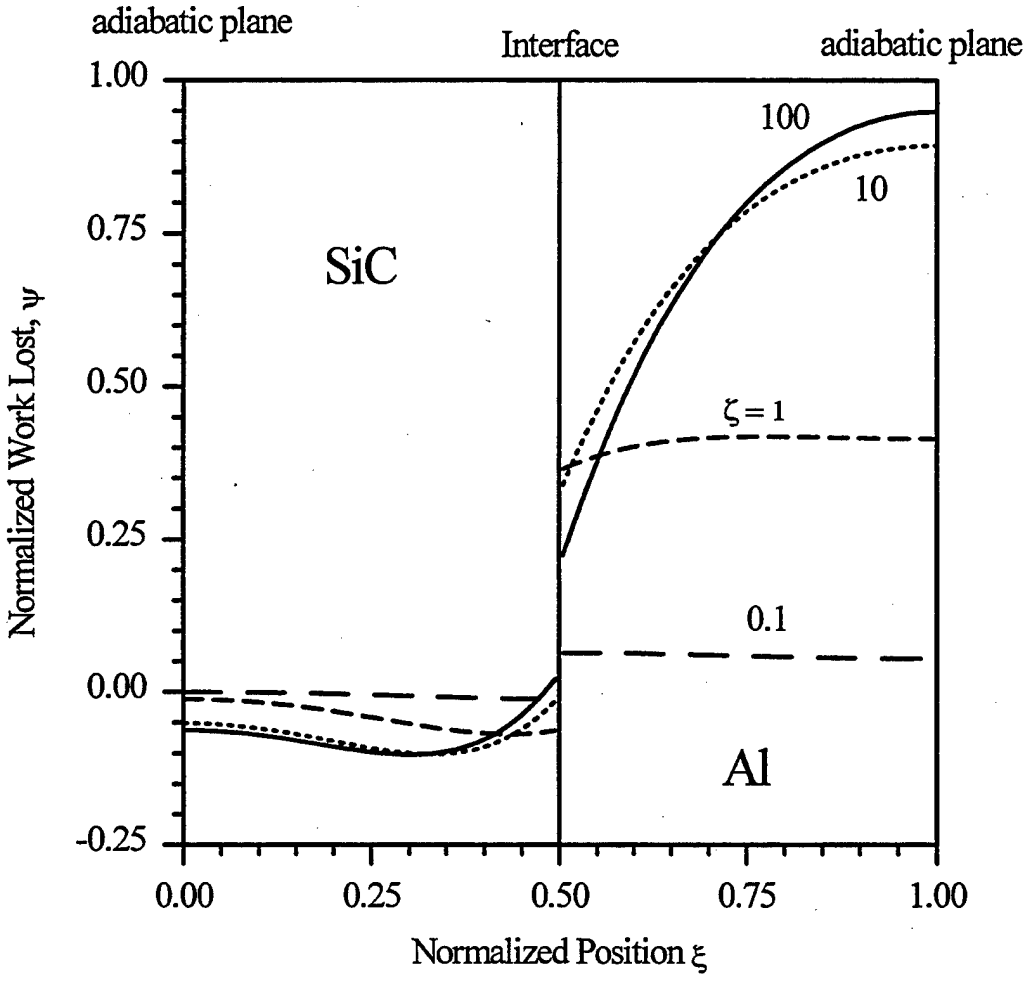

Figure 12. Normalized work lost ψ as a function of the normalized position ξ for problem (1) with an *imperfect* thermal interface, for the composite SiC-Al, for four normalized thermal contact conductances ζ, for a normalized frequency $\Omega_{SiC} = 10$, and for a SiC volume fraction of $V_f = 0.5$.

$$\chi = \frac{\Delta s}{\left((\alpha\sigma_{kk})^2/C\right)_2} \tag{128}$$

A physical feel for the denominator was given in the paragraph containing Eq. (126).

For the case of a thermally *perfect* interface, χ is plotted in Figure 13 versus the normalized position ξ with the normalized frequency Ω_{SiC} as a parameter. Note that the normalization of Δw and Δs was done in such a manner that setting $\psi = \chi$ corresponds to $\Delta w = T_o \Delta s$, i.e., one unit of normalized entropy produced corresponds to one unit of normalized work lost. Accordingly, ψ (Figures 11 and 12) and χ (Figure 13) are plotted on an identical scale. As in Section 3.1.2, pointwise $\psi \neq \chi$ or $\Delta w \neq T_o \Delta s$. As expected the entropy produced is maximum at the interface since the temperature gradients are greatest there (see Figure 8 and Eq. (11)), and is zero at the adiabatic planes, $\xi = 0$ and $\xi = 1$. Figure 14 shows the effect of a thermally imperfect interface on the local entropy produced for $\Omega_{SiC} = 10$. As the interface 'degrades', i.e. ζ decreases, the heat exchange between the slabs decreases, and the entropy production decreases.

The maximum elastic stored energy W per unit volume during a cycle is given by

$$W = \frac{1}{2E}\left[(1+\nu)\sigma_{lmo}\sigma_{lmo} - \nu\sigma_{kko}\sigma_{kko}\right] \tag{129}$$

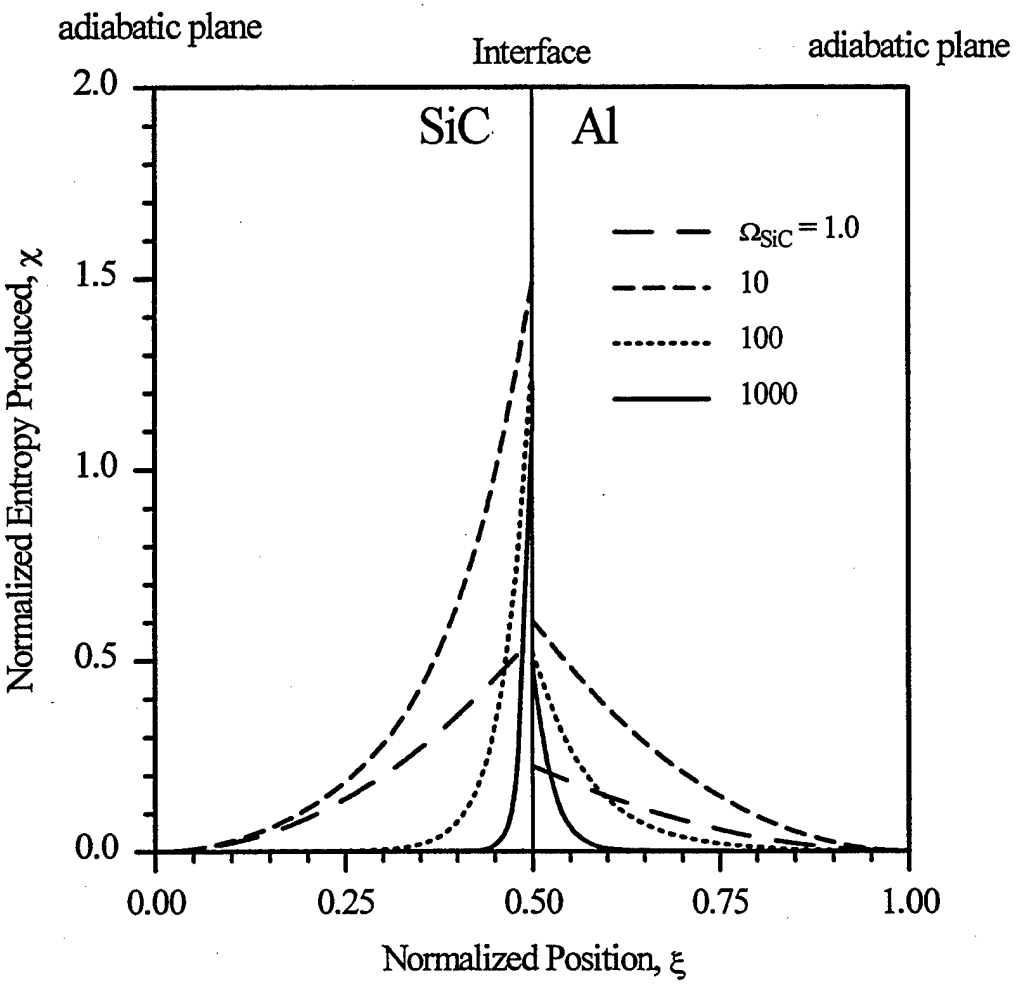

Figure 13. Normalized entropy produced χ as a function of the normalized position ξ for problem (1) with a *perfect* thermal interface, for the composite SiC-Al, for four values of the normalized frequency Ω_{SiC}, and for a SiC volume fraction of $V_f = 0.5$.

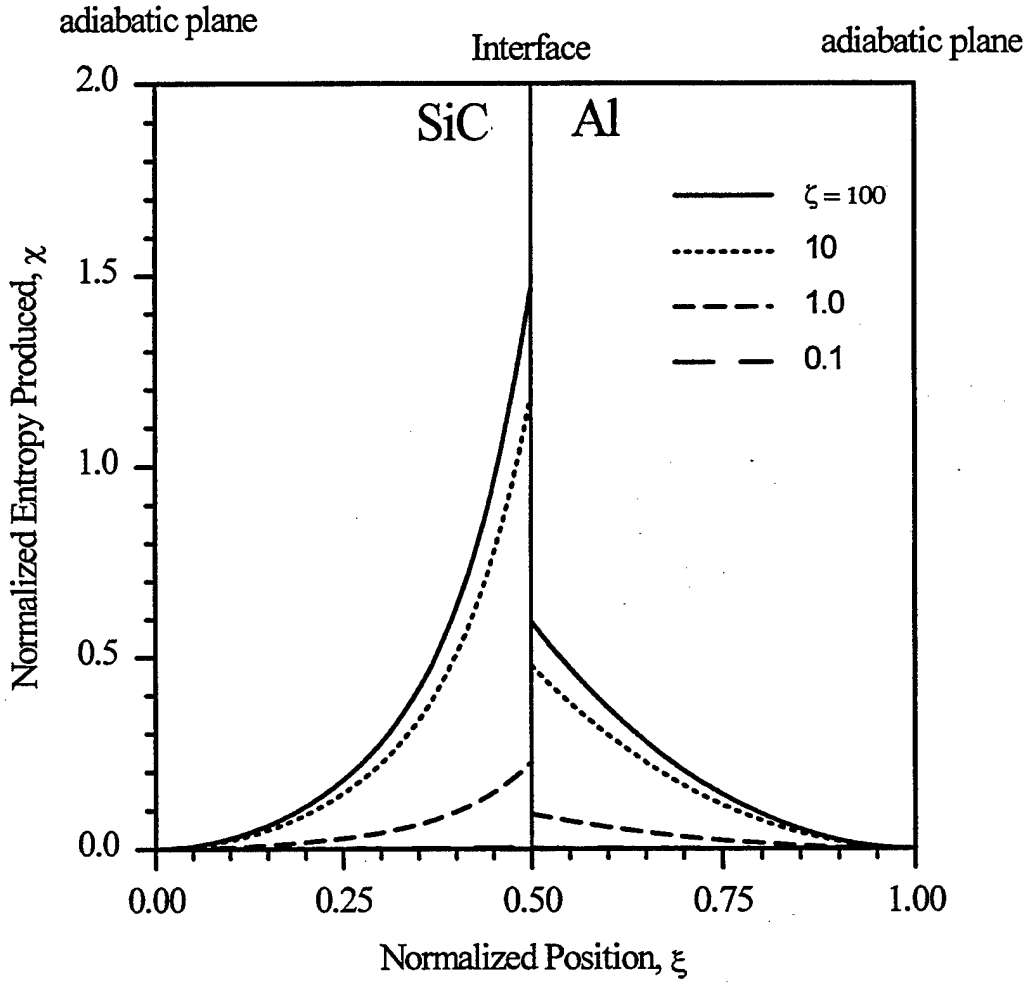

Figure 14. Normalized entropy produced χ as a function of the normalized position ξ for problem (1) with an *imperfect* thermal interface, for the composite SiC-Al, for four normalized thermal contact conductances ζ, for a normalized frequency $\Omega_{SiC} = 10$, and for a SiC volume fraction of $V_f = 0.5$.

where ν is Poisson's ratio. Substituting Eqs. (103) and (129) into Eq. (4) and using the results of this section, the specific damping capacity Ψ averaged over the volume of the unit cell for both problems (1) and (2) is

$$\Psi = \Psi_o \frac{\sum_{n=1}^{\infty} \frac{\Omega_1 \gamma_n^2}{\Omega_1^2 + \gamma_n^4} Q_n}{\frac{a}{b} + \left(1 - \frac{a}{b}\right)\frac{E_1}{E_2} F^2} \tag{130}$$

where $Q_n = R_n\left(I_1 a/b + I_2 F \alpha_2/\alpha_1\right)$. A modulus of elastothermodynamic damping has been defined as $\Psi_o = 2\pi E \alpha^2 T_o / C$. This parameter first appeared in Zener's work (1937) when he analyzed the thermoelastic damping of a homogeneous beam undergoing flexural vibrations. Zener called it the relaxation strength. The damping results of Milligan and Kinra (1993) for a linear inclusion in an infinite matrix were reproduced using the above equation by letting the parameter a/b become sufficiently small for a fixed value of Ω_1.

The damping of the SiC-Al composite with a thermally *perfect* interface is plotted in Figure 15 as a function of Ω_{SiC} for various SiC volume fractions, V_f. The equilibrium temperature T_o has been taken to be 300 K. As $\Omega_{SiC} \to 0$ essentially isothermal conditions are obtained and $\Psi \to 0$. At the other extreme, as $\Omega_{SiC} \to \infty$ essentially adiabatic conditions are obtained and, once again, $\Psi \to 0$. In between these two extremes, the peak damping occurs at a frequency which depends on the volume fraction. The maximum damping is slightly more than 0.5% at $\Omega_{SiC} \approx 10$ and $V_f \approx 0.5$. Now, for a homogeneous medium subjected to a homogeneous stress field, the damping is zero.

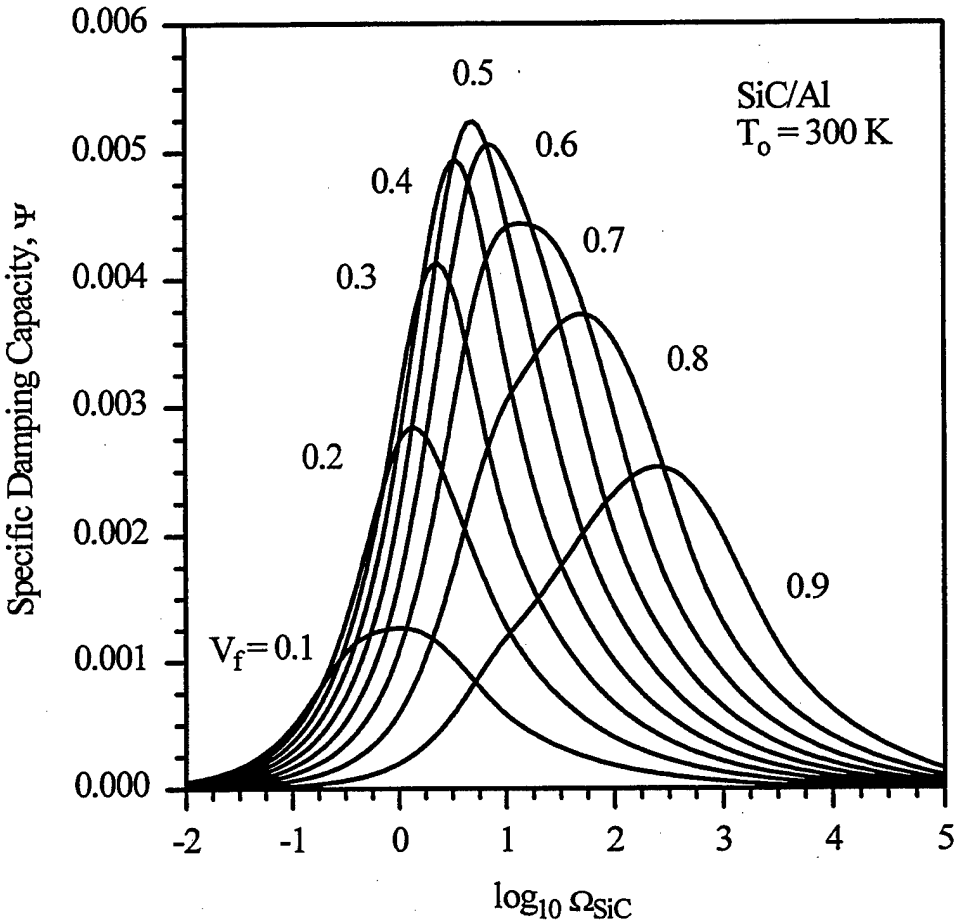

Figure 15. Specific damping capacity Ψ as a function of the normalized frequency Ω_{SiC} for various SiC volume fractions V_f, for the composite SiC-Al, for problem (1) with a thermally *perfect* interface.

Accordingly, in Figure 15 the damping goes to zero for $V_f \to 0$ and $V_f \to 1$ at any frequency. The effect of a thermally *imperfect* interface on the specific damping capacity is shown in Figure 16 for $\Omega_{SiC} = 10$ and $V_f = 0.5$. As expected from the previous discussion, as $\zeta \to 0$ (thermally isolated slabs), $\Psi \to 0$; Ψ increases monotonically with ζ; as $\zeta \to \infty$, Ψ increases to its value for a thermally perfect interface.

Finally, using the Simplex method of multivariable optimization (Press, et al, 1989, pp. 289-293), the optimum damping values for various inclusion materials in an Al, Mg, and Ti matrix, varying V_f and Ω_1, were calculated for both problems (1) and (2). These results are given in Table II. The thermomechanical properties of the materials are given in Table I.

Table 2 Optimum specific damping capacity for problems (1) and (2) with a thermally *perfect* interface for various inclusion and matrix materials, varying inclusion volume fraction V_f and the normalized frequency Ω_1.

	Problem (1)			Problem (2)		
	V_f	Ω_1	Ψ_{max}	V_f	Ω_1	Ψ_{max}
SiC-Al	0.51	5.1	0.0052	0.26	1.9	0.0002
Al_2O_3-Al	0.54	5.3	0.0027	0.27	2.8	0.0030
SiC-Mg	0.50	5.5	0.0074	0.22	1.4	0.0001
Al_2O_3-Mg	0.51	5.7	0.0005	0.22	2.3	0.0003
SiC-Ti	0.57	3.2	0.0008	0.34	0.9	0.0000
Al_2O_3-Ti	0.54	3.8	0.0001	0.37	2.0	0.0008

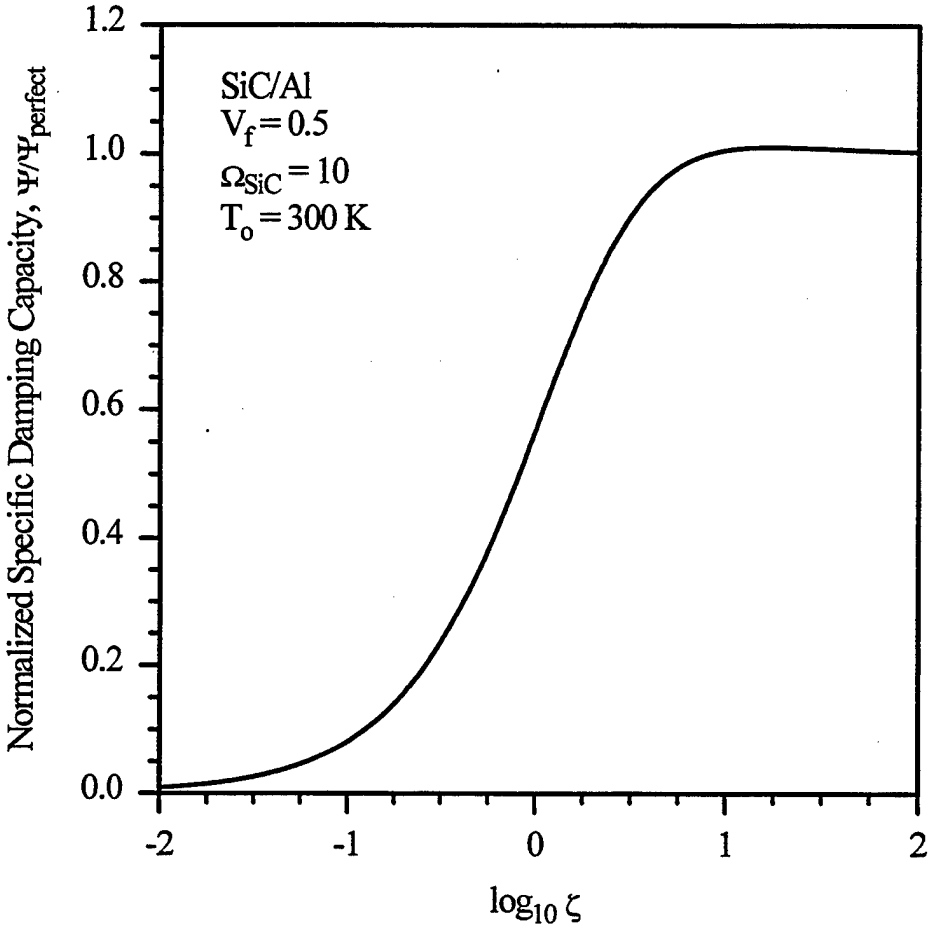

Figure 16. Normalized specific damping capacity $\Psi/\Psi_{perfect}$ as a function of the normalized film coefficient ζ, for problem (1) with a thermally *imperfect* interface, for the composite SiC-Al, for a normalized frequency $\Omega_{SiC} = 10$, and for a SiC volume fraction of $V_f = 0.5$.

3.4.2 Elastothermodynamic Damping in a Symmetric Three-Layer Plate

Consider a symmetric three-layer plate with thermally *perfect* interfaces as shown in Figure 17. In the following, all externally applied loads are assumed to be time-harmonic and in phase with each other, and the factor $e^{i\omega t}$ is implied, as is customary. It is assumed that the deformations in the plate are adequately described by the classical (thin) laminate theory based on the well-known Kirchoff hypothesis (CLT). Since the plate is symmetric in both the material properties and the geometry, there is no coupling between bending and extension. Herein, only bending is considered. Then, given the bending/twisting moments $M_x(x,y)$, $M_y(x,y)$, and $M_{xy}(x,y)$, the curvatures $\kappa_x(x,y)$, $\kappa_y(x,y)$, and $\kappa_{xy}(x,y)$, may be obtained by using the CLT (see Jones, 1975, for example). Our sign convention is that positive moments produce positive curvatures (see Figure 17); it is different from that of Jones (1975). With $\sigma_{zz} = \sigma_{zx} = \sigma_{zy} = 0$, the nonzero stresses are given by

$$\sigma_{xx} = -\frac{E}{1-\nu^2}\left(\kappa_x + \nu\kappa_y\right)z, \quad \sigma_{yy} = -\frac{E}{1-\nu^2}\left(\kappa_y + \nu\kappa_x\right)z, \quad \sigma_{xy} = -\frac{E}{1+\nu}\kappa_{xy}z \tag{131}$$

so that

$$\sigma_{kk} = -\frac{E}{1-\nu}\left(\kappa_x + \kappa_y\right)z \tag{132}$$

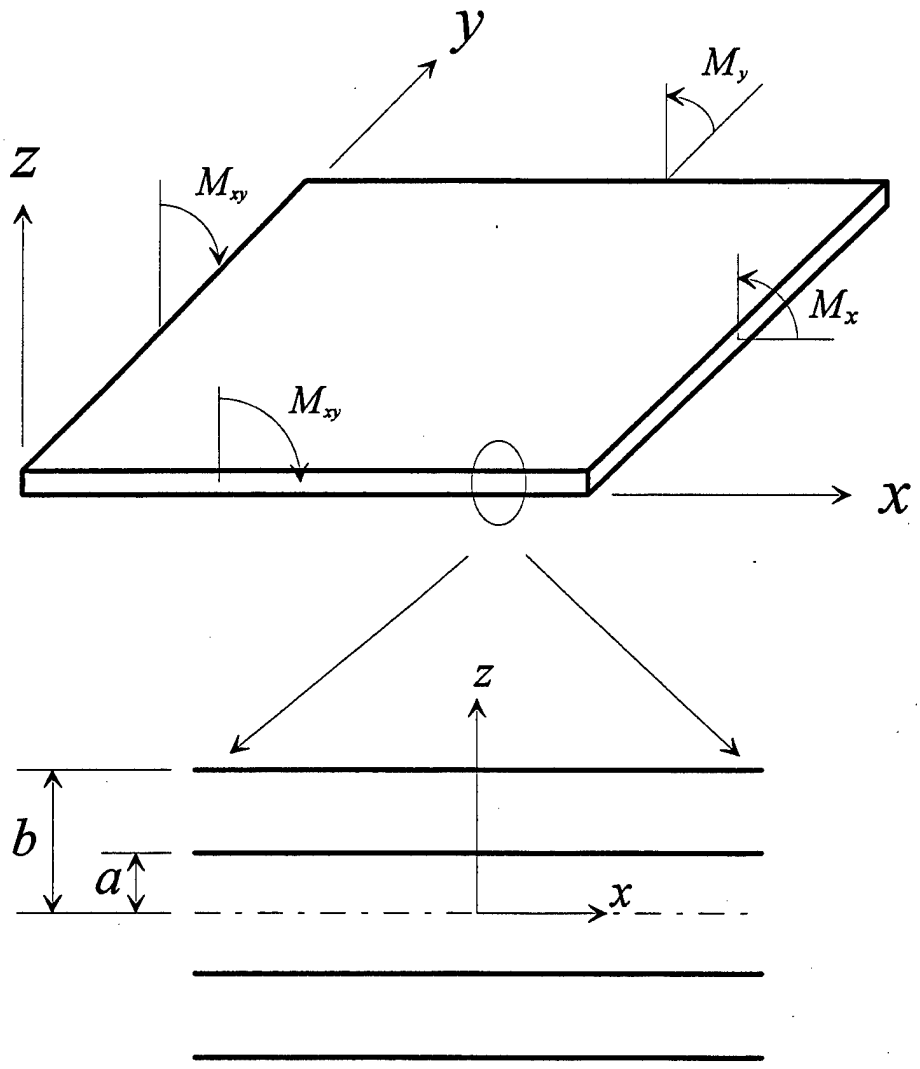

Figure 17. A symmetric three-layer plate with dimensions and moment sign convention.

Note that the hydrostatic stress field, σ_{kk}, is independent of the twist curvature, κ_{xy}, and, therefore, of the twisting moment, M_{xy}. In keeping with the assumptions in the CLT, the gradients of temperature in the x and y directions are very small compared to the gradients in the z-direction. From Eq. (11), the production of entropy depends upon the *square* of these temperature gradients. Therefore, for the purpose of calculating the total damping of the laminate, heat conduction in the x and y directions is neglected.

Note that σ_{kk} in Eq. (132) is an odd function of z. Since the operator in Eq. (15) is symmetric in z, it follows that V is an odd function of z, and $V = 0$ at $z = 0$. Thus, it is sufficient to consider only the upper half of the plate, $z > 0$. In the following the subscript $(\,)_1$ will refer to the inner layer of thickness $2a$, and the subscript $(\,)_2$ will refer to the two outer layers of thickness $(b-a)$; the total thickness of the plate is $2b$ (see Figure 17). The volume fraction of the outer layers is $V_f \equiv 1 - a/b$. Using the method of Ozisik (1980, pp. 294-334), the eigenfunctions for each of the laminae are

$$\phi_{1n}(z) = \sin(\gamma_n z/a) \tag{133}$$

$$\phi_{2n}(z) = A_n \cos(\eta_n z/b) + B_n \sin(\eta_n z/b) \tag{134}$$

where A_n and B_n are

$$A_n = -\frac{K\cos\gamma_n \cos\eta_n}{\sin\left(\eta_n\left(\frac{a}{b}-1\right)\right)}, \quad B_n = -\frac{K\cos\gamma_n \sin\eta_n}{\sin\left(\eta_n\left(\frac{a}{b}-1\right)\right)} \tag{135}$$

and γ_n, η_n, and K were defined in Eq. (112). The transcendental equation for the eigenvalues β_n is

$$\begin{vmatrix} -\sin\gamma_n & \cos(\eta_n a/b) & \sin(\eta_n a/b) \\ K\cos\gamma_n & \sin(\eta_n a/b) & -\cos(\eta_n a/b) \\ 0 & -\sin\eta_n & \cos\eta_n \end{vmatrix} = 0 \tag{136}$$

Using exactly the same procedure as in Section 3.4.1, the specific damping capacity for the three-layer composite plate was found to be

$$\Psi = \Psi_{o1} \frac{\sum_{n=1}^{\infty} \frac{\Omega_1 \gamma_n^2}{\Omega_1^2 + \gamma_n^4} Q_n}{\frac{1}{3}\left[\frac{1-\nu_1}{1+\nu_1}(a/b)^3 \frac{f_1(\kappa)}{f_3(\kappa)} + \frac{E_2}{E_1}\frac{(1-\nu_1)^2}{1-\nu_2^2}\left(1-(a/b)^3\right)\frac{f_2(\kappa)}{f_3(\kappa)}\right]} \tag{137}$$

where the normalized frequency $\Omega_1 = \omega C_1 a^2 / k_1$, and

$$Q_n = \frac{\left[(a/b)^2 I_1 + \frac{E_2}{E_1}\frac{1-\nu_1}{1-\nu_2}\frac{\alpha_2}{\alpha_1} I_2\right]^2}{\frac{a}{b} I_3 + \frac{C_2}{C_1} I_4} \tag{138}$$

$$\begin{aligned} f_j(\kappa) &= \int_{xy}\left[\kappa_x^2 + \kappa_y^2 + 2(1-\nu_j)\kappa_{xy}^2 + 2\nu_j \kappa_x \kappa_y\right] dxdy, \quad j = 1,2 \\ f_3(\kappa) &= \int_{xy}\left(\kappa_x + \kappa_y\right)^2 dxdy \end{aligned} \tag{139}$$

$$I_1 = \frac{1}{\gamma_n^2}\sin(\gamma_n) - \frac{1}{\gamma_n}\cos(\gamma_n)$$

$$I_2 = \frac{1}{\eta_n}\left\{ A_n\left[\frac{1}{\eta_n}\left(\cos(\eta_n) - \cos(\eta_n a/b)\right) + \sin(\eta_n) - \frac{a}{b}\sin(\eta_n a/b)\right] + \right.$$
$$\left. + B_n\left[\frac{1}{\eta_n}\left(\sin(\eta_n) - \sin(\eta_n a/b)\right) - \cos(\eta_n) + \frac{a}{b}\cos(\eta_n a/b)\right]\right\}$$

$$I_3 = \frac{1}{2} - \frac{1}{4\gamma_n}\sin(2\gamma_n)$$

$$I_4 = \frac{1}{2}\left(1 - \frac{a}{b}\right)\left(A_n^2 + B_n^2\right) + \frac{1}{4\eta_n}\left(A_n^2 - B_n^2\right)\left[\sin(2\eta_n) - \sin(2\eta_n a/b)\right]$$
$$- \frac{1}{2\eta_n} A_n B_n\left[\cos(2\eta_n) - \cos(2\eta_n a/b)\right]$$

(140)

The damping of the zinc-steel-zinc composite plate is plotted in Figure 18 as a function of Ω_{steel} for various values of V_f (the volume fraction of zinc), with the curvatures $\kappa_{xy} = 0$, $\kappa_x = \kappa_y = \text{constant}$, and $T_o = 300K$. For a given value of V_f, as $\Omega_{\text{steel}} \to 0$ essentially isothermal conditions are obtained, and $\Psi \to 0$. At the other extreme, as $\Omega_{\text{steel}} \to \infty$, away from the interfaces, essentially adiabatic conditions are obtained, and, once again $\Psi \to 0$. For comparison, Ψ for an uncoated steel plate $\left(V_f = 0.0\right)$ is also shown; the maximum damping is $\Psi_{\max} \cong 0.025$. At a "very small cost" of adding 20% zinc (by volume), $\Psi_{\max}$ increases to 0.055, i.e. by about 100%. When $V_f = 0.4$, $\Psi_{\max} \cong 0.1$, i.e., an increase of about 400%.

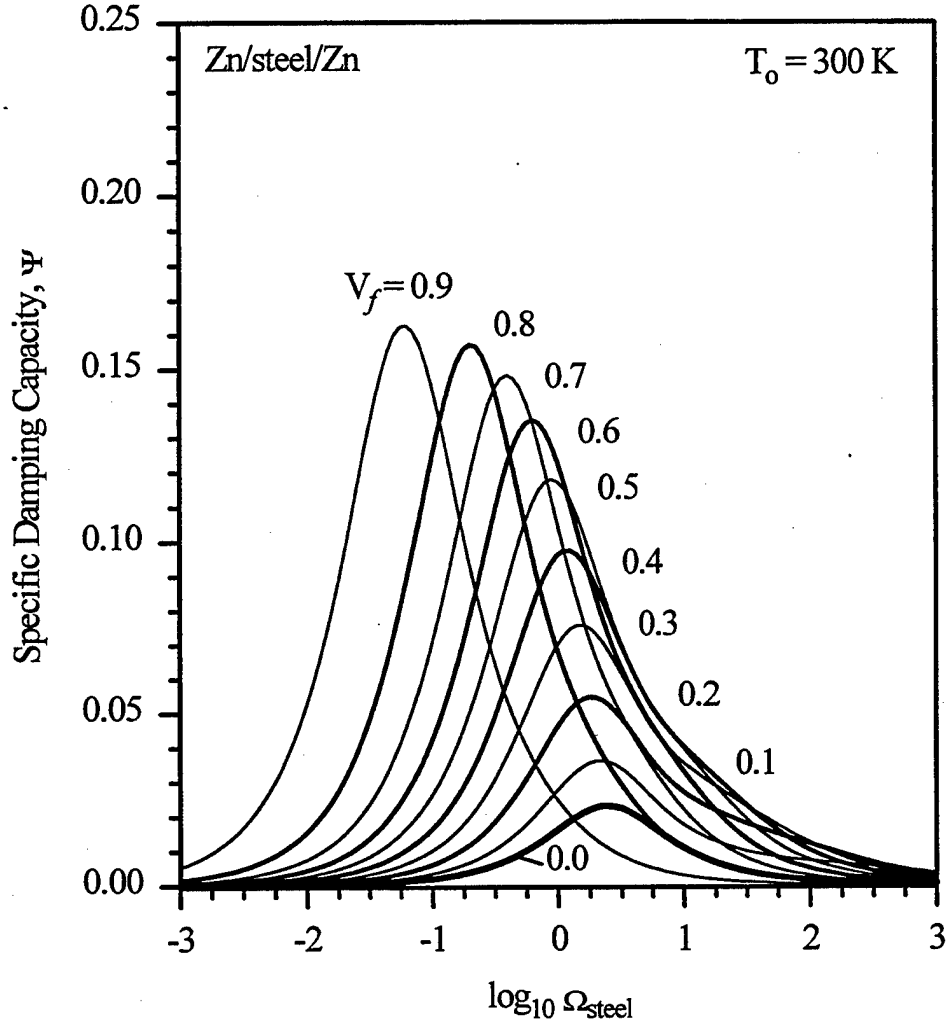

Figure 18. Specific damping capacity Ψ versus the normalized frequency Ω_{steel} for the symmetric three-layer plate zinc-steel-zinc with thermally *perfect* interfaces, for several zinc volume fractions V_f.

The special case of a homogeneous plate may be obtained from Eq. (137) by letting $V_f \to 0$. After some careful analysis, the following result was obtained

$$\Psi = \frac{1+\nu}{1-\nu}\frac{f_3(\kappa)}{f_1(\kappa)}\left[\Psi_o \frac{96}{\pi^4}\sum_{n=0}^{\infty}\frac{1}{(2n+1)^2}\frac{\Omega}{\Omega^2+(2n+1)^4}\right] \tag{141}$$

where an *unsubscripted* normalized frequency has been defined as $\Omega = \omega C(2a)^2/\pi^2 k$, so that the result will be directly comparable to a classic result by Zener (1937). Note that $2a$ is the thickness of the homogeneous plate. The expression in the square brackets in Eq. (141) is precisely the damping of a homogeneous Euler-Bernoulli beam subjected to in-plane bending (Zener, 1937). Thus, the following elegantly simple result follows immediately. For a *homogeneous plate*,

$$\Psi_{\text{plate}} = \lambda \Psi_{\text{beam}} \tag{142}$$

where $\lambda = (1+\nu)f_3(\kappa)/(1-\nu)f_1(\kappa)$. Consider the special case, $\kappa_{xy} = 0$, $\kappa_x = \kappa_y = \text{constant}$, and $\nu = 1/3$; then $\lambda = 3$. Therefore, $\Psi_{\text{plate}} = 3\Psi_{\text{beam}}$, i.e., the damping in a plate subjected to equal biaxial curvatures is three times the damping in a beam subjected to the same curvature in the plane of the beam. Furthermore, if $\kappa_{xy} = \kappa_y = 0$ then $\lambda = 2$, i.e., when subjected to identical curvatures, the plate damping is twice the beam damping. Zener (1937) made a clever observation that the series in Eq. (141) is accurately represented by merely its first term $(n = 0)$, and that $96/\pi^4 = 0.9855 \cong 1$. Then, Eq. (141) reduces to the well-known form for a standard anelastic solid

$$\Psi = \lambda\left[\Psi_o \frac{\Omega}{1+\Omega^2}\right] \tag{143}$$

3.4.3 Elastothermodynamic Damping in a Hollow Two-Layer Concentric Sphere

Consider a random particulate composite reinforced by hollow spheres of outer radius a with the volume fraction of inclusions given by V_f. As a first approximation to the elastothermodynamic damping of such a composite, we calculate the damping in a hollow two-layer concentric sphere with the inclusion occupying the space $h<r<a$ and the matrix occupying the space $a<r<b$ such that $(a/b)^3 = V_f$ as shown in Figure 19. Thus, the volume fraction of the inclusion in the two-layer composite sphere is equal to the volume fraction of inclusions in the random particulate composite. The surfaces $r=h$ and $r=b$ are assumed to be adiabatic and the interface $r=a$ may be thermally *imperfect*. The outer surface $r=b$ is subjected to a time-harmonic radial stress $\sigma_{rr} = \sigma e^{i\omega t}$. Unless otherwise stated, the subscripts $(\,)_1$ and $(\,)_2$ will refer to the inclusion and matrix, respectively.

It is assumed that the frequency of vibration is sufficiently small so that the inertia effects may be neglected and the dynamic stress field may be approximated by the corresponding static stress field times $e^{i\omega t}$. The static elasticity problem may be solved using standard methods (Little, 1973). Interestingly, the hydrostatic stress is constant in the inclusion and the matrix. The pertinent results are

$$\frac{(\sigma_{kk})_2}{(\sigma_{kk})_1} = \frac{K_2}{K_1}\frac{D_2}{D_1} \tag{144}$$

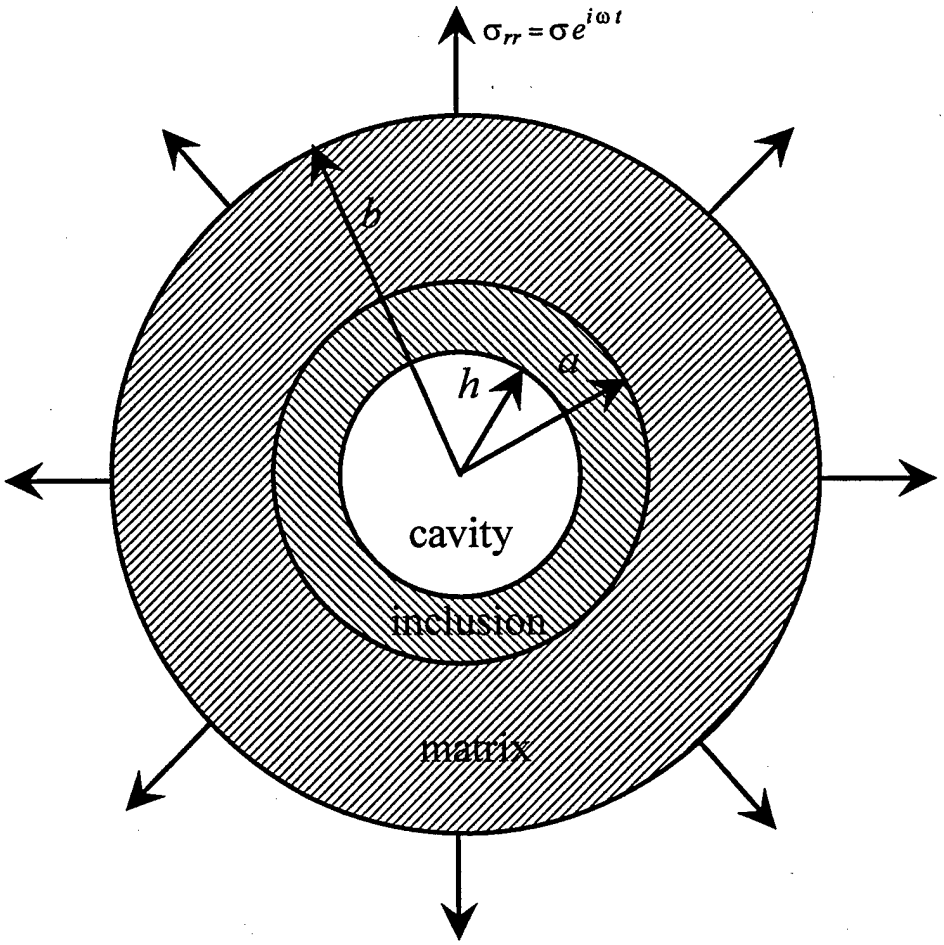

Figure 19. A two-layer concentric hollow sphere with dimensions shown.

$$\frac{\int_R W\,dR}{4\pi/3b^3} = \left[\begin{array}{r}\left(\tfrac{9}{2}K_1D_1^2 + 6\mu_1 D_3^2 (h/a)^3\right)\left(1-(h/a)^3\right)(a/b)^3 + \\ +\left(\tfrac{9}{2}K_2D_2^2 + 6\mu_2 D_4^2 (a/b)^3\right)\left(1-(a/b)^3\right)\end{array}\right] \quad (145)$$

where K is the bulk modulus, μ is the shear modulus, and the constants D_1, D_2, D_3, D_4 are given by

$$D_4 = \frac{\sigma}{\det}\left[1+\frac{4\mu_1}{3K_1}(a/h)^3 - \frac{4\mu_1}{3K_2}\left((a/h)^3-1\right)\right],\ D_3 = \frac{\sigma}{\det}\left(1+\frac{4\mu_2}{3K_2}\right)$$

$$D_2 = \frac{1}{3K_2}\left(4\mu_2(a/b)^3 D_4 + \sigma\right),\ D_1 = \frac{4\mu_1}{3K_1}(a/h)^3 D_3 \quad (146)$$

where

$$\det = -\left[1+\frac{4\mu_1}{3K_1}(a/h)^3\right]4\mu_2\left((a/b)^3-1\right)+\left[1+\frac{4\mu_2}{3K_2}(a/b)^3\right]4\mu_1\left((a/h)^3-1\right) \quad (147)$$

The eigenfunctions for each layer may be determined using the method of Ozisik (1980, pp. 294-334). The eigenfunction for each region is

$$\phi_{1n} = (1/x)\sin(\gamma_n x/a) + B_{1n}(1/x)\cos(\gamma_n x/a) \quad (148)$$

$$\phi_{2n} = A_{2n}(1/x)\sin(\eta_n x/b) + B_{2n}(1/x)\cos(\eta_n x/b) \quad (149)$$

where the constants B_{1n}, A_{2n}, B_{2n} are given by

$$B_{1n} = \frac{-a_{11}}{a_{12}},\quad A_{2n} = \frac{-1}{\Delta}a_{44}\left(a_{12}a_{21}-a_{22}a_{11}\right),\quad B_{2n} = \frac{a_{43}}{\Delta}\left(a_{12}a_{21}-a_{22}a_{11}\right) \quad (150)$$

where $\Delta = a_{12}\left(a_{23}a_{44}-a_{43}a_{24}\right)$, and γ_n, η_n are given by Eq. (112). The transcendental equation for the eigenvalues β_n is

$$\begin{vmatrix} a_{11} & a_{12} & 0 & 0 \\ a_{21} & a_{22} & a_{23} & a_{24} \\ a_{31} & a_{32} & a_{33} & a_{34} \\ 0 & 0 & a_{43} & a_{44} \end{vmatrix} = 0 \tag{151}$$

where the constants a_{ij} , $i, j \in \{1,2,3,4\}$ are given by

$$a_{11} = (\gamma_n h/a)\cos(\gamma_n h/a) - \sin(\gamma_n h/a),\ a_{12} = -(\gamma_n h/a)\sin(\gamma_n h/a) - \cos(\gamma_n h/a)$$

$$a_{21} = (k_1/k_2)(\gamma_n \cos\gamma_n - \sin\gamma_n),\ a_{22} = -(k_1/k_2)(\gamma_n \sin\gamma_n + \cos\gamma_n)$$

$$a_{23} = -(\eta_n a/b)\cos(\eta_n a/b) + \sin(\eta_n a/b)$$

$$a_{24} = (\eta_n a/b)\sin(\eta_n a/b) + \cos(\eta_n a/b)$$

$$a_{31} = (k_1/k_2)(-\gamma_n \cos\gamma_n + \sin\gamma_n) - (fa/k_2)\sin\gamma_n$$

$$a_{32} = (k_1/k_2)(\gamma_n \sin\gamma_n + \cos\gamma_n) - (fa/k_2)\cos\gamma_n$$

$$a_{33} = (fa/k_2)\sin(\eta_n a/b),\ a_{34} = (fa/k_2)\cos(\eta_n a/b)$$

$$a_{43} = \eta_n \cos(\eta_n) - \sin(\eta_n),\ a_{44} = -\eta_n \sin(\eta_n) - \cos(\eta_n) \tag{152}$$

Using exactly the same procedure as in Section 3.4.1 the specific damping capacity for the entire spherical composite was found to be

$$\Psi = \frac{\Psi_{B1} \sum_{n=1}^{\infty} \frac{\Omega_1 \gamma_n^2}{\Omega_1^2 + \gamma_n^4} Q_n}{\frac{1}{27}\left[\begin{array}{l} \frac{1}{2}(a/b)^3\left(1-(h/a)^3\right) + \frac{2}{3}\frac{\mu_1}{K_1}(D_3/D_1)^2(a/b)^3(h/a)^3\left(1-(h/a)^3\right) \\ \frac{K_2}{2K_1}(D_2/D_1)^2\left(1-(a/b)^3\right) + \frac{2\mu_2}{3K_1}(D_4/D_1)^2(a/b)^3\left(1-(a/b)^3\right) \end{array}\right]} \tag{153}$$

where $\Omega_1 = \omega C_1 a^2/k_1$, a modulus of damping for this problem is defined as $\Psi_B = \pi T_o K \alpha^2/C$, and Q_n is defined as

$$Q_n = \frac{\left[(a/b)^2 I_1 + \frac{\alpha_2}{\alpha_1}\frac{(\sigma_{kk})_2}{(\sigma_{kk})_1} I_2\right]^2}{\frac{a}{b} I_3 + \frac{C_2}{C_1} I_4} \tag{154}$$

with

$$I_1 = \frac{1}{\gamma_n}\left\{\left[\frac{1}{\gamma_n}\left(\sin(\gamma_n) - \sin(\gamma_n h/a)\right) - \cos(\gamma_n) + \frac{h}{a}\cos(\gamma_n h/a)\right] + \right.$$
$$\left. + B_{1n}\left[\frac{1}{\gamma_n}\left(\cos(\gamma_n) - \cos(\gamma_n h/a)\right) + \sin(\gamma_n) - \frac{h}{a}\sin(\gamma_n h/a)\right]\right\}$$

$$I_2 = \frac{1}{\eta_n}\left\{A_{2n}\left[\frac{1}{\eta_n}\left(\sin(\eta_n) - \sin(\eta_n a/b)\right) - \cos(\eta_n) + \frac{a}{b}\cos(\eta_n a/b)\right] + \right.$$
$$\left. + B_{2n}\left[\frac{1}{\eta_n}\left(\cos(\eta_n) - \cos(\eta_n a/b)\right) + \sin(\eta_n) - \frac{a}{b}\sin(\eta_n a/b)\right]\right\}$$

$$I_3 = \frac{1}{2}\left(1 - \frac{h}{a}\right)\left(1 + B_{1n}^2\right) + \frac{1}{4\gamma_n}\left(B_{1n}^2 - 1\right)\left[\sin(2\gamma_n) - \sin(2\gamma_n h/a)\right]$$
$$- \frac{1}{2\gamma_n} B_{1n}\left[\cos(2\gamma_n) - \cos(2\gamma_n h/a)\right]$$

$$I_4 = \frac{1}{2}\left(1-\frac{a}{b}\right)\left(A_{2n}^2 + B_{2n}^2\right) + \frac{1}{4\eta_n}\left(B_{2n}^2 - A_{2n}^2\right)\left[\sin(2\eta_n) - \sin(2\eta_n a/b)\right] - \frac{1}{2\eta_n} A_{2n} B_{2n}\left[\cos(2\eta_n) - \cos(2\eta_n a/b)\right] \tag{155}$$

The damping is plotted in Figure 20 for the composite Al_2O_3-Al with a thermally *perfect* interface for various inclusion volume fractions with $h/a = 0$ (solid sphere). Even though the theoretical maximum volume fraction of an actual particulate composite containing spherical inclusions of uniform size is 0.74, the damping is plotted for $V_f > 0.7$ for completeness. The maximum damping is approximately 0.01 for $V_f \approx 0.5$ and $\Omega_1 \approx 30$ (cf. Section 3.4.1, Table 2).

Figure 21 shows the effect of the cavity ratio h/a on the damping of the Al_2O_3-Al composite with a thermally *perfect* interface for $V_f = 0.5$ and several normalized frequencies. The damping of the composite is relatively unaffected by the hollow interior within the range $0 < h/a < 0.5$. The limiting case $h/a = 1$ corresponds to a spherical shell. For this case, since the hydrostatic stress is constant, the thermoelastic effect is homogeneous, and hence there is no conduction of heat. Therefore, the damping is zero.

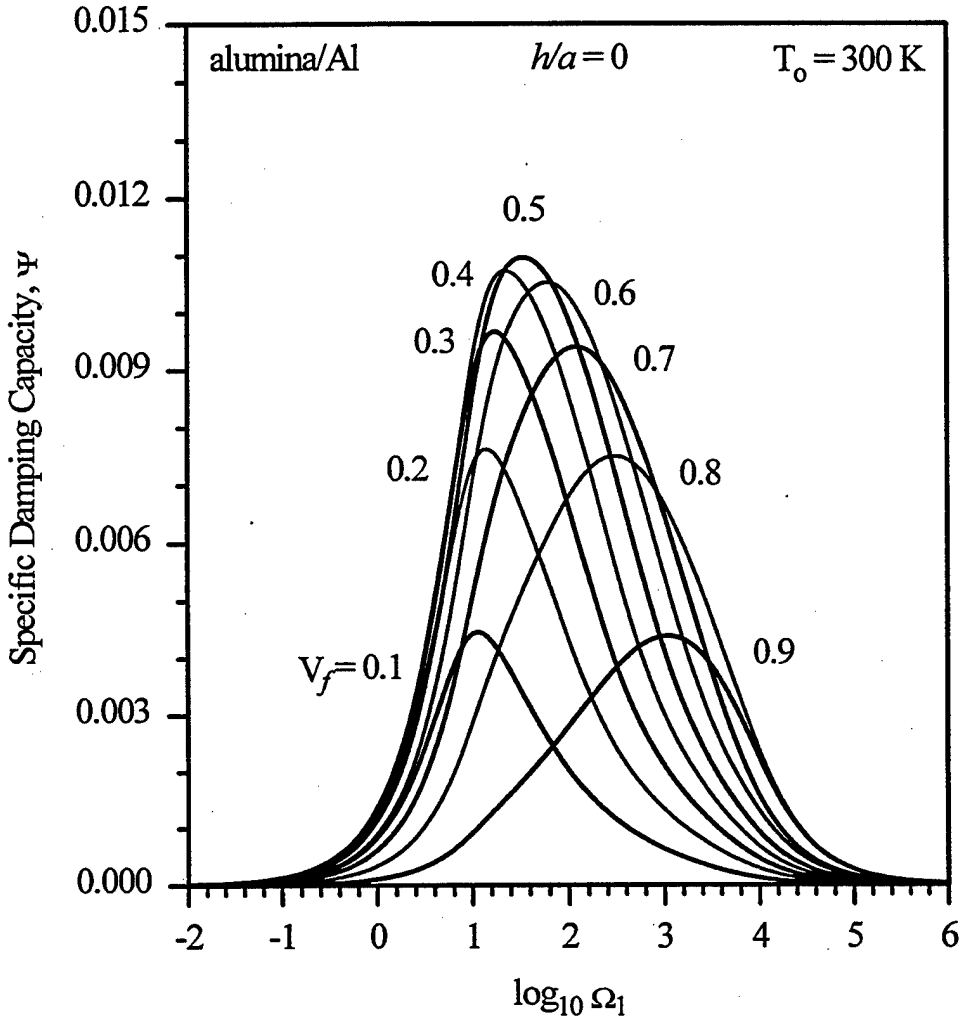

Figure 20. Specific damping capacity Ψ as a function of the normalized frequency Ω_1 for the spherical composite Al_2O_3-Al with a thermally *perfect* interface, for various Al_2O_3 volume fractions V_f, with $h/a = 0$.

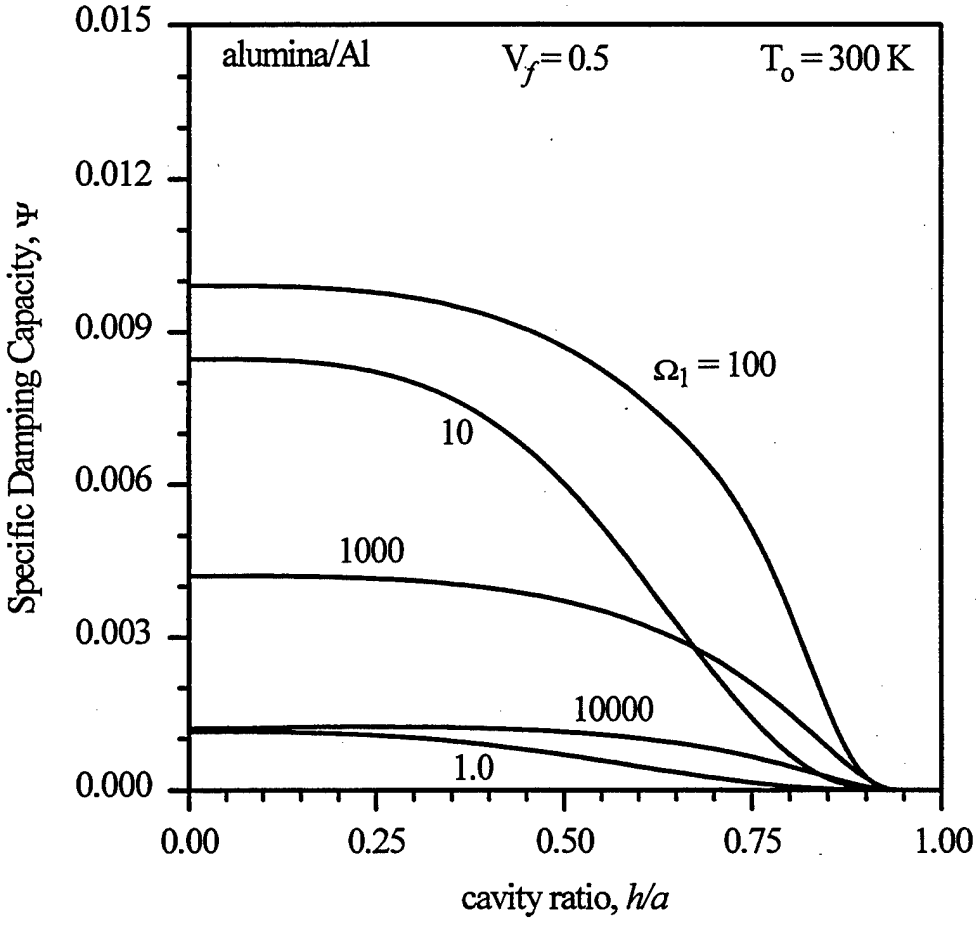

Figure 21. Specific damping capacity Ψ as a function of the cavity ratio h/a for the spherical composite Al_2O_3-Al with a thermally *perfect* interface for various normalized frequencies Ω_1 and $V_f = 0.5$.

Finally, using the Simplex method of multivariable optimization (Press, et al, 1989, pp. 289-293), the optimum damping values for SiC and Al_2O_3 inclusions in an Al, Mg, and Ti matrix, varying V_f and Ω_1 with $h/a = 0$, were calculated. These results are given in Table 3. The thermomechanical properties of the materials are given in Table 1.

Table 3. Optimum specific damping capacity for the composite sphere with a thermally *perfect* interface and $h/a = 0$, for various inclusion and matrix materials, varying volume fraction V_f and the normalized frequency Ω_1.

	V_f	Ω_1	Ψ_{max}
SiC-Al	0.44	36	0.028
Al_2O_3-Al	0.47	32	0.011
SiC-Mg	0.46	46	0.042
Al_2O_3-Mg	0.47	46	0.022
SiC-Ti	0.44	15	0.004
Al_2O_3-Ti	0.44	21	0.000

4. ELASTOTHERMODYNAMIC DAMPING IN CRACKED MEDIA

In this section, a Griffith crack subjected to a *time-harmonic* loading in Modes I, II, and III is considered. An *approximate* analysis is given for the temperature field, the work lost, and the entropy produced in the vicinity of the Griffith crack.

4.1 STRESS FIELD

Consider an infinite plate of an isotropic homogeneous material (in either plane stress or plane strain) containing a Griffith crack occupying the line $-a < x < a,\ y = 0$. It is assumed that the frequency of vibration is sufficiently small (or, alternatively, the wavelength is very large compared to the crack length) so that the inertia effects may be neglected and the dynamic stress field may be approximated by the corresponding static stress field times $e^{i\omega t}$. The hydrostatic component of the static stress field is given by (Westergaard, 1939; Paris and Sih, 1965)

Mode I:
$$\sigma_{kk} = 2\kappa\sigma\,\mathrm{Re}\frac{z}{\sqrt{z^2 - a^2}} \tag{156}$$

Mode II:
$$\sigma_{kk} = 2\kappa\tau\,\mathrm{Im}\frac{z}{\sqrt{z^2 - a^2}} \tag{157}$$

Mode III:
$$\sigma_{kk} = 0 \tag{158}$$

where $z = x + iy$, $\kappa = 1$ for plane stress and $1+\nu$ for plane strain, ν is Poisson's ratio, and σ and τ characterize the stress field at infinity: $\sigma_{11} = \sigma_{22} = \sigma$ and $\sigma_{12} = 0$ for Mode I; $\sigma_{11} = \sigma_{22} = 0$ and $\sigma_{12} = \tau$ for Mode II.

4.2 MODE III

First, the trivial case of Mode III, where σ_{kk} is zero everywhere, is dismissed. Since σ_{kk} is zero everywhere, the thermoelastic effect, Eq. (1), disappears. There are no changes in temperature, no entropy produced and no work converted into heat. Attention is now turned to Modes I and II. Since closed-form solutions were obtained for Mode II but not for Mode I, Mode II results will be given first.

4.3 MODE II

4.3.1 Temperature Field

The governing equation for the fluctuating temperature field is given by Eq. (15),

$$\nabla^2 V - \frac{i\omega C}{k} V + \frac{1}{k} g(\mathbf{x}) = 0 \tag{159}$$

where the inhomogeneous stress term has been written as a heat generation term $g(\mathbf{x})$ given by

$$g(\mathbf{x}) = -(i\omega)\alpha T_o \sigma_{kk}(\mathbf{x}) \tag{160}$$

where $\sigma_{kk}(\mathbf{x})$ is given by Eq. (157). In Mode II $\sigma_{kk}(\mathbf{x})$ is an odd function of x and y. Therefore, with the exception of the crack faces, $-a < x < a$, $y = 0^{\pm}$, $\sigma_{kk} \equiv 0$ on the planes $x = 0$ and $y = 0$. Since the operator in Eq. (159) is

symmetric in x and y, V is an odd function of x and y and, with the exception of the crack faces, $-a < x < a$, $y = 0^{\pm}$, $V \equiv 0$ on $x = 0$ and $y = 0$. The crack faces are taken to be adiabatic, i.e. $\partial V/\partial y = 0$. Therefore, instead of the full plane shown in Figure 22(a) it is sufficient to consider the quarter plane shown in Figure 22(b) with the following thermal boundary conditions

$$\begin{aligned} &(1) \quad V = 0 \quad && x = 0, 0 \le y \le \infty \\ &(2) \quad V = 0 \quad && y = 0, a < x < \infty \\ &(3) \quad \frac{\partial V}{\partial y} = 0 \quad && y = 0^{+}, 0 < x < a \end{aligned} \tag{161}$$

Attempts to obtain an exact solution to this problem led to intractable mathematics. An approximate solution is now developed. Accordingly, a number of assumptions intended to reduce the algebraic effort will be introduced. Once the approximate solution is obtained, the reasonableness of the assumptions introduced en route will be demonstrated.

The temperature field, Eq. (159), is driven by σ_{kk} via the heat generation term, Eq. (160). The rate of entropy production is driven by the *square* of the spatial gradients of temperature, Eq. (11). Sufficiently far away from the crack $\sigma_{kk} \to 0$, $\nabla T \to 0$, and the elastothermodynamic effects (work lost and entropy produced) disappear. Accordingly, attention is focused on the region surrounding the crack. A polar coordinate system (r,θ) is introduced at the right crack tip $z = a$ as shown in Figure 23. In Figure 24 the *exact* σ_{kk} contours are plotted for the region $0 < x < 2a$, $0 < y < a$, and in Figure 25 the *exact* σ_{kk} is plotted as solid lines for $0 < r < a$ and $\theta = 0, \pi/4, \pi/2, 3\pi/4, \pi$.

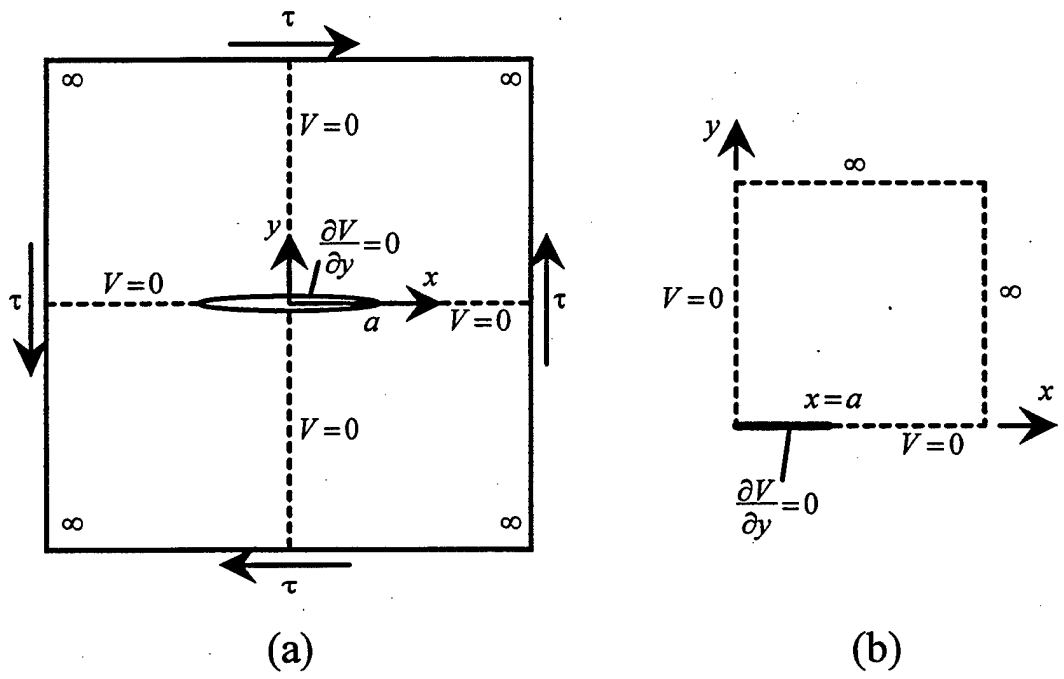

Figure 22. (a) A Griffith crack of length $2a$ in Mode II loading with a rectangular coordinate system (x,y). The crack faces are assumed to be adiabatic. Because σ_{kk} is an odd function of x and y, $V=0$ on $x=0$, and on $y=0$ except on the crack faces. (b) The reduced quarter-plane heat-conduction problem.

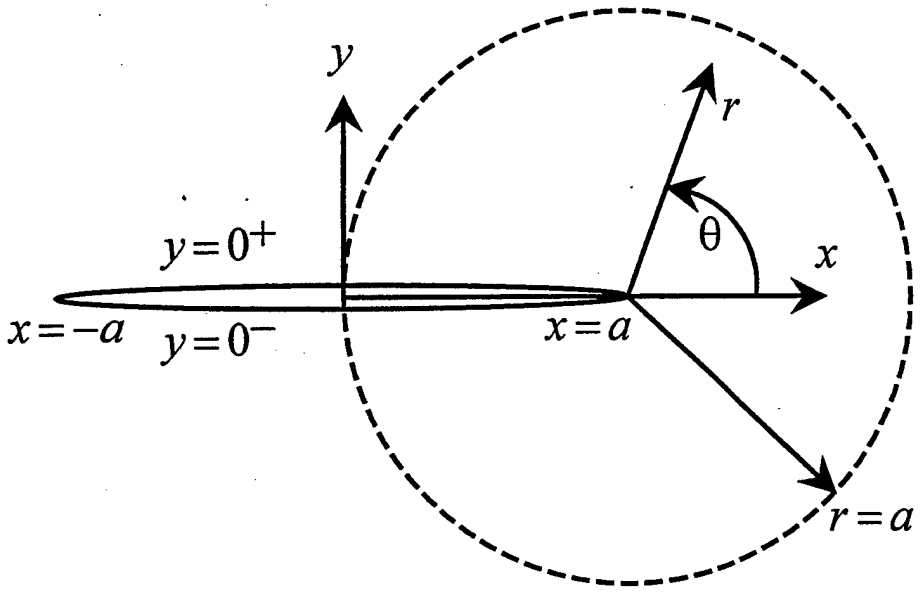

Figure 23. A Griffith crack with a polar coordinate system (r,θ) at the crack tip.

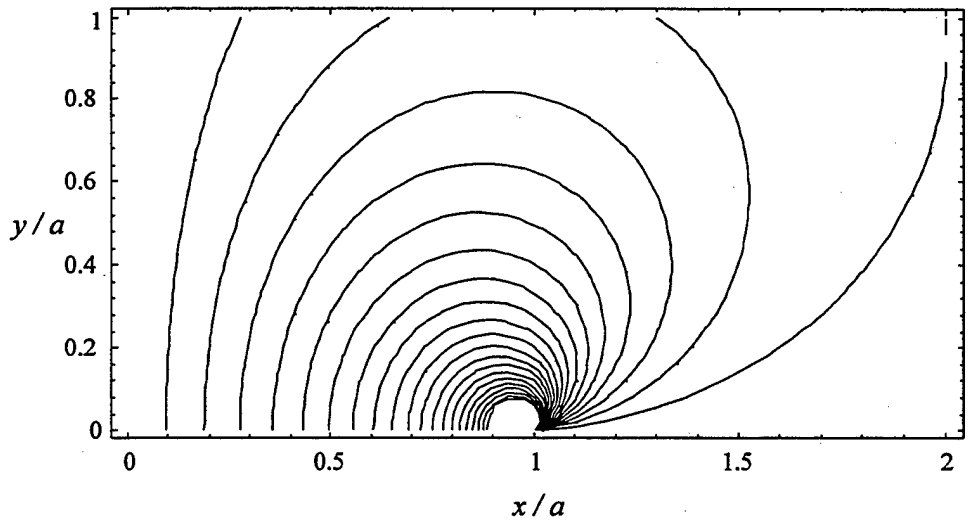

Figure 24. Mode II normalized hydrostatic stress contours, $\sigma_{kk}/\kappa\tau$. ($x/a = 1$ corresponds to the right crack tip. The full field may be constructed by using the odd symmetry of the problem. The range of the contours is –0.1 (lower left) to –2.0 (left of crack tip) with increments of –0.1.)

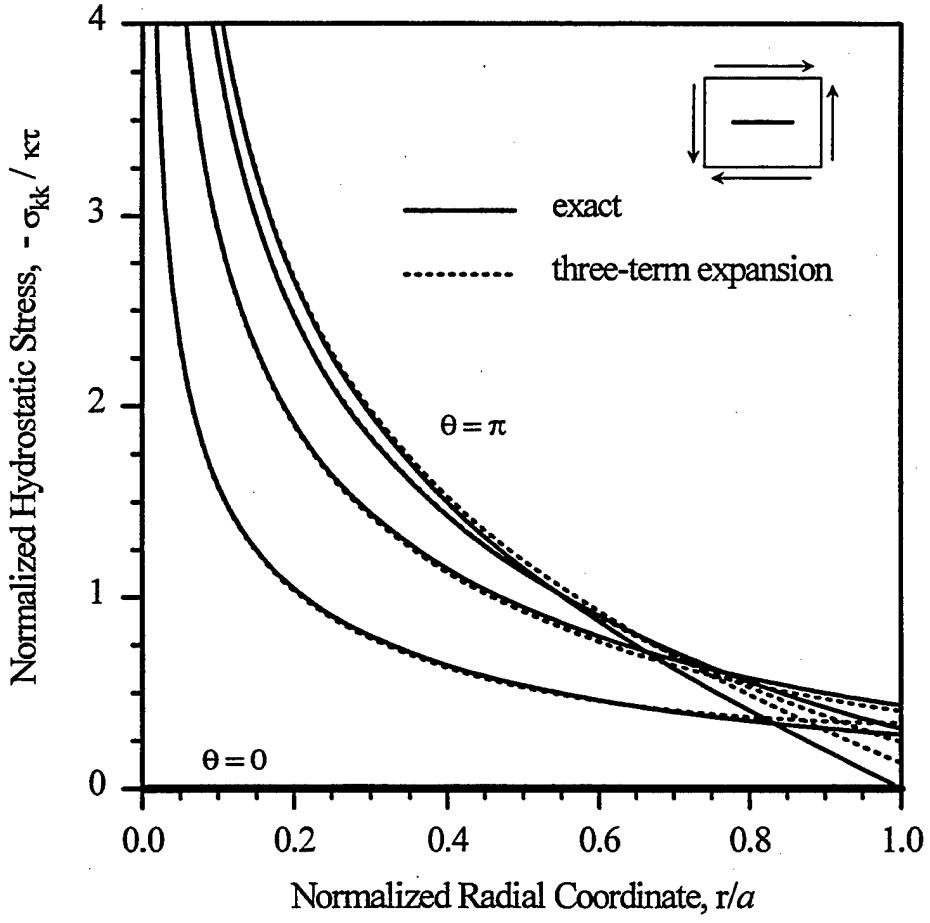

Figure 25. Comparison between the exact σ_{kk} and its three-term expansion for $\theta = 0, \pi/4, \pi/2, 3\pi/4, \pi$. Mode II.

For a positive applied shear stress, the hydrostatic stress field in the first quadrant ($x>0, y>0$) is compressive; accordingly, in Figure 25 *negative* σ_{kk} has been plotted. Moreover, the Griffith crack causes a mode conversion of the remotely applied pure shear stress ($\sigma_{kk} \equiv 0$) to a hydrostatic stress field near the crack. As expected on the basis of symmetry, $\sigma_{kk} \equiv 0$ on the ray $\theta = 0$, and $\sigma_{kk} = 0$ at the point $r = a$, $\theta = \pi$ ($x = y = 0$). By virtue of the fact that σ_{kk} is an odd function of x, for $\theta = \pi$, as r increases from a to $2a$ ($-a < x < 0$) σ_{kk} increases from zero to plus-infinity. (It is for this reason that, in the next paragraph, our Laurent series expansion of σ_{kk} will be limited to $r < a$.) Thus, in Mode II the Griffith crack localizes the hydrostatic stress field to the region between the crack tips. Later it will be shown that the exact opposite is true for Mode I: the Griffith crack localizes the hydrostatic stress field to the region exterior to the crack tips.

Next, an approximation to σ_{kk} is constructed. Eq. (157) was expanded into a Laurent series in $z/2a$ about the tip $z = a$. In linear elastic fracture mechanics (LEFM), a characterization of the crack-tip stress field is generally considered adequate. This is not the case here. Here, interest is in the conversion of mechanical energy into heat throughout the plate due to the presence of a crack. A solution is sought that is valid in as large a region surrounding the crack as possible. Accordingly, one-, two-, three-, and four-term expansions were compared with the exact σ_{kk}. The expansion was limited to the disk $r < a$, $-\pi < \theta < \pi$. It was found that the four-term expansion is not a significant improvement over the three-term expansion (Essentially, the error changes sign). Furthermore, retaining each additional

term entails a significant amount of additional algebraic effort. Therefore, the series was truncated at three terms. In the disk $0<r/a<1$, $-\pi<\theta<\pi$, the exact σ_{kk} given by Eq. (157) will be approximated by

$$\sigma_{kk}=2\kappa\tau\left[\frac{-1}{2}\sin(\theta/2)\sqrt{\frac{2a}{r}}+\frac{3}{4}\sin(\theta/2)\sqrt{\frac{r}{2a}}-\frac{5}{16}\sin(3\theta/2)\left(\frac{r}{2a}\right)^{3/2}\right] \qquad \begin{matrix}0<r<a\\ -\pi<\theta<\pi\end{matrix} \tag{162}$$

This approximate σ_{kk} is compared with the exact σ_{kk} in Figure 25. The comparison is considered a good engineering approximation. (At the risk of stating the obvious, outside the disk $r=a$, Eq. (162) is a poor approximation to Eq. (157). For example, as noted earlier, on $\theta=\pi$, $a<r<2a$, the exact σ_{kk} increases from zero to plus infinity whereas the approximate $\sigma_{kk}\to(9/8)\kappa\tau$.)

Next, approximations to the heat-conduction problem shown in Figure 22(b) are considered. A normalized frequency Ω and a diffusion length l are introduced as

$$\Omega=\omega Ca^2/k\,, \qquad l=\sqrt{2k/\omega C} \tag{163}$$

so that $\Omega=2(a/l)^2$ or $l=a(2/\Omega)^{1/2}$. A "physical feel" for the diffusion length may be obtained as follows. Consider a semi-infinite rod occupying $0\le x<\infty$ at an equilibrium temperature T_o, subjected to a time-harmonic temperature $V=V_o e^{i\omega t}$ at the end $x=0$. In the interior the temperature variation is given by $V(x)=V_o\exp(-(1+i)x/l)$. Thus, at $x=l$, $|V/V_o|=1/e$, and so on. Returning to the problem at hand, observe that the source term $g(\mathbf{x})$ in Eq. (159) is square-root singular at the crack tip. When l is comparable to the

half-crack length a, $\Omega = O(1)$, a strong thermal interaction between the crack tip and the isothermal wall at $x = 0$ is anticipated. In order to capture this physics one must obtain the exact solution; the approximate solution will not do that. Suppose Ω is large compared to one, say $\Omega \geq 10$, then $(a/l) \geq 2.24$. Therefore, a rather weak interaction between the crack tip and the isothermal wall at $x = 0$ is anticipated. In the following it is assumed that there is *no* interaction between the crack tip and the wall at $x = 0$. This allows for the construction of a much simpler heat-conduction problem *associated* with the actual heat-conduction problem shown in Figure 22(b). Appropriately, it will be called the "associated heat-conduction problem"; this is shown in Figure 26. Since the wall is "thermally unaware" of the crack tip at $x = a$, it can be moved from $x = 0$ to $x = -\infty$ with impunity; concurrently, the adiabatic line $0 < x < a$ stretches out to the adiabatic line $-\infty < x < a$.

Attention is now turned to the heat generation term $g(r,\theta)$. In the interior of the half-disk, $r < a$, $0 \leq \theta \leq \pi$, $g(r,\theta)$ for the associated problem is taken to be that given by the three-term expansion, Eqs. (160) and (162). Returning to Figure 25, at $r = a$, σ_{kk} is rather small; more significantly, the gradients of σ_{kk} are small. Therefore, in the associated problem we set $g(r,\theta) \equiv 0$ in $a \leq r < \infty$, $0 \leq \theta \leq \pi$. Once the solution to the associated problem is obtained, the solution in the left quarter-plane, $x < 0$, $y > 0$ will be immediately discarded. The solution in the right quarter plane, $x > 0$, $y > 0$, will be taken to be the solution for the actual problem shown in Figure 22(b). As noted earlier, the solution in the full plane, Figure 22(a), can be readily

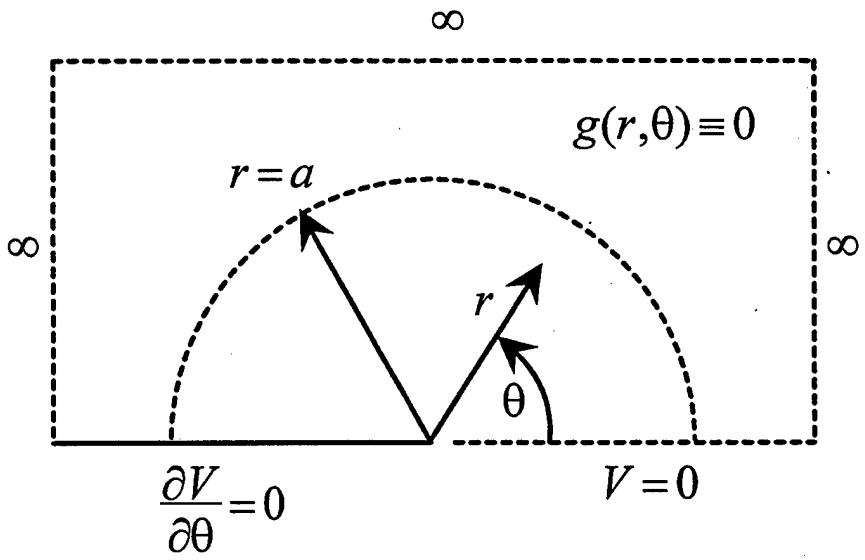

Figure 26. The "associated heat conduction problem" with zero heat generation outside the disk of radius *a*. Mode II.

constructed using the symmetries in σ_{kk} and V. Finally, it is intuitively obvious that as Ω becomes very large, i.e. as the diffusion length becomes very small compared to the crack length, the approximate solution will become increasingly more accurate.

The associated heat-conduction problem is given by

$$\frac{\partial^2 V}{\partial r^2}+\frac{1}{r}\frac{\partial V}{\partial r}+\frac{1}{r^2}\frac{\partial^2 V}{\partial \theta^2}-\frac{C}{k}i\omega V+\frac{1}{k}g(r,\theta)=0,\quad 0\le\theta\le\pi,\ 0<r<\infty \tag{164}$$

$$\begin{aligned} &V=0 \quad \text{at} \quad \theta=0,\quad 0<r<\infty \\ &\frac{\partial V}{\partial \theta}=0 \quad \text{at} \quad \theta=\pi,\quad 0<r<\infty \end{aligned} \tag{165}$$

where

$$g(r,\theta)=\begin{cases} -(i\omega)\alpha T_o\,\sigma_{kk}(r,\theta) & 0\le\theta\le\pi,\ 0<r\le a \\ 0 & 0\le\theta\le\pi,\ a<r<\infty \end{cases} \tag{166}$$

Next, an exact solution to the associated heat-conduction problem is obtained. An integral transform-inversion formula is first developed to remove the θ-variable in Eq. (164). It is assumed that the fluctuating temperature field $V(r,\theta)$ may be represented in the form

$$V(r,\theta)=\sum_{n=0}^{\infty} C_n(r)\sin((n+1/2)\theta) \tag{167}$$

where the $\sin((n+1/2)\theta)$ are the eigenfunctions arising from solving the corresponding homogeneous heat conduction problem. Multiplying Eq. (167) by $\sin((m+1/2)\theta)$ and integrating from 0 to π with respect to θ yields

$$C_n(r)=\frac{2}{\pi}\tilde{V}(r) \tag{168}$$

where the integral transform of V is defined as

$$\tilde{V}(r) = \int_0^{\pi} V(r,\theta)\sin\left((n+1/2)\theta\right) d\theta \tag{169}$$

The inversion formula is obtained by substituting Eq. (168) into Eq. (167) yielding

$$V(r,\theta) = \frac{2}{\pi}\sum_{n=0}^{\infty}\tilde{V}(r)\sin((n+1/2)\theta) \tag{170}$$

Next, taking the integral transform of Eq. (164), integrating the θ-derivative term by parts, and using the boundary conditions Eq. (165) results in

$$\frac{\partial^2\tilde{V}}{\partial r^2} + \frac{1}{r}\frac{\partial\tilde{V}}{\partial r} - \left(\frac{C}{k}i\omega + \frac{(n+1/2)^2}{r^2}\right)\tilde{V} = -\frac{1}{k}\tilde{g}(r), \quad 0 < r < \infty \tag{171}$$

where the transform of the heat generation term, $\tilde{g}(r)$, is given by

$$\tilde{g}(r) = \begin{cases} -(i\omega)\alpha T_o \kappa\tau\dfrac{\pi\sqrt{2}}{2}\left[\left(\dfrac{-1}{\sqrt{r/a}} + \dfrac{3}{4}\sqrt{r/a}\right)\delta_{n0} - \left(\dfrac{5}{32}(r/a)^{3/2}\right)\delta_{n1}\right] & 0 < r \le a \\ 0 & a < r < \infty \end{cases} \tag{172}$$

where $\delta_{n0} = 0$ for $n \neq 0$, $\delta_{n0} = 1$ for $n = 0$, and similarly $\delta_{n1} = 0$ for $n \neq 1$, $\delta_{n1} = 1$ for $n = 1$. Eq. (171) is an inhomogeneous modified Bessel's equation of order $(n+1/2)$. Two independent solutions to the homogeneous equation are $I_{(n+1/2)}\left(\sqrt{i\Omega}\, r/a\right)$ and $K_{(n+1/2)}\left(\sqrt{i\Omega}\, r/a\right)$, where $I_{(n+1/2)}$ is the modified Bessel function of the first kind of order $(n+1/2)$, and $K_{(n+1/2)}$ is the modified Bessel function of the second kind of order $(n+1/2)$ (McLachlan, 1955);

recall $\Omega = \omega a^2/D$. Equation Eq. (171) may be solved using the method of Green's function (Arfken, 1985) or equivalently, the method of variation of parameters (Boyce and DiPrima, 1986) resulting in

$$\tilde{V}(r) = K_{(n+1/2)}\left(\sqrt{i\Omega}\, r/a\right)\int_0^{r/a} u\, I_{(n+1/2)}\left(\sqrt{i\Omega}\, u\right)\left(a^2\tilde{g}(u)/k\right)du + \\ + I_{(n+1/2)}\left(\sqrt{i\Omega}\, r/a\right)\int_{r/a}^{\infty} u\, K_{(n+1/2)}\left(\sqrt{i\Omega}\, u\right)\left(a^2\tilde{g}(u)/k\right)du \tag{173}$$

Substituting Eq. (172) into Eq. (173) and the result into Eq. (170) gives

$$\Theta(r,\theta) = -\sqrt{2}\, i\Omega\left\{\sin(\theta/2)\left[K_{1/2}\left(\sqrt{i\Omega}\, r/a\right)\int_0^{r/a} I_{1/2}\left(u\sqrt{i\Omega}\right)\left(-\sqrt{u}+\tfrac{3}{4}u^{3/2}\right)du + \right.\right. \\ \left. + I_{1/2}\left(\sqrt{i\Omega}\, r/a\right)\int_{r/a}^{1} K_{1/2}\left(u\sqrt{i\Omega}\right)\left(-\sqrt{u}+\tfrac{3}{4}u^{3/2}\right)du\right] + \\ \sin(3\theta/2)\left[K_{3/2}\left(\sqrt{i\Omega}\, r/a\right)\int_0^{r/a} I_{3/2}\left(u\sqrt{i\Omega}\right)\left(-\tfrac{5}{32}u^{5/2}\right)du + \right. \\ \left.\left. + I_{3/2}\left(\sqrt{i\Omega}\, r/a\right)\int_{r/a}^{1} K_{3/2}\left(u\sqrt{i\Omega}\right)\left(-\tfrac{5}{32}u^{5/2}\right)du\right]\right\} \\ \text{for } 0 < r \le a,\ 0 \le \theta \le \pi. \tag{174}$$

where a normalized fluctuating temperature Θ for Mode II has been introduced as $\Theta = V/\left(\tau\kappa T_o\alpha/C\right)$. (A physical feel for the denominator may be developed as follows. If a rod is subjected to a uniaxial tension of magnitude τ under adiabatic conditions, it will cool by an amount $\tau T_o\alpha/C$.) The Bessel functions appearing in Eq. (174) are of half-integer order and may be expressed in terms of elementary functions as follows (Abramowitz and Stegun, 1970)

$$I_{1/2}(z)=\sqrt{\frac{2}{\pi z}}\sinh(z),\quad K_{1/2}(z)=\sqrt{\frac{\pi}{2z}}\exp(-z)$$
$$I_{3/2}(z)=\sqrt{\frac{2}{\pi z}}\left[\cosh(z)-\frac{1}{z}\sinh(z)\right],\quad K_{3/2}(z)=\sqrt{\frac{\pi}{2z}}\left(1+\frac{1}{z}\right)e^{-z} \tag{175}$$

The integrals appearing in Eq. (174) were calculated explicitly and are given by

$$\int_0^{r/a} I_{1/2}\left(u\sqrt{i\Omega}\right)\left(-\sqrt{u}+\tfrac{3}{4}u^{3/2}\right)du=$$
$$=\sqrt{\frac{2}{\pi}}\frac{1}{(i\Omega)^{3/4}}\left[1+\left(\frac{3}{4}\frac{r}{a}-1\right)\cosh\left(\sqrt{i\Omega}\,r/a\right)-\frac{3}{4\sqrt{i\Omega}}\sinh\left(\sqrt{i\Omega}\,r/a\right)\right]$$

$$\int_{r/a}^1 K_{1/2}\left(u\sqrt{i\Omega}\right)\left(-\sqrt{u}+\tfrac{3}{4}u^{3/2}\right)d\xi=$$
$$=\sqrt{\frac{\pi}{2}}\frac{1}{(i\Omega)^{3/4}}\left[\left(\frac{1}{4}-\frac{3}{4}\frac{1}{\sqrt{i\Omega}}\right)e^{-\sqrt{i\Omega}}+\left(-1+\frac{3}{4}\frac{r}{a}+\frac{3}{4\sqrt{i\Omega}}\right)e^{-\sqrt{i\Omega}\,r/a}\right]$$

$$\int_0^{r/a} I_{3/2}\left(u\sqrt{i\Omega}\right)\left(u^{5/2}\right)du=$$
$$=\sqrt{\frac{2}{\pi}}\frac{1}{(i\Omega)^{3/4}}\left[-\frac{3}{\sqrt{i\Omega}}\frac{r}{a}\cosh\left(\sqrt{i\Omega}\,r/a\right)+\left(\left(\frac{r}{a}\right)^2+\frac{3}{i\Omega}\right)\sinh\left(\sqrt{i\Omega}\,r/a\right)\right]$$

$$\int_{r/a}^1 K_{3/2}\left(u\sqrt{i\Omega}\right)\left(u^{5/2}\right)du=$$
$$=\sqrt{\frac{\pi}{2}}\frac{1}{(i\Omega)^{3/4}}\left[\left(\left(\frac{r}{a}\right)^2+\frac{3}{i\Omega}\left(1+\sqrt{i\Omega}\frac{r}{a}\right)\right)e^{-\sqrt{i\Omega}\,r/a}-\left(1+\frac{3}{i\Omega}\left(1+\sqrt{i\Omega}\right)\right)e^{-\sqrt{i\Omega}}\right] \tag{176}$$

Next, the crack-tip temperature field is examined. For a finite Ω (finite l), expanding Eq. (174) about $r = 0$ and retaining only the first term yields

$$\Theta = A(\Omega)\sqrt{\frac{r}{a}}\sin(\theta/2), \qquad r << l \tag{177}$$

where the complex function $A(\Omega)$ is given by

$$A(\Omega) = \left[-\sqrt{2i\Omega}\left(e^{-\sqrt{i\Omega}} - 1\right)\right] + \left[\frac{3\sqrt{2}}{4}\left(e^{-\sqrt{i\Omega}}\left(\sqrt{i\Omega} + 1\right) - 1\right)\right] \tag{178}$$

The two bracketed terms correspond, respectively, to the first $\left(1/\sqrt{r}\right)$ and second $\left(\sqrt{r}\right)$ terms of σ_{kk} in Eq. (162); the third term $\left(r^{3/2}\right)$ does not contribute to $A(\Omega)$. Moreover, a careful examination of the complete series expansion of σ_{kk} revealed that the contribution to $A(\Omega)$ of all higher-order terms ($r^{5/2}$ and higher) is also zero. Now suppose for a moment that the thermal conductivity is zero, then from Eq. (1), $\Theta = \left(-\sigma_{kk}/\kappa\tau\right)$, i.e., together with σ_{kk} the temperature is also square-root singular at the crack tip. In this context, it is a remarkable observation that for any $k > 0$, however small, the temperature at the crack tip is zero at all frequencies, Eq.(177).

Next, the high-frequency behavior of the crack-tip temperature field is considered. Intuitively, as Ω becomes very large ($l << a$), it is expected that the elastothermodynamic effects will become increasingly localized near the crack tip. It is expected that the crack-tip solution will become independent of a. As $\Omega \to \infty$, the second bracketed term in Eq. (178), which corresponds to the second $\left(\sqrt{r}\right)$ term of σ_{kk}, Eq. (162), vanishes, and $A(\Omega) \to \sqrt{2i\Omega}$. Equation Eq. (177) reduces to

$$\Theta = \sqrt{2i\Omega}\sqrt{\frac{r}{a}}\sin(\theta/2), \qquad r << l << a \tag{179}$$

It is important to observe that Θ in Eq. (179) corresponds only to the square-root singular stress field in Eq. (162). In LEFM it is customary to work with dimensional quantities, e.g., K_{II}. Accordingly, Eq. (179) is written in a dimensional form as

$$V(r,\theta) = T_o e^{i\pi/4}\frac{\kappa}{\pi}\frac{\alpha}{\sqrt{kC}}\sqrt{\omega}K_{II}\sqrt{2\pi r}\sin(\theta/2), \qquad r << l << a \tag{180}$$

where $K_{II} = \tau\sqrt{\pi a}$. Note that $V \sim \sqrt{\omega}$. In LEFM, for a fixed K_{II}, the crack-tip stress field for all Mode II problems is identical, and is given by the first term in Eq. (162): $\sigma_{kk} = (-2\kappa)\sin(\theta/2)K_{II}/(2\pi r)^{1/2}$. Similarly, for a fixed K_{II} and ω, the high-frequency crack-tip temperature field for all Mode II problems is identical, and is given by Eq. (180) (Obviously, for plates made up of different materials, the temperature field depends on the thermal property, $\alpha/\sqrt{kC}$.).

In polar form $\Theta = \|\Theta\|\exp(i\Phi)$, where $\|\Theta\|$ is the magnitude and Φ is the phase of Θ. Returning to Eq. (174), in Figure 27 the magnitude of Θ is plotted for $0 \le r \le a$, $\theta = 0, \pi/4, \pi/2, 3\pi/4, \pi$, and $\Omega = 1, 10, 100, 1000$. It is recognized that the approximate solution may begin to lose accuracy below $\Omega = 10$. Nevertheless, Θ is plotted for $\Omega = 1$ to give a "feel" for it. The fluctuating temperature field obtained using the two-term expansion for σ_{kk} is also included for comparison. Physically, at low frequencies heat has sufficient time to diffuse during each cycle so that essentially isothermal conditions are

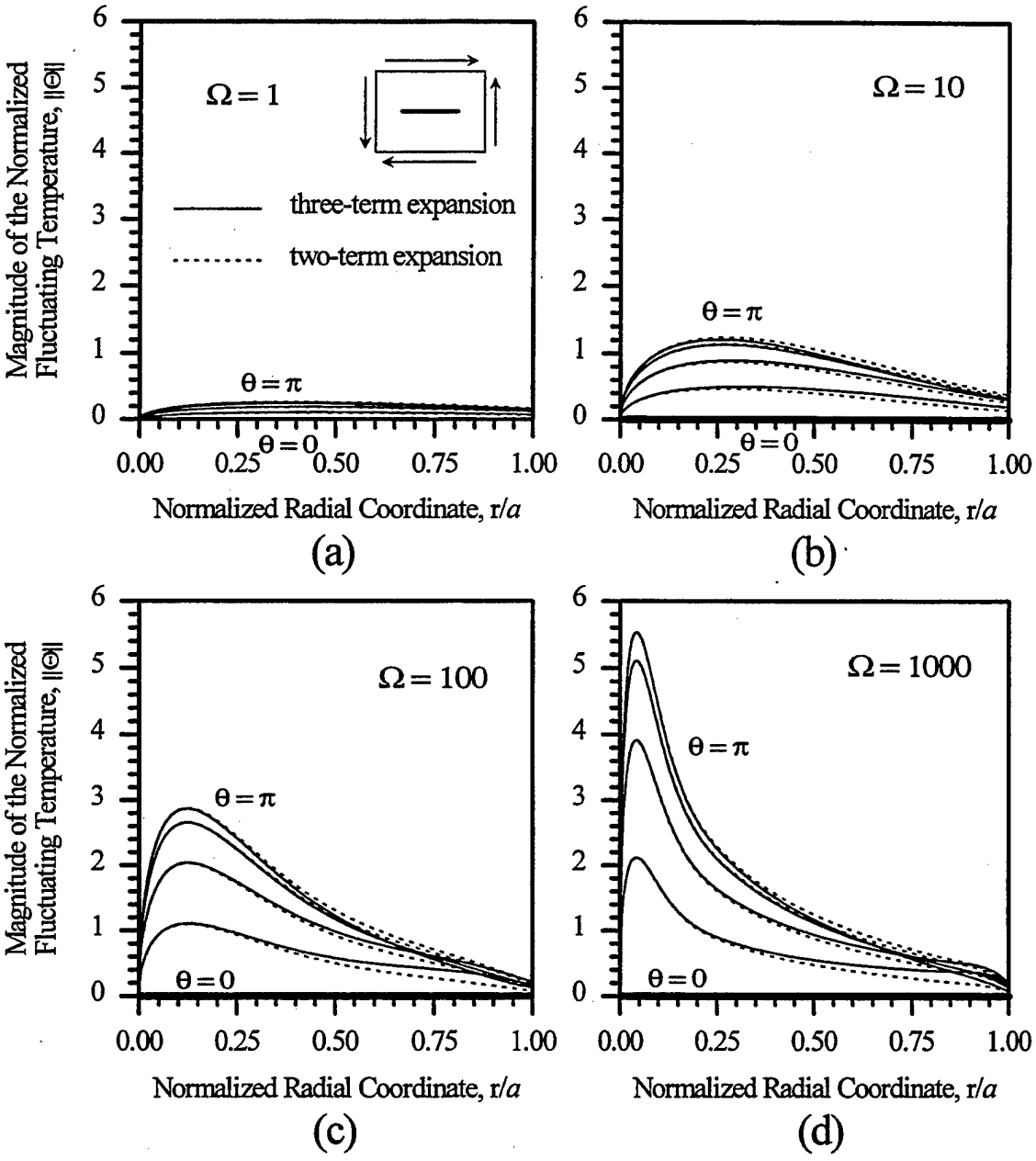

Figure 27. Magnitude of the normalized fluctuating temperature as a function of the normalized radial coordinate for $\theta = 0, \pi/4, \pi/2, 3\pi/4, \pi$. (a) $\Omega = 1$; (b) $\Omega = 10$; (c) $\Omega = 100$; (d) $\Omega = 1000$. The fluctuating temperature at the crack tip is always zero. Mode II.

obtained. This case is evidenced by $\Omega = 1$ in Figure 27. Conversely, at high frequencies, heat has very little time to diffuse and, away from the crack tip, essentially adiabatic conditions areobtained. Under adiabatic conditions, from (1), $\Theta = (-\sigma_{kk}/\kappa\tau)$. This explains the quantitative agreement, away from the crack tip, between Θ in Figure 27 and $(-\sigma_{kk}/\kappa\tau)$ in Figure 25, particularly at $\Omega = 1000$. Close to the crack tip, the temperature gradients in the radial direction are square-root singular (see Eq. (177)) and, therefore, truly adiabatic conditions are never attained even at very high frequencies. This explains the difference between Θ and $(-\sigma_{kk}/\kappa\tau)$ close to the crack tip. This argument is now explored mathematically. For any $r \in (0,a)$, it is easy to show from Eqs. (174) and (176) that $\lim_{\Omega\to\infty} \Theta(r,\theta) = (-\sigma_{kk}/\kappa\tau)$. However, as $r \to 0$, σ_{kk} becomes unbounded, whereas Θ is a bounded continuous function on the *open interval* $(0,a)$. Therefore, Θ does not converge *uniformly* to $(-\sigma_{kk}/\kappa\tau)$ on the open interval $(0,a)$.

In Figure 28 the phase of the fluctuating temperature, Φ, is plotted for $0 \le r \le a$, $\theta = \pi/4, \pi/2, 3\pi/4, \pi$, and $\Omega = 1, 10, 100, 1000$. The phase of Θ is not shown for $\theta = 0$ since $\Theta \equiv 0$ for this case. The phase of the fluctuating temperature field obtained using the two-term expansion for σ_{kk} is also included for comparison. Note that in Eq. (174) the difference between the solutions corresponding to the two-term and three-term expansions for σ_{kk} is the $\sin(3\theta/2)$ term. Thus, the temperature solution corresponding to the two-term expansion for σ_{kk} may be separated in terms of the θ-coordinate and the radial coordinate, i.e. Θ corresponding to the two-term solution has the form

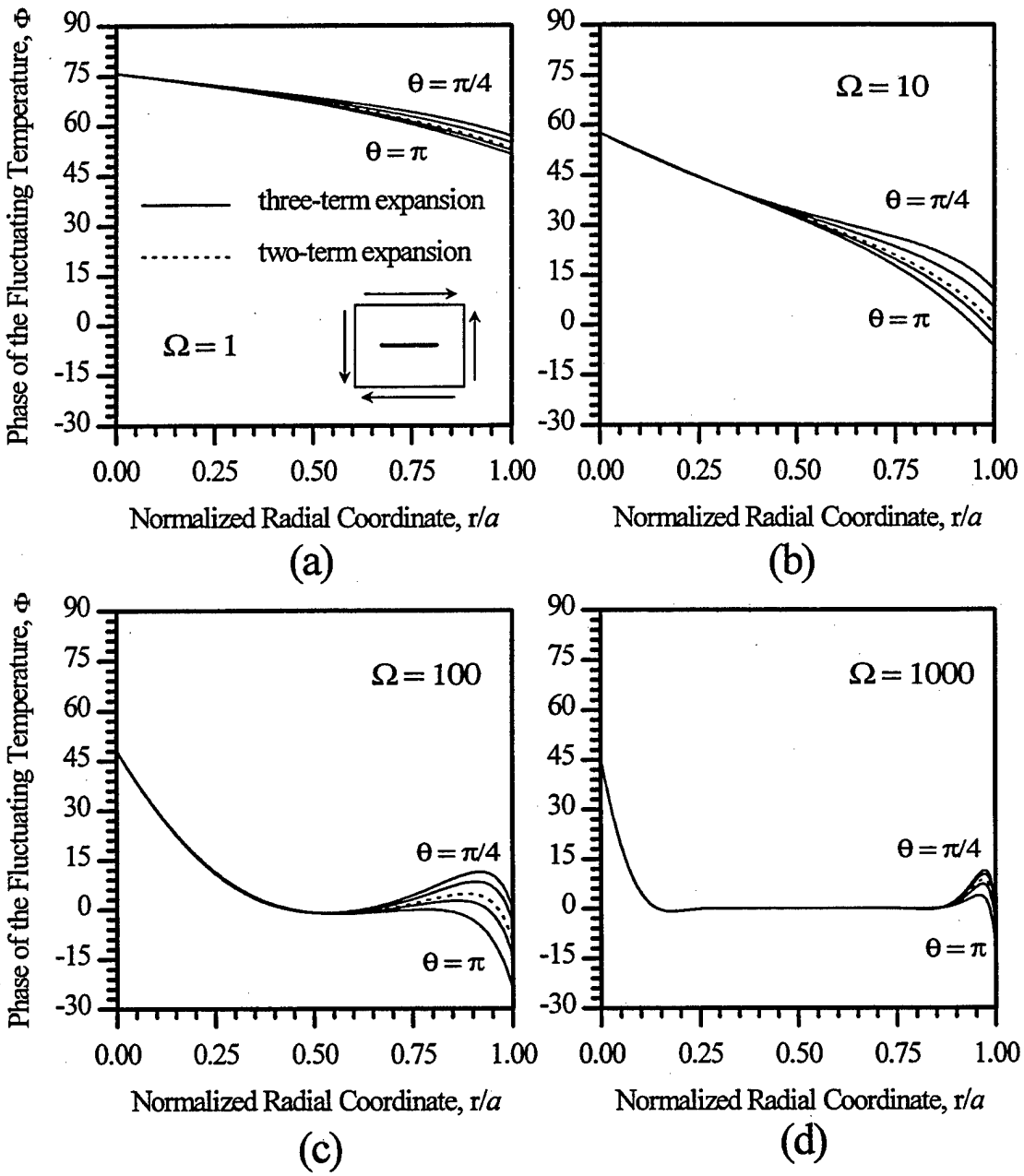

Figure 28. Phase of the fluctuating temperature as a function of the normalized radial coordinate for $\theta = \pi/4, \pi/2, 3\pi/4, \pi$. (a) $\Omega = 1$; (b) $\Omega = 10$; (c) $\Omega = 100$; (d) $\Omega = 1000$. In the case of the two-term expansion, Φ is independent of θ. Mode II.

$\Theta \sim \sin(\theta/2)$ x(some complex-valued function of r). It follows that the phase of the fluctuating temperature field corresponding to the two-term expansion for σ_{kk} is independent of θ. This result is evidenced in Figure 28. Furthermore, from Figure 27 it is clear that the $\sin(3\theta/2)$ term in Eq. (174) makes a significant contribution to Θ only for $r > a/2$. Therefore, the phase of the temperature solution corresponding to the three-term expansion for σ_{kk} is virtually independent of θ for $r < a/2$. For $\Omega << 1$, the problem is essentially isothermal, and we observed that Φ is nearly $\pi/2$ (plots not included). Conversely, for $\Omega = 1000$, away from the crack tip, the problem is essentially adiabatic, and Φ is nearly zero. At the crack tip, for high frequencies, Eq. (180) predicts a phase $\Phi = \pi/4$, which is evidenced in Figure 28c, and 28d. In summary, as Ω increases from zero to infinity, the phase decreases from $\pi/2$ to $\pi/4$ at the crack tip, and from $\pi/2$ to zero away from the crack tip.

4.3.2 Work Lost

The conversion of external work into heat at a point is now examined. A normalized work lost ψ is defined as $\psi = \Delta w / \left(\tau^2 \kappa^2 T_o \alpha^2 / C\right)$ for Mode II. A "physical feel" for the denominator may be developed as follows. A rod of one unit volume at an equilibrium temperature T_o is subjected to a uniaxial tension of magnitude τ under adiabatic conditions; then $V = -\tau T_o \alpha / C$. While holding τ fixed, the rod is allowed to absorb heat from a reservoir at T_o until it returns to its equilibrium temperature T_o. Next, the rod is unloaded adiabatically; then $V = +\tau T_o \alpha / C$. Once again, the rod is allowed to give up

heat to a reservoir at T_o until the rod temperature becomes T_o. The *total* work lost during this cycle is $\tau^2 T_o \alpha^2 / C$. By way of example, for steel, $\alpha = 12\text{x}10^{-6} K^{-1}$ and $C = 3.8\text{x}10^6 J/m^3 K$. If we choose $\tau = 100 MPa$, $T_o = 300K$, and $\kappa = 1$ (plane stress), then $\Delta w = 114 J/m^3$. Interestingly, the temperature increase of the rod due to this conversion of work into internal heat energy is only $\Delta T = 3\text{x}10^{-5} K$. For use in the next section, the *total* entropy produced during this cycle is $\tau^2 \alpha^2 / C$. For the example under consideration, $\Delta s = 0.38 J/m^3 K$. Substituting Eq. (162) into Eq. (24) and noting the difference in notation, yields

$$\psi(r,\theta) = -2\pi\left[\sin(\theta/2)\left(\frac{-1}{2}\sqrt{\frac{2a}{r}} + \frac{3}{4}\sqrt{\frac{r}{2a}}\right) - \frac{5}{16}\sin(3\theta/2)\left(\frac{r}{2a}\right)^{3/2}\right]\text{Im}(\Theta(r,\theta))$$

$$\text{for } 0 < r \le a,\ 0 \le \theta \le \pi. \quad (181)$$

where Θ is given by Eq. (174). As expected, $\psi \equiv 0$ on $\theta = 0$ because $\sigma_{kk} \equiv 0$ on $\theta = 0$.

The crack-tip work-lost field is now examined. For a finite Ω, expanding Eq. (181) in (r/a) about $r = 0$ and retaining upto the linear term, yields

$$\psi = \pi\sqrt{2}(\text{Im}\, A)\sin^2(\theta/2) +$$
$$+\pi\left[-\Omega\sin^2(\theta/2) - \frac{3}{2\sqrt{2}}(\text{Im}\, A)\sin^2(\theta/2) + \sqrt{2}(\text{Im}\, B)\sin(\theta/2)\sin(3\theta/2)\right]\left(\frac{r}{a}\right)$$

$$r << l \quad (182)$$

where, as before, the complex function $A(\Omega)$ is given by Eq. (178), and the new complex function $B(\Omega)$ is given by

$$B(\Omega)=\frac{-\sqrt{2}}{6}\left[3-\left(i\Omega+3\left(1+i\Omega\right)\right)e^{-\sqrt{i\Omega}}\right] \tag{183}$$

The first term in Eq. (182) contains contributions from the first two terms of σ_{kk} in Eq. (162), but not from any higher-order terms. Next, the three terms inside the square brackets in Eq. (182) are examined: The first term, $-\Omega\sin^2(\theta/2)$, corresponds only to the first term of σ_{kk} in Eq. (162); the second term, $-\left(3/2\sqrt{2}\right)(\mathrm{Im}\,A)\sin^2(\theta/2)$, contains contributions only from the first two terms of σ_{kk} in Eq. (162); the third term, $\sqrt{2}(\mathrm{Im}\,B)\sin(\theta/2)\sin(3\theta/2)$, contains contributions only from the first and third terms of σ_{kk} in Eq. (162). More importantly, if the series expansion Eq. (162) had been carried out to infinity, none of these three terms would have contained contributions from any of the higher-order terms in Eq. (162). Finally, the complex function $B(\Omega)$ corresponds only to the third term of σ_{kk} in Eq. (162).

Next, the limit of the work lost, ψ, as $r\to 0$ is examined; from Eq. (182)

$$\psi=\pi\sqrt{2}(\mathrm{Im}\,A)\sin^2(\theta/2) \tag{184}$$

Note that analogous to the crack-tip stress field in Eq. (162) and the crack-tip temperature field in Eq. (177), the limit of ψ also depends upon the direction θ along which the limit is taken. For $\theta=\pi$, ψ at the crack tip is plotted against Ω in Figure 29. For $\Omega<10$, ψ is plotted as a dashed line to remind the reader that these values may be inaccurate. The slope changes from one as $\Omega\to 0$ to 1/2 as $\Omega\to\infty$.

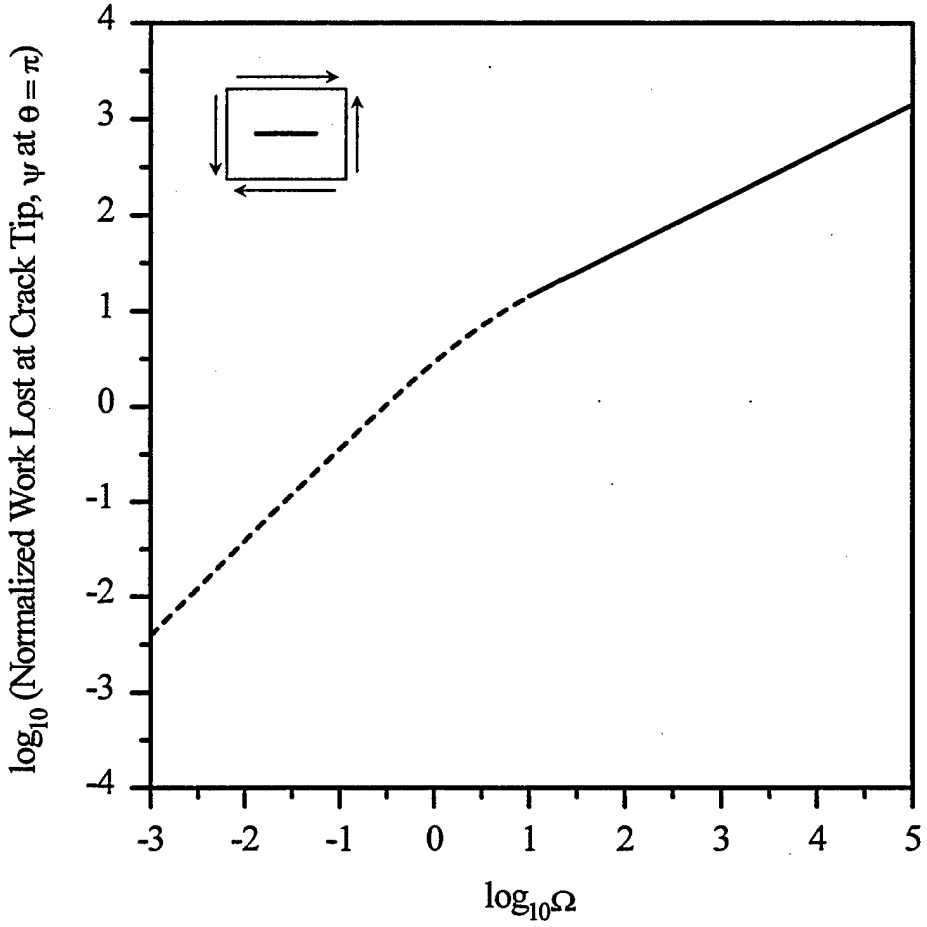

Figure 29. Normalized work lost at the crack tip, ψ at $\theta = \pi$, as a function of the normalized frequency Ω. The dashed line indicates the range of Ω in which the solution may be inaccurate. The slope decreases from one at low frequencies to 1/2 at high frequencies. Mode II.

Next, the high-frequency behavior of the work lost at the crack tip is examined. As $\Omega \to \infty$, $\mathrm{Im}\, A(\Omega) \to \sqrt{\Omega}$, $\mathrm{Im}\, B(\Omega) \to 0$, and Eq. (182) reduces to

$$\psi = \pi\left(\sqrt{2\Omega} - \Omega(r/a)\right)\sin^2(\theta/2) \ , \quad r << l << a \tag{185}$$

or, in dimensional form

$$\Delta w = T_o \kappa^2 \alpha^2 \left[\frac{\sqrt{2}}{\sqrt{kC}}\sqrt{\omega} - \frac{\omega r}{k}\right] K_{II}^2 \sin^2(\theta/2) \ , \quad r << l << a \tag{186}$$

Note that $\Delta w \sim \sqrt{\omega}$ at the crack tip. As in the case of the temperature V in Eq. (180), Δw in Eq. (186) corresponds only to the square-root singular stress field in Eq. (162). Therefore, for a fixed K_{II} and ω, Eq. (186) describes the universal high-frequency work lost field at the crack tip for all Mode II problems.

Returning to Eq. (181), in Figure 30 ψ is plotted for $0 \le r \le a$, $\theta = 0, \pi/4, \pi/2, 3\pi/4, \pi$, and $\Omega = 1, 10, 100, 1000$. Once again, even though it may be quite inaccurate, ψ is plotted for $\Omega = 1$ to give a "feel" for it. Note that the Figure for $\Omega = 1000$ has a different scale. The work lost obtained using the two-term expansion for σ_{kk} is also included for comparison. The results obtained with the two-term and three-term expansions are virtually indistinguishable for all four values of Ω. This result provides some justification for our assumption to truncate the Laurent series, Eq. (162), at three terms. The work lost is essentially confined to the interior of the disk $r = a$. This provides an a posteriori justification for replacing the actual

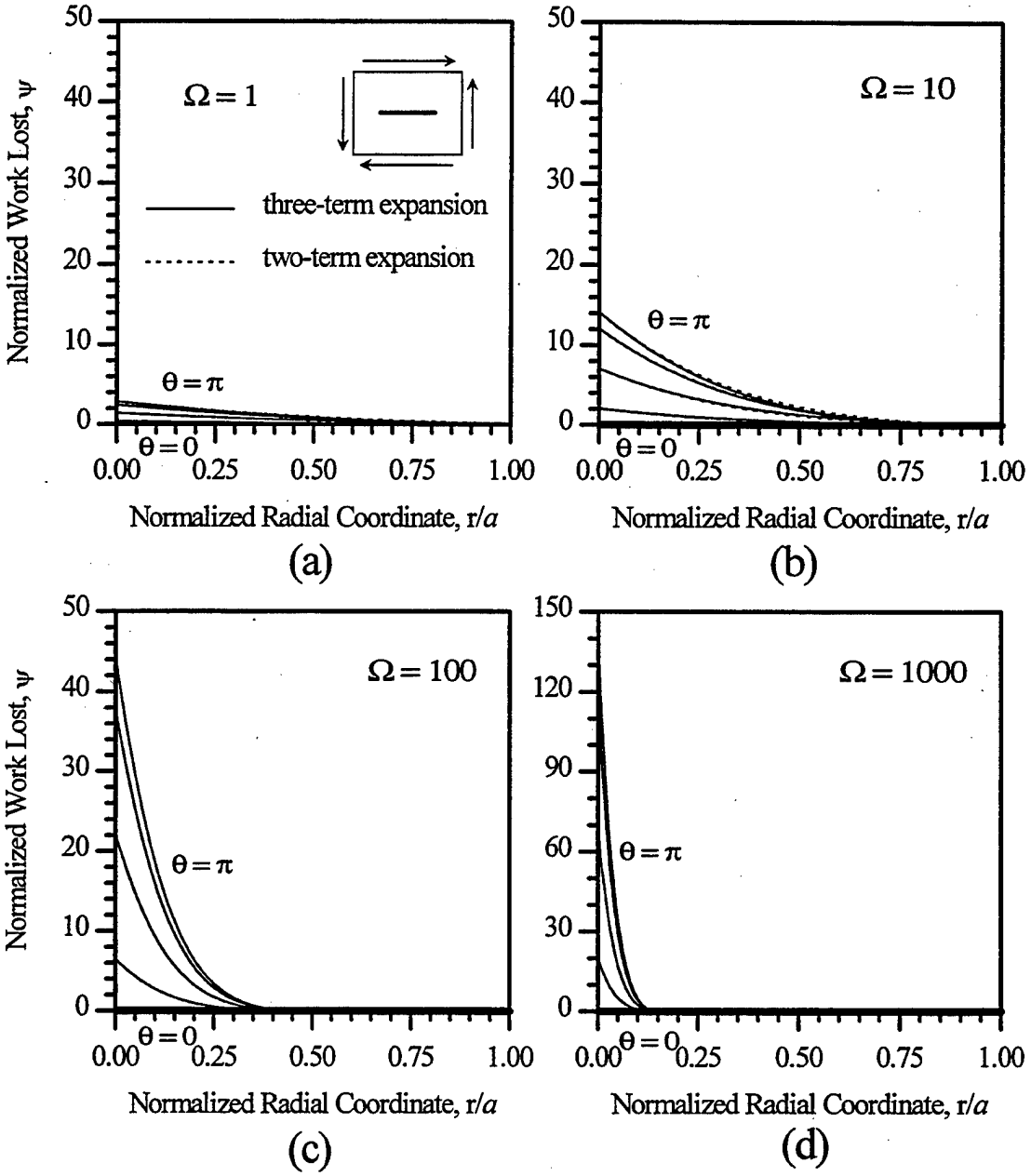

Figure 30. Normalized work lost as a function of the normalized radial coordinate for $\theta = 0, \pi/4, \pi/2, 3\pi/4, \pi$. (a) $\Omega = 1$; (b) $\Omega = 10$; (c) $\Omega = 100$; (d) $\Omega = 1000$. The work lost corresponding to the two-term and the three-term expansions is virtually indistinguishable. The work lost is essentially confined to the interior of the disk $r = a$. Mode II.

$g(r,\theta)$ - which is very small any way - with zero for $r > a$. As a check on our solution, we note that in the exact solution on the plane $x = 0$, $V \equiv 0$, and therefore $\psi \equiv 0$. In the approximate solution the only point that coincides with the plane $x = 0$ is $(r = a, \theta = \pi)$. In Figure 30 at $(r = a, \theta = \pi)$, ψ is zero for all Ω, thus giving credence to our approximate solution. In physical terms, at low frequencies essentially isothermal conditions are obtained, and the work lost is nearly zero throughout. This case is evidenced by $\Omega = 1$ in Figure 30. Conversely, at high frequencies, away from the crack tip, essentially adiabatic conditions are obtained, and again the work lost is zero. Explicitly, from Eq. (181), for any $r \in (0,a)$, $\lim_{\Omega \to \infty} \psi(r,\theta) = 0$. From Eq. (186) we see that $\psi \sim \sqrt{\omega}$ at the crack tip. Therefore, as in the case of the temperature, ψ does not converge uniformly to its adiabatic limit, $\psi(r,\theta) = 0$, on the open interval $(0,a)$.

4.3.3 Entropy Produced

The production of entropy at a point is now examined. A normalized entropy produced is defined as $\chi = \Delta s / (\tau^2 \kappa^2 \alpha^2 / C)$. A physical feel for the denominator was discussed in the preceding section. Rederiving Eq. (27) in polar coordinates and noting the difference in notation, gives

$$\chi(\mathbf{x},\omega) = \frac{\pi}{\Omega}\left[\frac{\partial\Theta}{\partial(r/a)}\frac{\partial\overline{\Theta}}{\partial(r/a)} + \frac{1}{(r/a)^2}\frac{\partial\Theta}{\partial\theta}\frac{\partial\overline{\Theta}}{\partial\theta}\right] \tag{187}$$

where Θ is given by Eq. (174).

First, the crack-tip entropy field is examined. For a finite Ω (finite l), expanding Eq. (187) about $r = 0$ and retaining only the first term yields

$$\chi = \frac{\pi A\overline{A}}{4\Omega}\frac{a}{r}, \qquad r << l \tag{188}$$

where $A(\Omega)$ is given by Eq. (178). As in the case of Θ in Eq. (177), χ in Eq. (188) contains contributions from the first two terms of σ_{kk} in Eq. (162), but not from any higher-order terms. Observe that χ exhibits a $1/r$ type singularity at the crack tip, and is independent of θ. A *normalized* entropy intensity factor is defined as

$$S_{II} = \lim_{r\to 0}\left(\frac{2}{\pi}\frac{r}{a}\chi\right) = \frac{A\overline{A}}{2\Omega} \tag{189}$$

Figure 31 shows the dependence of S_{II} on Ω. For $\Omega < 10$, S_{II} is plotted as a dashed line to indicate that these values may be inaccurate.

Next, the high-frequency behavior of the crack-tip entropy field is considered. For $\Omega \to \infty$, $A\overline{A}/\Omega \to 2$ so that $S_{II} \to 1$; therefore

$$\chi = \frac{\pi}{2}\frac{a}{r}, \qquad r << l << a \tag{190}$$

or in dimensional form

$$\Delta s = \frac{\pi\kappa^2\alpha^2}{C}\frac{K_{II}^2}{2\pi r}, \qquad r << l << a \tag{191}$$

In the spirit of LEFM, a *dimensional* entropy intensity factor is defined as

$$M_{II} = \lim_{r\to 0}(2\pi r\,\Delta s) = \frac{\pi\kappa^2\alpha^2}{C}K_{II}^2 \tag{192}$$

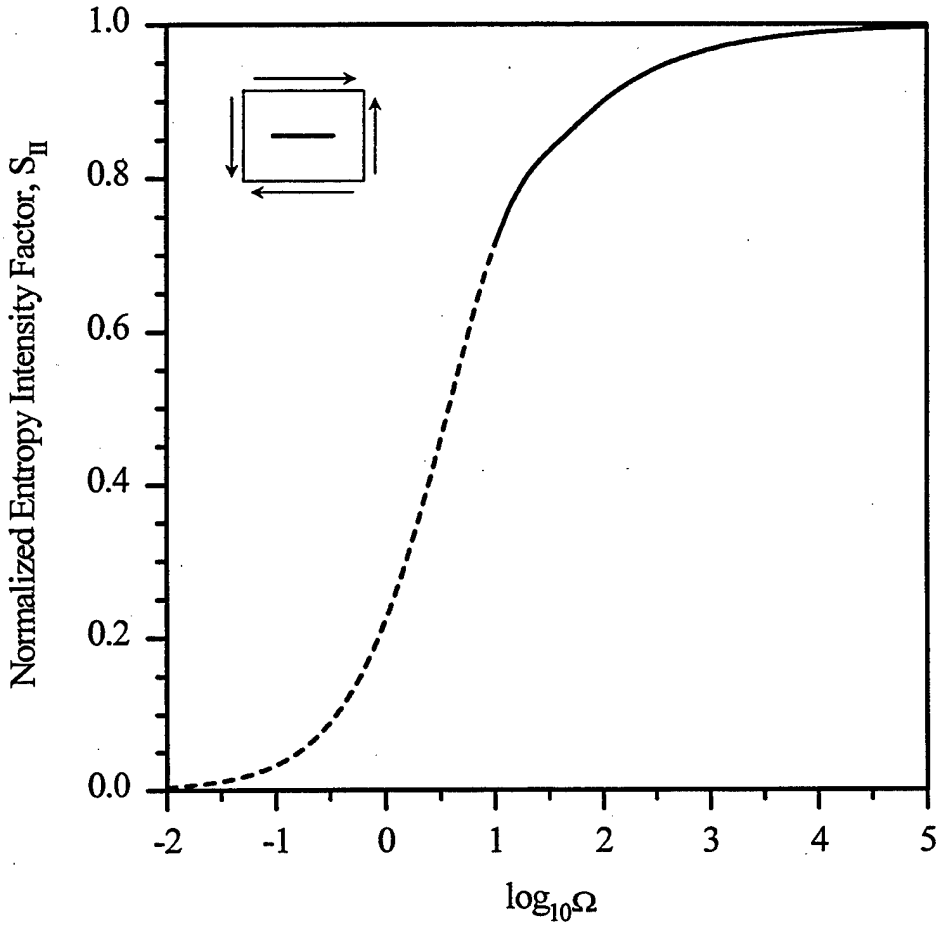

Figure 31. Normalized entropy intensity factor, S_{II}, as a function of the normalized frequency Ω. The dashed line indicates the range of Ω in which the solution may be inaccurate. Mode II.

so that

$$\Delta s = \frac{M_{II}}{2\pi r}, \qquad r << l << a \tag{193}$$

Note that in the high-frequency limit, χ in Eq. (190) is frequency independent (cf. the temperature $\Theta \sim \sqrt{\Omega}$, Eq. (179), and the lost work $\psi \sim \sqrt{2\Omega} - \Omega(r/a)$, Eq. (185)). As in the case of the temperature V in Eq. (180) and the work lost Δw in Eq. (186), Δs in Eq. (191) corresponds only to the square-root singular stress field in Eq. (162). Therefore, for a fixed K_{II}, Eq. (191) describes the universal high-frequency crack-tip entropy field for all Mode II problems.

In Figure 32, χ is plotted for $0 \le r \le a$, $\theta = 0, \pi/4, \pi/2, 3\pi/4, \pi$, and $\Omega = 1, 10, 100, 1000$. The entropy produced using the two-term expansion for σ_{kk} is also included for comparison. Once again the results obtained with the two-term and three-term expansions are virtually indistinguishable for all the Ω shown, lending further credence to our decision to truncate the series at three terms. Note that the normalization of Δw and Δs was done in such a manner that setting $\psi = \chi$ corresponds to $\Delta w = T_o \Delta s$, i.e. one unit of normalized entropy produced corresponds to one unit of normalized work lost. Accordingly, ψ (Figure 30) and χ (Figure 32) are plotted using identical scales (except Figure 30d). As in the case of ψ, as $r \to a$, χ is negligibly small for all Ω. This provides further justification for replacing $g(r,\theta)$ - which was very small any way - with zero for $r > a$. It is instructive to compare the lost work (Figure 30) and the entropy produced (Figure 32). The lost work is identically zero on $\theta = 0$ (in front of the crack), increases monotonically

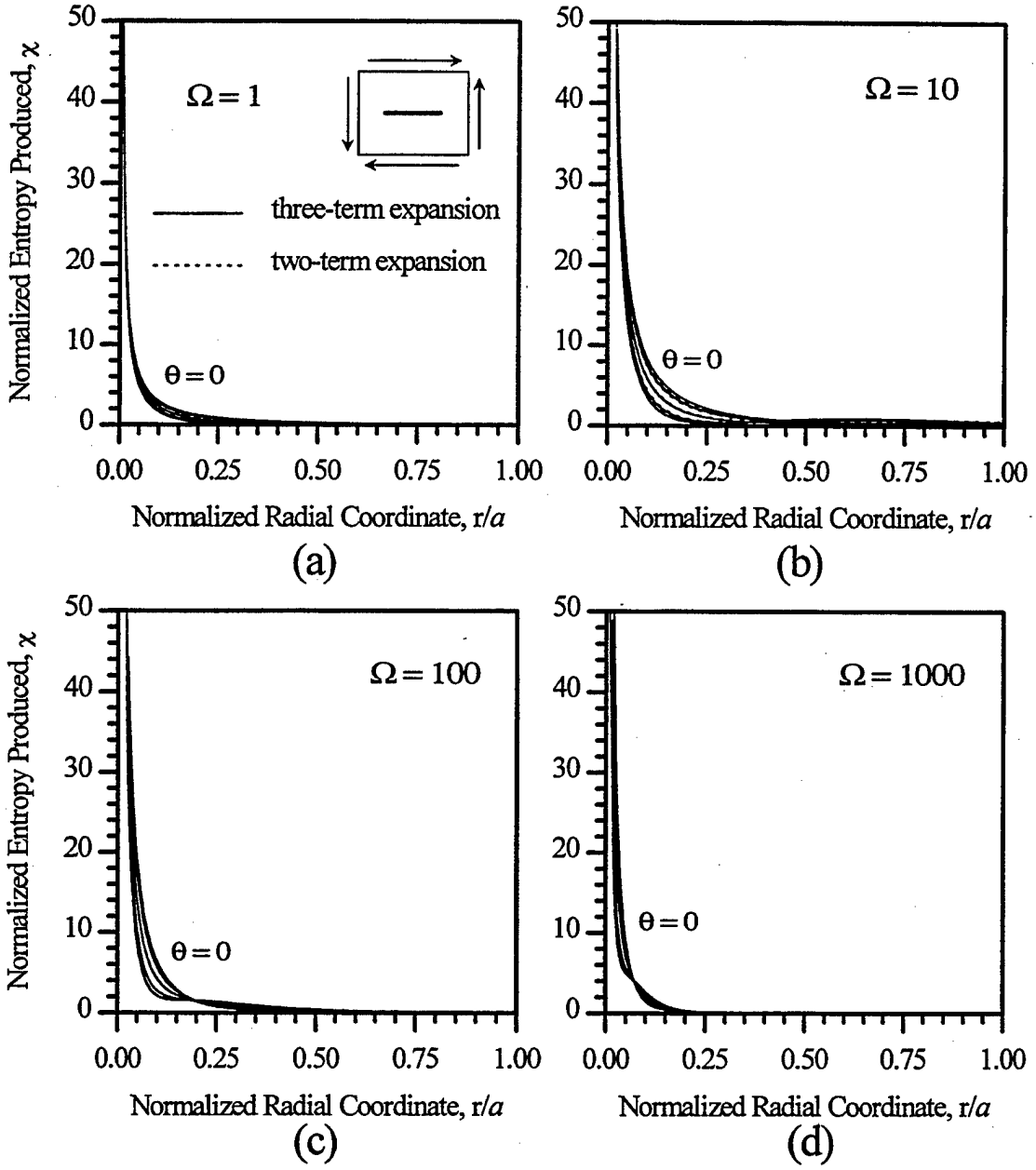

Figure 32. Normalized entropy produced as a function of the normalized radial coordinate for $\theta = 0, \pi/4, \pi/2, 3\pi/4, \pi$. (a) $\Omega = 1$; (b) $\Omega = 10$; (c) $\Omega = 100$; (d) $\Omega = 1000$. The entropy produced goes to infinity as $(1/r)$ at the crack tip. The entropy produced corresponding to the two-term and the three-term expansions is virtually indistinguishable. Mode II.

with θ, and becomes maximum on $\theta = \pi$ (crack faces). Close to the crack-tip, the exact opposite is true for χ. (This does not come as a surprise. In Section 3.1.2 it was shown that in the case of an Euler-Bernoulli beam, $\chi \equiv 0$ on the adiabatic boundaries and maximum on the neutral axis, whereas $\psi \equiv 0$ on the neutral axis and maximum on the boundaries). In Figure 32 for $\Omega = 100$ and $\Omega = 1000$ there is a fairly sharp cross-over visible at $r/a = 0.2$ and $r/a = 0.08$, respectively. For r/a greater than the cross-over point, χ is lowest on $\theta = 0$ and increases with θ. For any $r \in (0,a)$, in the high frequency limit, Eq. (187) reduces to $\lim_{\Omega\to\infty} \chi(r,\theta) = 0$. On the other hand, from Eq. (190), χ is unbounded at the crack tip. Therefore, as in the case of Θ and ψ, χ does not converge uniformly to the adiabatic limit on the open interval $(0,a)$.

4.3.4 Total Work Lost

The total work lost throughout the plate (of unit thickness) per cycle is given by

$$\Delta W = \int_{-\infty}^{\infty}\int_{-\infty}^{\infty} \Delta w \, dx dy \tag{194}$$

However, in the previous section it was argued that virtually all of the external work is lost in the interior of the disk $r < a$. Accordingly, Eq. (194) is approximated with

$$\Delta W = 2\int_{-\pi}^{\pi} d\theta \int_0^a \Delta w \, r \, dr \tag{195}$$

where the factor of 2 accounts for the two crack tips. With reference to Figure 30, it is clear that the solution for Δw obtained using the two-term

expansion for σ_{kk} is virtually identical to the solution obtained using the three-term expansion. Therefore, for simplicity the two-term solution will be used. (This solution is obtained by omitting the $\sin(3\theta/2)$ terms in Es. (174) and (181).) We now define a normalized total work lost, $\Psi = \Delta W/W$, where $W = 2\pi a^2\left(\kappa^2\tau^2\alpha^2 T_o/C\right)$. (Note that the term in parenthesis is the term that arose naturally in the discussion of the work lost, ψ. Once again, the factor of 2 accounts for the two crack tips.) Then

$$\Psi = 2\pi\,\mathrm{Im}\left\{\tfrac{1}{i\Omega}\left[\tfrac{3}{4} - \sqrt{i\Omega} + e^{-\sqrt{i\Omega}}\left(\sqrt{i\Omega} - 3\right)\left(\tfrac{1}{2} - \tfrac{1}{16}\cosh\left(\sqrt{i\Omega}\right) - \tfrac{3}{16}\tfrac{1}{\sqrt{i\Omega}}\sinh\left(\sqrt{i\Omega}\right)\right)\right]\right\} \tag{196}$$

In Figure 33, Ψ is plotted as a function of Ω. For $\Omega < 10$ we have plotted Ψ as a dashed line to indicate that these values may be inaccurate. As expected, as $\Omega \to 0$, essentially isothermal conditions are obtained and $\Psi \to 0$. As $\Omega \to \infty$, away from the crack tip, essentially adiabatic conditions are obtained, and once again $\Psi \to 0$. The maximum work lost occurs at approximately $\Omega = 10$.

The *exact* solution for the total work lost in an Euler-Bernoulli beam of a rectangular cross-section may be obtained by substituting Eq. (41) into Eq. (3), yielding

$$\Psi = \frac{\Delta W}{W} = \frac{192}{\pi^2}\sum_{\substack{n=1\\ \text{odd}}}^{\infty}\frac{\Omega}{n^2\left(n^4\pi^4 + \Omega^2\right)} \quad \text{(beam)} \tag{197}$$

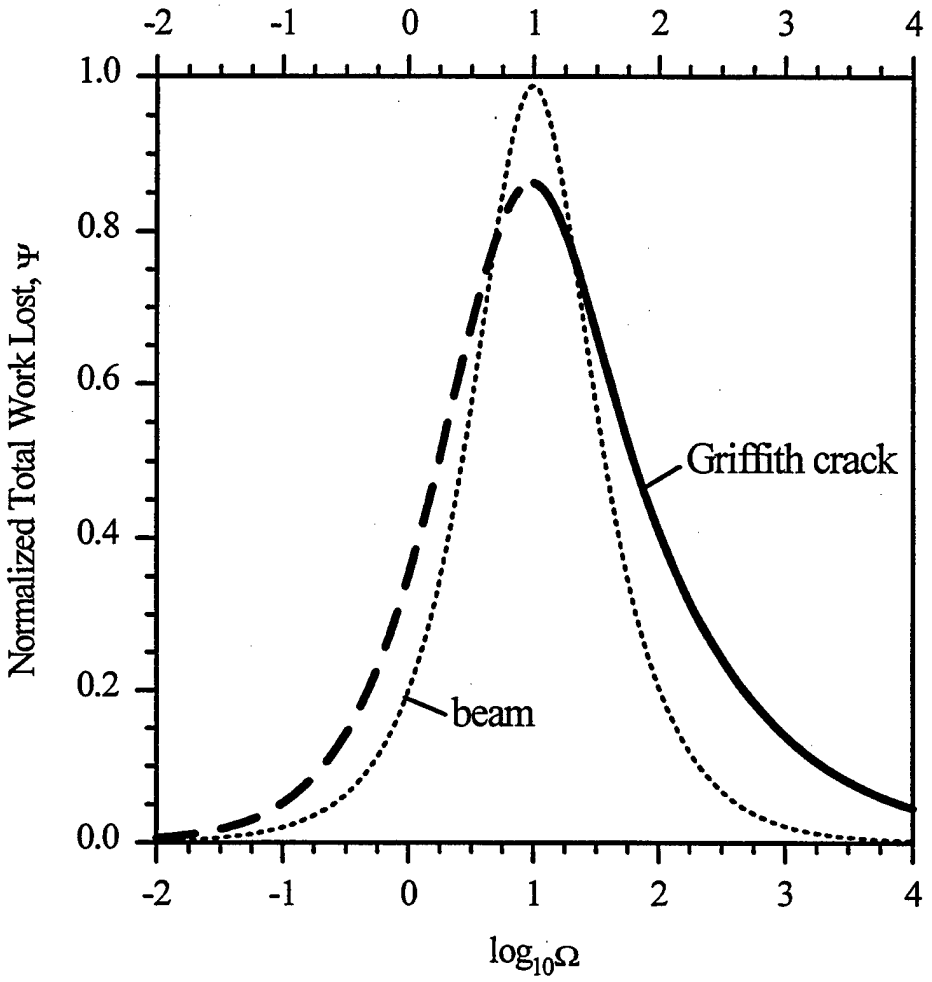

Figure 33. Normalized total work lost as a function of the normalized frequency. The dashed line indicates the range where the solution may be inaccurate. Mode II. The corresponding results for an Euler-Bernoulli beam are also included for comparison (dotted line). The close resemblance between the two elastothermodynamic responses comes as a pleasant surprise. The peak occurs at virtually the same normalized frequency, $\Omega = 10$.

where $W = (\pi E \alpha^2 T_o / C) W_o$, W_o is the maximum stored elastic energy during the cycle, E is the Young's modulus, $\Omega = \omega C h^2 / k$ (cf. $\Omega = \omega C a^2 / k$ for the Griffith crack), and h is the total height of the beam in the plane of the vibrations. This result was originally derived by Zener (1937) using a different approach. Moreover, Eq. (197) has been repeatedly verified by several experimentalists, e.g., Berry (1955) or Nowick and Berry (1972, Ch. 17). The *exact* solution for the beam (dotted line) and our *approximate* solution for the crack are compared in Figure 33. In spite of the obvious differences in the essential nature of the two boundary value problems, there is a close resemblance between their elastothermodynamic responses. The peak occurs at virtually the same normalized frequency Ω; the semi crack length (a) and the beam height (h) play the same role in the definition of Ω. Furthermore, there is a similarly close resemblance between the approximate elastothermodynamic response of the Griffith crack and the *exact* response of a periodic array of slabs (Section 3.4.1), the symmetric three-layer plate (Section 3.4.2), and the composite sphere (Section 3.4.3). This comparison lends further credence to the simplifying assumptions introduced in obtaining the approximate solution to the Mode II crack problem.

4.4 MODE I

4.4.1 Temperature Field

A Mode I Griffith crack subjected to a biaxial tension is shown in Figure 34a. The hydrostatic stress field is given by Eq. (156), and is an even function of x and y. The temperature field is governed by Eqs. (159) and (160). Since the operator in Eq. (159) is symmetric in x and y, V is an even function of x and y. Moreover, the crack faces are assumed to be adiabatic. Therefore, the entire planes $x=0$ and $y=0$ are adiabatic. Thus, it is only necessary to consider the positive quarter plane $(x\geq 0, y\geq 0)$ with the adiabatic boundary conditions

$$\begin{aligned} &(1)\quad \frac{\partial V}{\partial x}=0 \quad x=0, 0<y<\infty \\ &(2)\quad \frac{\partial V}{\partial y}=0 \quad y=0, 0<x<\infty \end{aligned} \tag{198}$$

This is shown in Figure 34b. Attempts to solve this heat conduction problem also led to intractable mathematics so an approximate solution is again sought.

First, an approximation to σ_{kk} is considered. As in the case of Mode II, we introduce a polar coordinate system (r,θ) at the right crack tip $z=a$ (see Figure 23), and expand Eq. (156) in a Laurent series in $z/2a$ about the point $z=a$. Retaining the first three terms we obtain

$$\sigma_{kk}=2\kappa\sigma\left[\cos(\theta/2)\left(\frac{1}{2}\sqrt{\frac{2a}{r}}+\frac{3}{4}\sqrt{\frac{r}{2a}}\right)-\frac{5}{16}\cos(3\theta/2)\left(\frac{r}{2a}\right)^{3/2}\right] \quad 0<r<2a \tag{199}$$

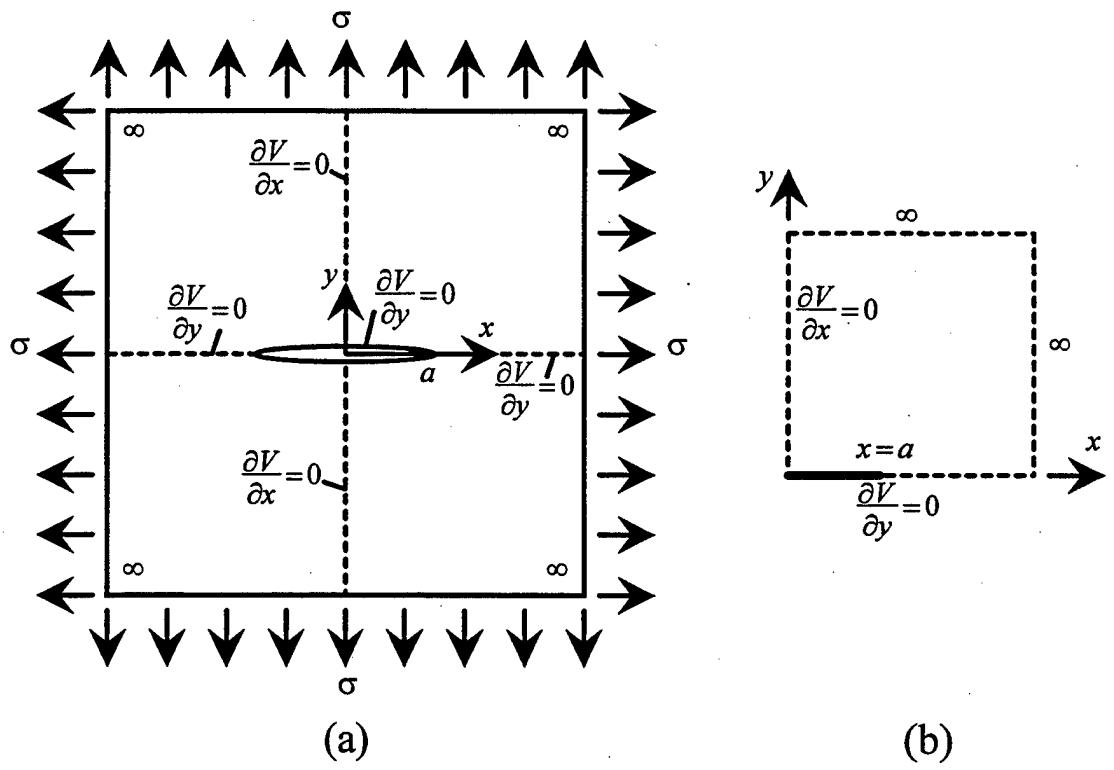

Figure 34. (a) A Griffith crack of length $2a$ in Mode I loading with a rectangular coordinate system (x,y). The crack faces are assumed to be adiabatic. Because σ_{kk} is an even function of x and y, the planes $x=0$ and $y=0$ are adiabatic. (b) The reduced quarter-plane heat-conduction problem.

In Figure 35 the *exact* σ_{kk} contours (using Eq. (156)) are plotted for the region $0<x<2a$, $0<y<a$, and in Figure 36 the *exact* σ_{kk} and its three-term approximation, Eq. (199), are compared for $0<r/a<2$ (cf. $0<r/a<1$ for Mode II). The comparison is quite good. A similar comparison was carried our for a four-term expansion; it was found that the fourth term does not yield any significant improvement. Therefore, the series was truncated at three terms. Note that in Mode I, the exact $\sigma_{kk}=0$ on the crack faces and, for any r increases to its maximum value on $\theta=0$. The exact opposite is true for Mode II: the exact σ_{kk} is maximum on the crack faces and, for any r, decreases to zero on $\theta=0$ (cf. Figure 25). As a visual aid, one might say that a Griffith crack tends to localize the hydrostatic stress field *outside* the crack tips in Mode I, and *inside* the crack tips in Mode II. Returning to Figure 36 in spite of the singularity at the other crack tip $(r=2a,\theta=\pi)$, the comparison is considered to be surprisingly good out to $r<2a$. This may be attributed to the fact that $\sigma_{kk}=0$ on the crack faces, $0<r<2a$, $\theta=\pm\pi$.

The approximations introduced in the paragraph containing Eq. (162) are also used for Mode I. The resulting "associated heat-conduction problem" is shown in Figure 37. Next, we consider the heat generation term $g(r,\theta)$. Inside the region $0\le\theta\le\pi$, $0<r<2a$, the exact $g(r,\theta)$ (Eqs. (156) and (160)) is approximated by the three-term expansion (Eqs. (199)and (160)). Now, as $r\to\infty$ (for any θ), the *exact* $\sigma_{kk}/\kappa\sigma\to 2$. As $r\to 2a$ (for any θ), the *approximate* $\sigma_{kk}/\kappa\sigma$ is very nearly two (see Figure 36).

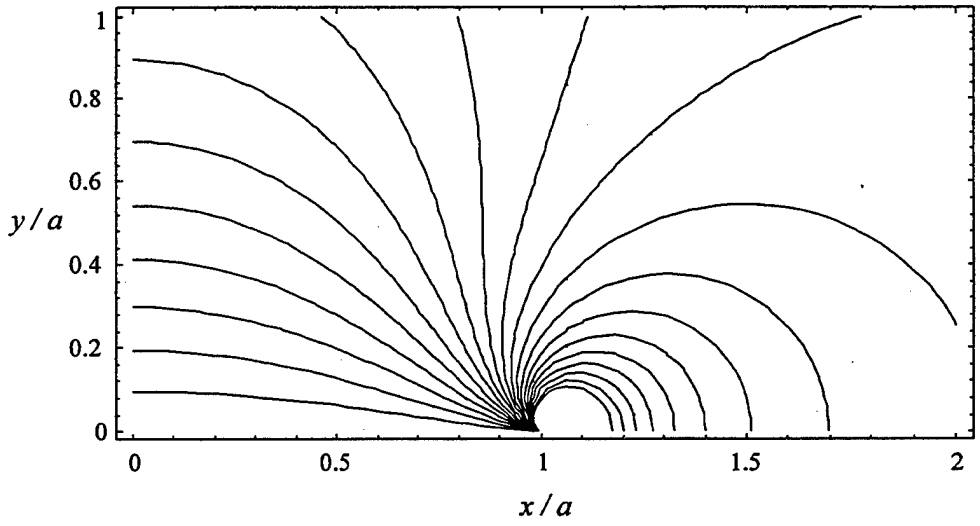

Figure 35. Mode I normalized hydrostatic stress contours, $\sigma_{kk}/\kappa\sigma$. ($x/a = 1$ corresponds to the right crack tip. The full field may be constructed by using the even symmetry of the problem. The range of the contours is 0.1 (lower left) to 2.0 (right of crack tip) with increments of 0.1.)

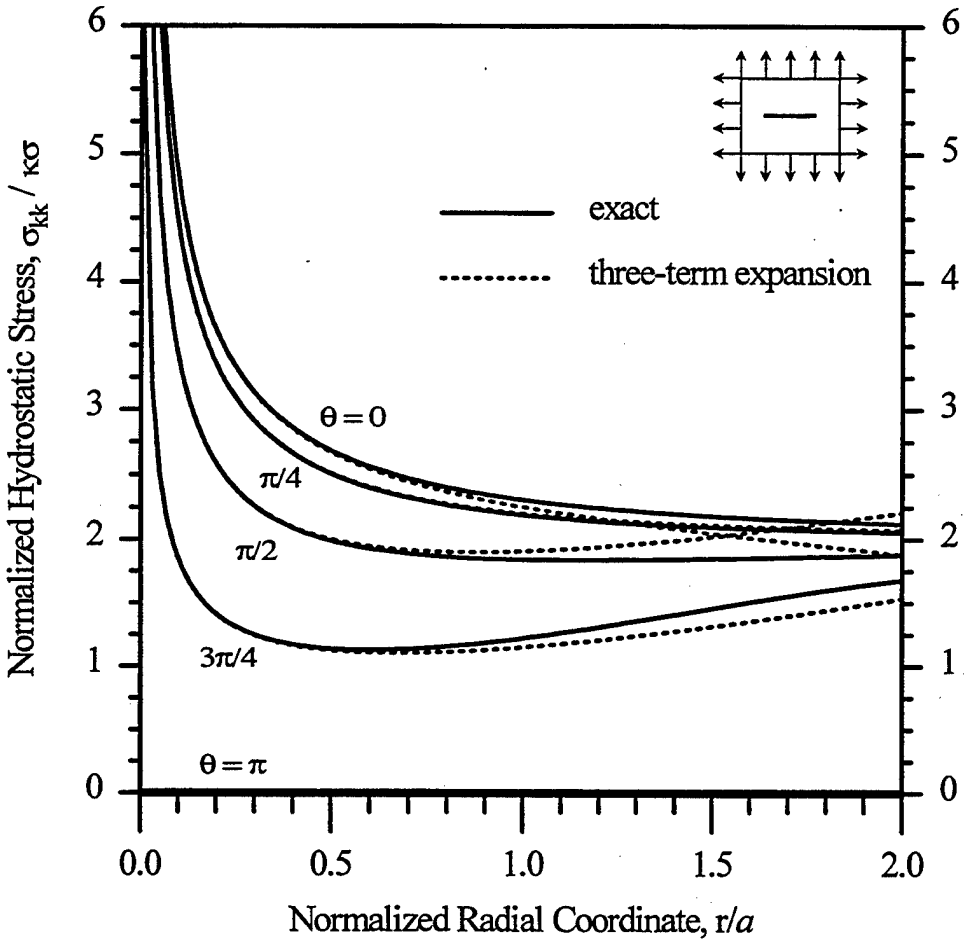

Figure 36. Comparison between the exact σ_{kk} and its three-term expansion for $\theta = 0, \pi/4, \pi/2, 3\pi/4, \pi$. Mode I.

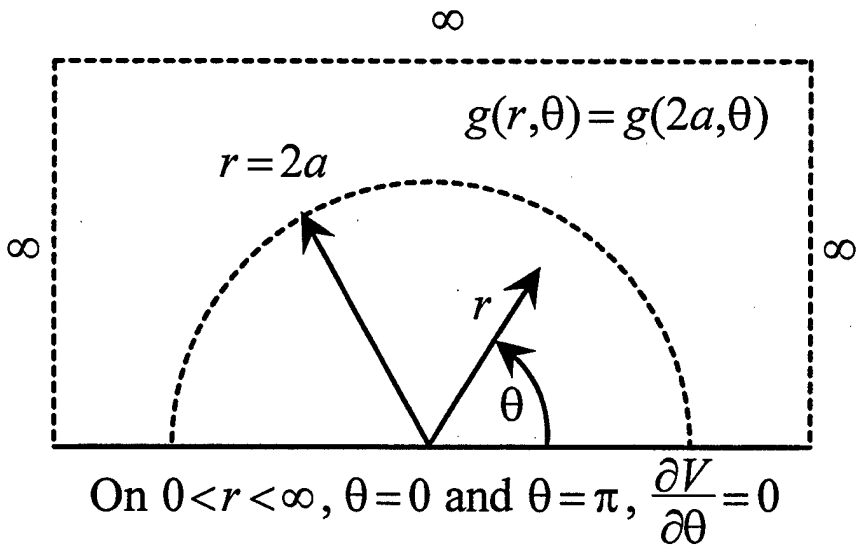

Figure 37. The "associated heat conduction problem" with a nonzero heat generation, $g(r,\theta) = g(2a,\theta)$, outside the disk of radius $2a$. Mode I.

A jump discontinuity in stress would lead to steep gradients in temperature which, in turn, would lead to spurious entropy production Eq. (11). In order to avoid this situation, in the associated heat-conduction problem, $g(r,\theta)$ is set equal to $g(2a,\theta)$ in the exterior of the half-disk, i.e. in $0 \le \theta \le \pi$, $2a \le r < \infty$ (cf. Mode II where we set $g(r,\theta) \equiv 0$, in $0 \le \theta \le \pi$, $a \le r < \infty$). As in the case of Mode II, once the solution to the associated heat-conduction problem in $y > 0$, the solution in the left quarter-plane, $x < 0$, $y > 0$, will be discarded; the solution in the right quarter plane, $x > 0$, $y > 0$, will be taken as an approximation to the exact solution of the problem shown in Figure 34b. The solution in the full plane, Figure 34a, can then be constructed using the even symmetries of V.

The associated heat-conduction problem for Mode I is given by

$$\frac{\partial^2 V}{\partial r^2} + \frac{1}{r}\frac{\partial V}{\partial r} + \frac{1}{r^2}\frac{\partial^2 V}{\partial \theta^2} - \frac{C}{k} i\omega V + \frac{1}{k} g(r,\theta) = 0, \quad 0 \le \theta \le \pi, \; 0 < r < \infty \tag{200}$$

$$\frac{\partial V}{\partial \theta} = 0 \quad \text{at} \quad \theta = 0, \pi, \quad 0 < r < \infty \tag{201}$$

where

$$g(r,\theta) = \begin{cases} -(i\omega)\alpha T_o \sigma_{kk}(r,\theta) & 0 \le \theta \le \pi, \; 0 < r \le 2a \\ -(i\omega)\alpha T_o \sigma_{kk}(2a,\theta) & 0 \le \theta \le \pi, \; 2a < r < \infty \end{cases} \tag{202}$$

An *exact* solution to this problem was obtained by using an integral transform method analogous to that used for Mode II; the solution is

$$\Theta(r,\theta) = -\sqrt{2}\, i\Omega \sum_{n=0}^{\infty} \frac{\cos(n\theta)}{N_n} \cdot$$

$$\cdot \left\{ K_n\left(\sqrt{i\Omega}\, r/a\right) \int_0^{r/a} I_n\left(u\sqrt{i\Omega}\right) \left[\frac{2(-1)^{n+1}}{4n^2-1} \left(\sqrt{u} + \frac{3}{4}u^{3/2}\right) - \frac{5}{32}\frac{6(-1)^n}{4n^2-9} u^{5/2} \right] du + \right.$$

$$+ I_n\left(\sqrt{i\Omega}\, r/a\right) \left[\int_{r/a}^{2} K_n\left(u\sqrt{i\Omega}\right) \left[\frac{2(-1)^{n+1}}{4n^2-1} \left(\sqrt{u} + \frac{3}{4}u^{3/2}\right) - \frac{5}{32}\frac{6(-1)^n}{4n^2-9} u^{5/2} \right] du + \right.$$

$$\left. \left. + \left[\frac{2(-1)^{n+1}}{4n^2-1} \left(\sqrt{2} + \frac{3}{4}(2)^{3/2}\right) - \frac{5}{32}\frac{6(-1)^n}{4n^2-9} (2)^{5/2} \right] \int_2^{\infty} K_n\left(u\sqrt{i\Omega}\right) du \right] \right\}$$

$$\text{for } 0 < r \le 2a \qquad (203)$$

where $N_n = \pi$ for $n = 0$ and $\pi/2$ for $n = 1,2,3,\ldots$, and a normalized fluctuating temperature Θ for Mode I has been defined as $\Theta = V/(\sigma\kappa T_o \alpha/C)$ (cf. Mode II, where $\Theta = V/(\tau\kappa T_o \alpha/C)$). Unfortunately, the integrals could not be evaluated in a closed form. Therefore, numerical integration was used. The Bessel functions and the associated integrals were evaluated using version 2.0 of the IMSL subroutines CBINS, CBKS, and QDAG with the parameters ERRREL set equal to 0.005 and ERRABS set equal to 0.0. The improper integrals were evaluated by taking the upper limit to be a large constant in place of infinity. It was found that an upper limit of 10 was sufficiently accurate for graphing purposes for the range of frequencies considered. Furthermore, it was found that the first eleven terms in the summation in Eq. (203) were sufficient.

Unlike Eq. (174), Eq. (203) could not be reduced to a closed form. Therefore, an expression for the crack-tip temperature field could not be derived (cf. Eq. (177) for Mode II). However, it was proven from Eq. (203)

that for any finite Ω, the temperature is bounded at the crack tip. So far, for maximum accuracy, the solution has been constructed in the half-disk, $r < 2a$; the approximation to $g(r,\theta)$ starts at $r = 2a$. However, from the symmetries of $V(x,y)$ it is obvious that only the solution in the half-disk $r < a$ is needed (see Figure 34b). Accordingly, in Figure 38 the magnitude of Θ is plotted for $0 \le r/a \le 1$, $\theta = 0, \pi/4, \pi/2, 3\pi/4, \pi$, and $\Omega = 1, 10, 100, 1000$. For the reasons discussed in the paragraph following Eq. (163), it is recognized that the approximate solution may not be accurate for $\Omega < 10$. Nevertheless, Θ is plotted for $\Omega = 1$ to give a "feel" for it. The results using a two-term expansion for σ_{kk} are also shown for comparison. For a given r the temperature magnitude decreases monotonically from a maximum at $\theta = 0$ to a minimum at $\theta = \pi$ (cf. Figure 27 where it is the exact opposite). It is clear that for $\Omega = 1$, heat has plenty of time to diffuse, and essentially isothermal conditions are obtained. Now examine the other extreme, $\Omega = 1000$. If truly adiabatic conditions are obtained then $\Theta = -\sigma_{kk}/\kappa\sigma$. By overlaying Figure 36 and Figure 38d, drawn to the same scale, we observed that beyond some distance away from the crack tip, essentially adiabatic conditions are in fact achieved at $\Omega = 1000$. Due to the limitations of evaluating Θ numerically, we were only able to calculate Θ for $r/a > 0.01$.

In Figure 39 the phase of the fluctuating temperature, Φ, is plotted for $0 \le r \le a$, $\theta = 0, \pi/4, \pi/2, 3\pi/4, \pi$, and $\Omega = 1, 10, 100, 1000$. The phase of the fluctuating temperature field obtained using the two-term expansion for σ_{kk} is also included for comparison. Note that in contrast to Eq. (174), in Eq. (203) the temperature solution corresponding to the two-term expansion for σ_{kk}

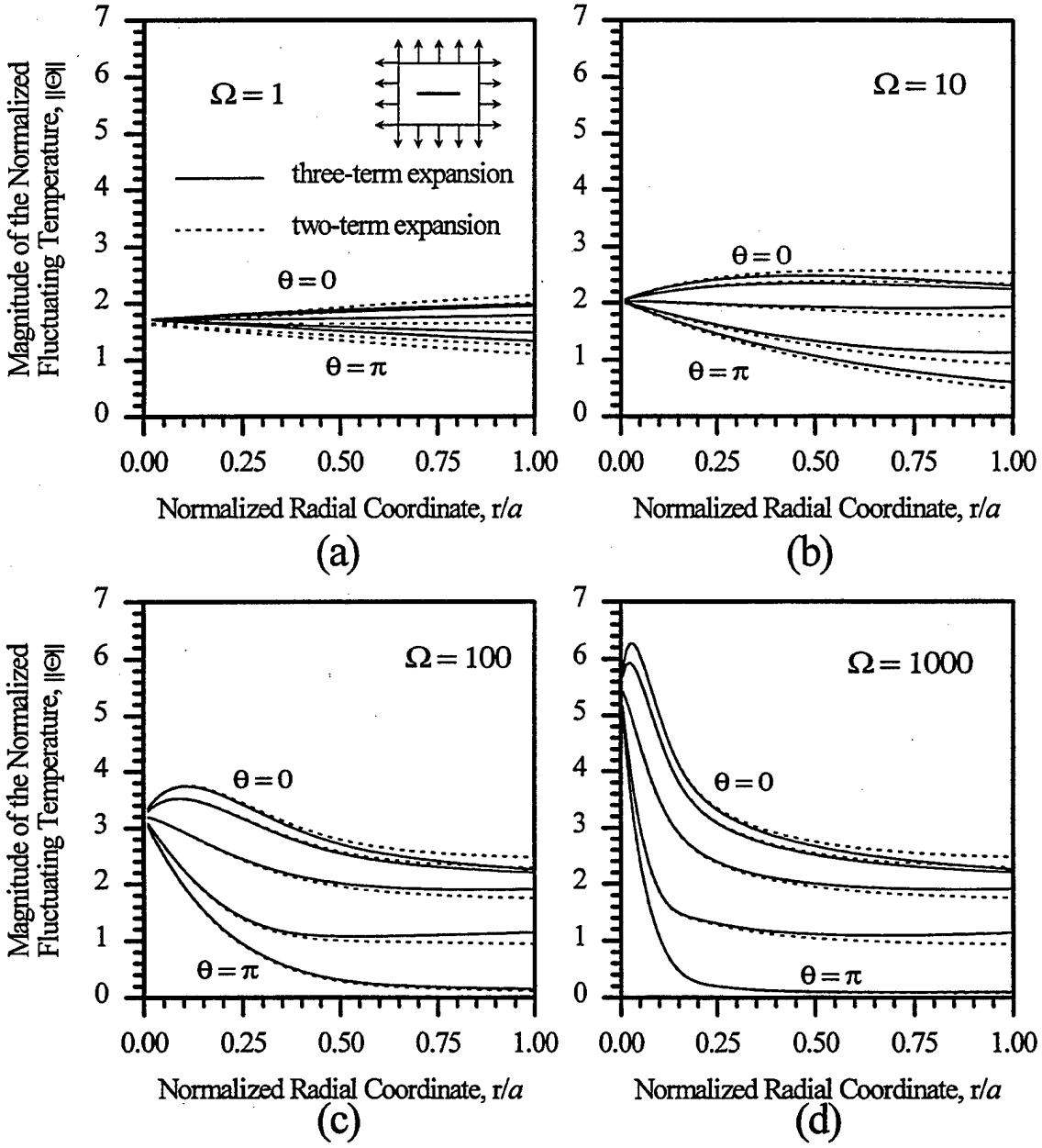

Figure 38. Magnitude of the normalized fluctuating temperature as a function of the normalized radial coordinate for $\theta = 0, \pi/4, \pi/2, 3\pi/4, \pi$. (a) $\Omega = 1$; (b) $\Omega = 10$; (c) $\Omega = 100$; (d) $\Omega = 1000$. The fluctuating temperature is bounded at the crack tip. Mode I.

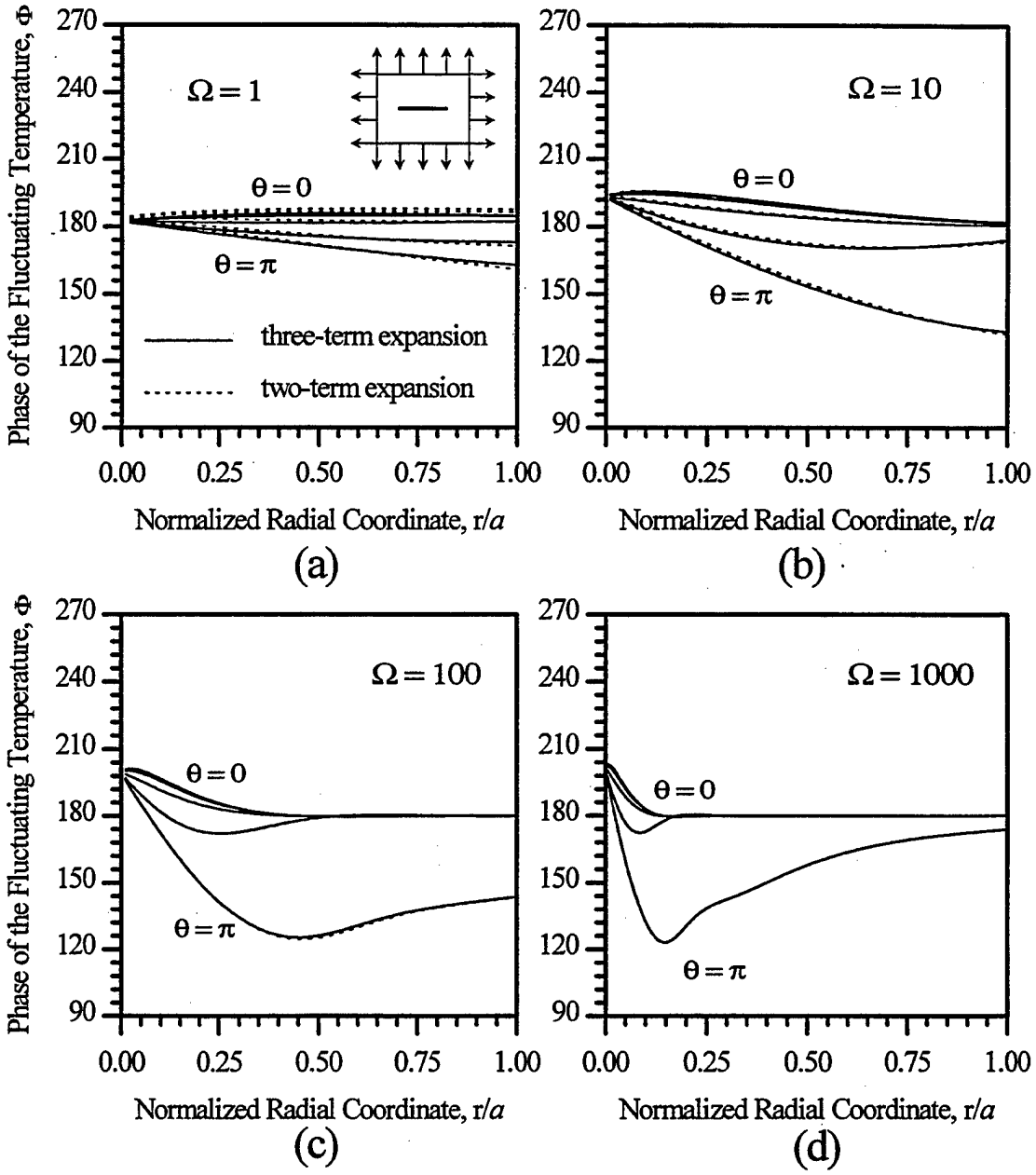

Figure 39. Phase of the fluctuating temperature as a function of the normalized radial coordinate for $\theta = 0, \pi/4, \pi/2, 3\pi/4, \pi$. (a) $\Omega = 1$; (b) $\Omega = 10$; (c) $\Omega = 100$; (d) $\Omega = 1000$. Mode I.

can not be separated in terms of the θ-coordinate and the radial coordinate. There is a much stronger θ-dependence in Mode I (Figure 39) as compared to Mode II (Figure 28). Observe that for large frequencies, $\Omega \approx 1000$, the problem is essentially adiabatic away from the crack tip, and the fluctuating temperature is out phase with the applied stress by approximately π. Conversely, for small frequencies, $\Omega \approx 1$, the problem is essentially isothermal and once again, the fluctuating temperature is out phase with the applied stress by approximately π. As the frequency increases, spatial variations in Φ become increasingly localized near the crack tip.

4.4.2 Work Lost

For Mode I, a normalized work lost ψ is defined as $\psi = \Delta w/\left(\sigma^2\kappa^2 T_o\alpha^2/C\right)$ (cf. $\psi = \Delta w/\left(\tau^2\kappa^2 T_o\alpha^2/C\right)$ for Mode II). Substituting Eq. (199) into Eq. (24) and noting the difference in notation, yields

$$\psi(r,\theta) = -2\pi\left[\cos(\theta/2)\left(\frac{1}{2}\sqrt{\frac{2a}{r}}+\frac{3}{4}\sqrt{\frac{r}{2a}}\right)-\frac{5}{16}\cos(3\theta/2)\left(\frac{r}{2a}\right)^{3/2}\right]\mathrm{Im}\,\Theta(r,\theta)$$

$$\text{for } 0<r\le 2a. \quad (204)$$

where Θ is given by Eq. (203). As expected, in view of Eq. (24), on $\theta=\pi$, $\psi \equiv 0$ because $\sigma_{kk} \equiv 0$ (cf. Mode II where $\psi \equiv 0$ on $\theta = 0$). Since the temperature is bounded at the crack tip, it follows from Eq. (204) that the work lost exhibits a $1/\sqrt{r}$ singularity at the crack tip. A dimensionless work-lost intensity factor ψ_I is defined for Mode I as

$$\psi_I = \lim_{r\to 0}\left(\sqrt{r/a}\,\psi\right)\Big|_{\theta=0} \quad (205)$$

To obtain this limit, we used a rational function extrapolation (Press, 1989, pp. 83-86). Figure 40 shows the frequency dependence of ψ_I in the range $10 < \Omega < 1000$ (The frequency range was limited due to numerical difficulties in evaluating Eq. (203).).

In Figure 41 ψ is plotted for $0 \le r \le a$, $\theta = 0, \pi/4, \pi/2, 3\pi/4, \pi$, and $\Omega = 1, 10, 100, 1000$. The results obtained using a two-term expansion for σ_{kk} are also shown for comparison. For a given *r*, the maximum ψ occurs for $\theta = 0$. There are regions where ψ becomes *negative*. A similar result was found in Section 3.4.1 where it was noted that the only constraint imposed by the second law of thermodynamics is that the *total* entropy produced throughout the cracked plate (a closed thermodynamic system which does not exchange heat with its surroundings) during one cycle of loading is either zero or positive, i.e. $\Delta S \ge 0$. It follows from Eq. (35) that $T_o \Delta S \equiv \Delta W \ge 0$, i.e., the *total* work lost throughout the cracked plate during one cycle should be zero or positive. It then follows that $\int_R \psi \, dR \ge 0$. From a visual examination of Figure 41, it is apparant that this second-law constraint is clearly satisfied.

4.4.3 Entropy Produced

A normalized entropy produced per unit volume, χ, for Mode I is defined as $\chi = \Delta s / (\sigma^2 \kappa^2 \alpha^2 / C)$ (cf. $\chi = \Delta s / (\tau^2 \kappa^2 \alpha^2 / C)$ in Mode II). Then χ is still given by Eq. (187), and for brevity the expression resulting from the substitution of Eq. (203) into Eq. (187) is not given herein. It was proven that the entropy produced is bounded at the crack tip. In Figure 42, χ is plotted for

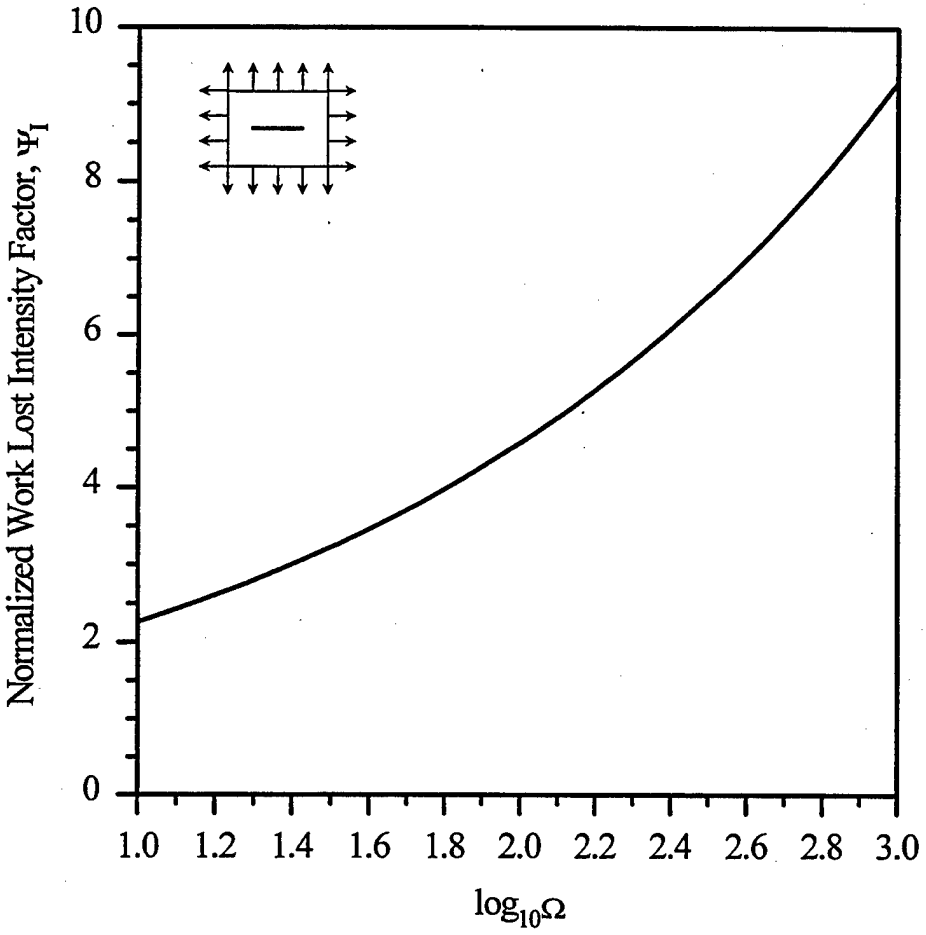

Figure 40. Normalized work lost intensity factor, ψ_I, as a function of the normalized frequency Ω. Mode I.

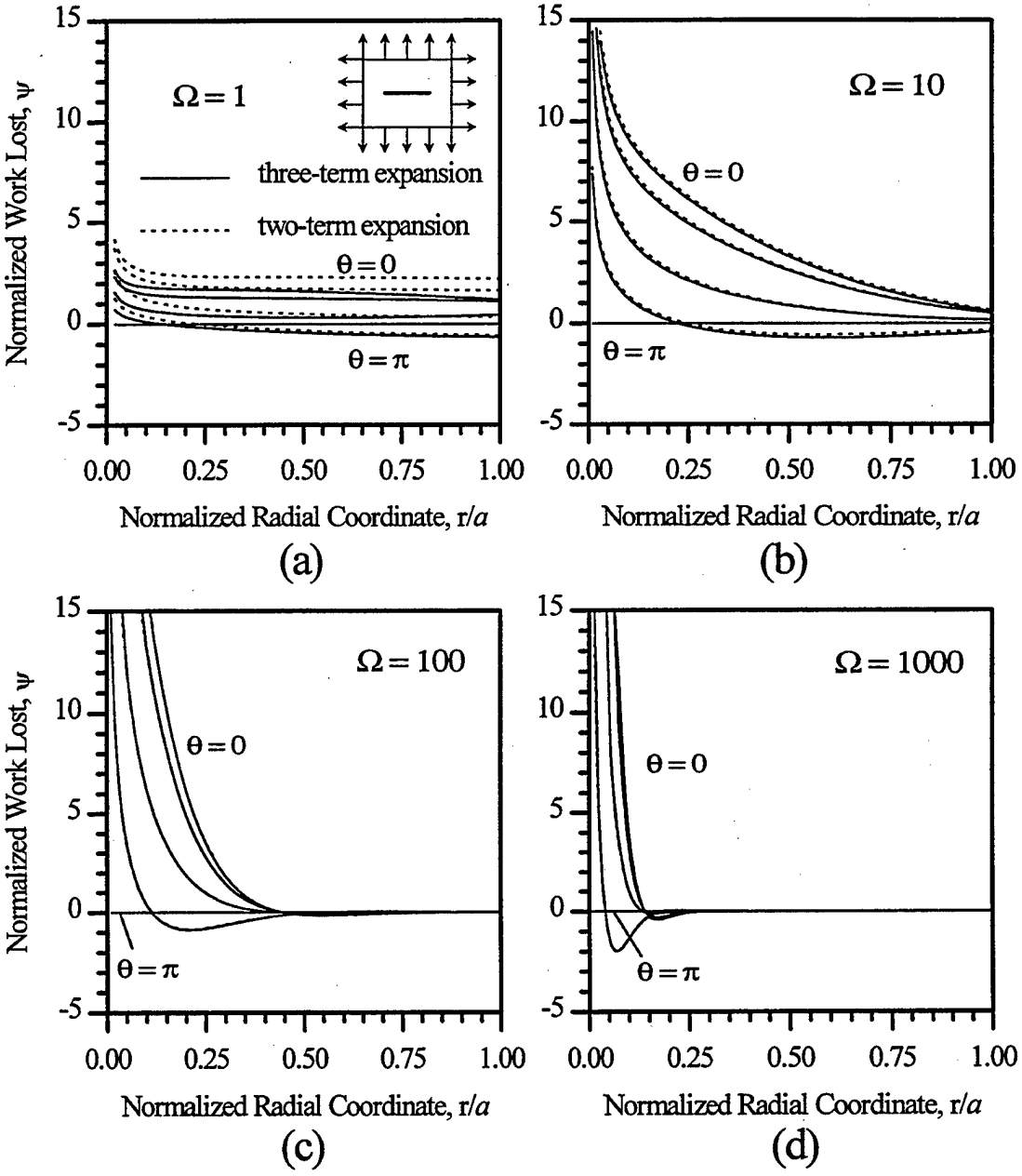

Figure 41. Normalized work lost ψ as a function of the normalized radial coordinate for $\theta = 0, \pi/4, \pi/2, 3\pi/4, \pi$. (a) $\Omega = 1$; (b) $\Omega = 10$; (c) $\Omega = 100$; (d) $\Omega = 1000$. The work lost goes to infinity as $\left(1/\sqrt{r}\right)$ at the crack tip. Mode I.

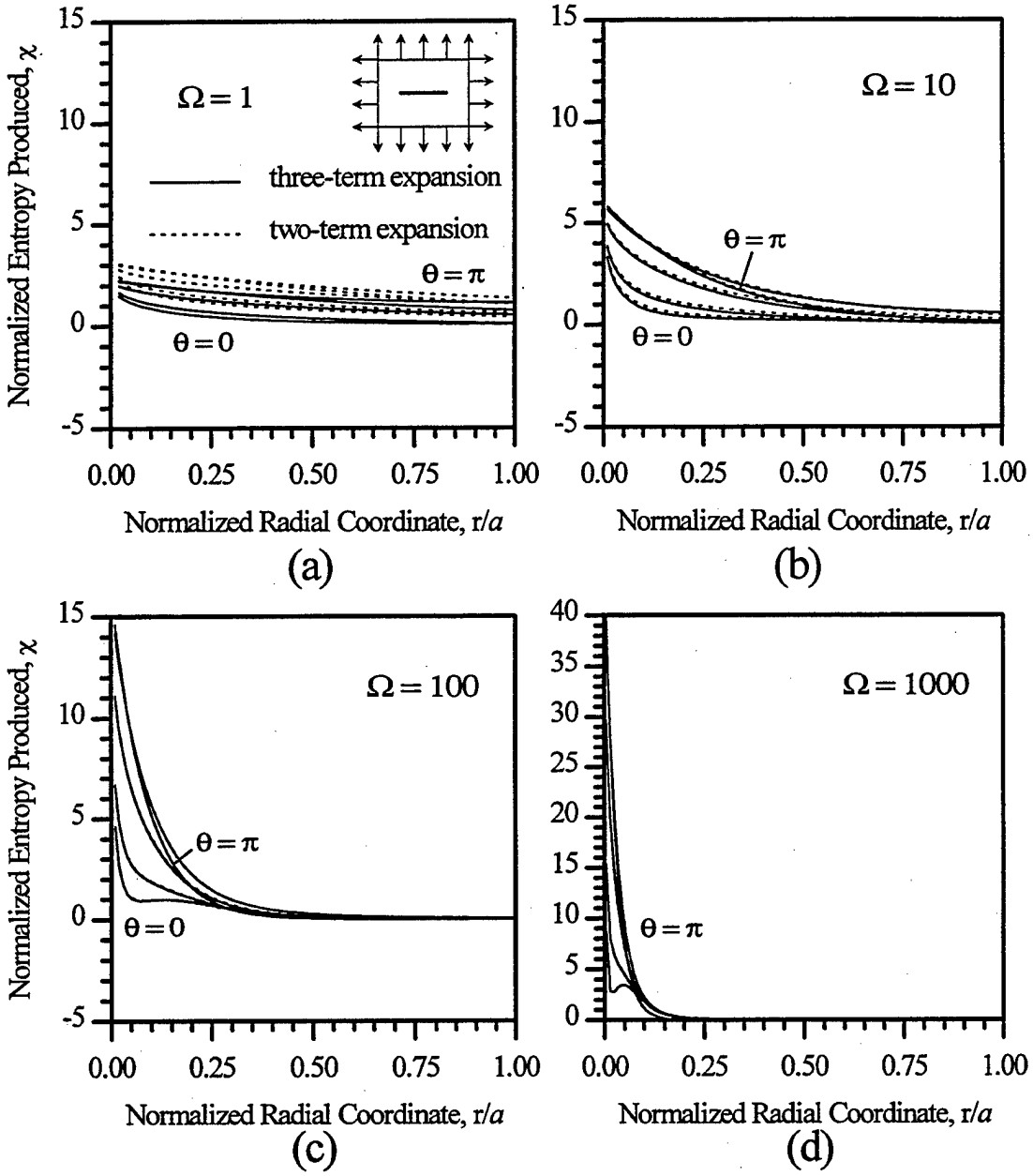

Figure 42. Normalized entropy produced as a function of the normalized radial coordinate for $\theta = 0, \pi/4, \pi/2, 3\pi/4, \pi$. (a) $\Omega = 1$; (b) $\Omega = 10$; (c) $\Omega = 100$; (d) $\Omega = 1000$. The entropy produced is bounded at the crack tip. Mode I.

$0 \le r \le a$, $\theta = 0, \pi/4, \pi/2, 3\pi/4, \pi$, and $\Omega = 1, 10, 100, 1000$. Note that the figure for $\Omega = 1000$ is plotted on a different scale. The entropy obtained using the two-term expansion for σ_{kk} is also included for comparison. As was done in Mode II, ψ (Figure 41) and χ (Figure 42) are plotted using identical scales (except Figure 42d). Sufficiently close to the crack tip, for a given radial location, the entropy produced is minimum on $\theta = 0$ and increases to a maximum on $\theta = \pi$. As a check on the approximate solution, note that in the exact solution for Mode I, at the point $(x = 0, y = 0)$, $\partial V/\partial x \equiv 0$ and $\partial V/\partial y \equiv 0$, and therefore $\chi \equiv 0$. In the approximate solution the point $(x = 0, y = 0)$ corresponds to the point $(r = a, \theta = \pi)$. In Figure 42 at $(r = a, \theta = \pi)$, χ is clearly not zero for $\Omega = 1$, nearly zero for $\Omega = 10$, and virtually zero for $\Omega = 100$ and $\Omega = 1000$.

5. SUMMARY

Using the linear one-way coupled theory of elastothermodynamic relaxation, the elastothermodynamic damping of composite and cracked media was examined. Two descriptions of elastothermodynamic damping were established: (1) the mechanical description and (2) the entropic description. An integral-transform technique was developed to solve for the temperature field of a general composite medium with arbitrary heat generation. With this solution, a general expression for the damping of the composite material was derived. This general solution for the elastothermodynamic damping was then specialized to a solution for a composite material consisting of N-isotropic layers in a rectangular, cylindrical, and spherical coordinate system (i.e. an N-layer slab, cylinder, and sphere, respectively). With this specialized result the elastothermodynamic damping of laminated, fiber-reinforced, and particulate composites was examined. Finally, an approximate analysis was given for the temperature field, the work lost, and the entropy produced in the vicinity of a Griffith crack for Modes I, II, and III.

REFERENCES

Abramowitz, M. and Stegun, I., eds., 1970, *Handbook of Mathematical Functions,* Dover, New York, pp. 443-444.

Alblas, J., 1961, "On the General Theory of Thermo-Elastic Friction," *Applied Scientific Research*, Vol. 10, Sect. A, pp. 349-362.

Alblas, J., 1981, "A Note on the Theory of Thermoelastic Damping," *Journal of Thermal Stresses*, Vol. 4, pp. 333-355.

Arfken, G., 1985, *Mathematical Methods for Physicists*, Academic Press, New York, pp. 897-909.

Armstrong, B., 1984, "Models for Thermoelastic Attenuation of Waves in Heterogeneous Solids," *Geophysics*, Vol. 49, No. 7, pp. 1032-1040.

Berry, B., 1955, "Precise Investigation of the Theory of Damping by Transverse Thermal Currents," *Journal of Applied Physics*, Vol. 26, No. 10, pp. 1221-1224.

Bhagat, R., Amateau, M., and Smith, E., 1989, "Damping Behavior of Planar Random Carbon Fiber Reinforced 6061 Al Matrix Composites Fabricated by High-Pressure Infiltration Casting," *Journal of Composites Technology and Research*, Vol. 11, No. 3, pp. 113-116.

Biot, M, 1956, "Thermoelasticity and Irreversible Thermodynamics," *Journal of Applied Physics*, Vol. 27, No. 3, pp. 240-253.

Bishop, J. and Kinra, V., 1992, "Some Improvements in the Flexural Damping Measurement Technique," in *M^3D: Mechanics and Mechanisms of Material Damping, ASTM STP 1169*, Eds.: V. Kinra and A. Wolfenden,

American Society for Testing and Materials, Philadelphia, Pennsylvania, pp. 457-470.

Boley, B. and Weiner, J., 1960, *Theory of Thermal Stresses,* John Wiley & Sons, New York.

Boyce, W. and DiPrima, R., 1986, *Elementary Differential Equations and Boundary Value Problems*, 4th ed., John Wiley & Sons, New York, pp.156-162.

Brillouin, L., 1953, *Wave Propagation in Periodic Structures*, Dover, New York, p. 70.

Budiansky, B., and Sumner, E., 1983, "Bulk Thermoelastic Attenuation of Composite Materials," *Journal of Geophysical Research*, Vol. 88, No. B12, pp. 10343-10348.

Callen, H., 1985, *Thermodynamics and an Introduction to Thermostatistics,* 2nd ed., John Wiley & Sons, New York, pp. 91-130.

Chadwick, P., 1962, "Thermal Damping of a Vibrating Elastic Body," *Mathematika*, Vol. 9, pp. 38-48.

de Batist, R., 1972, *Internal Friction of Structural Defects in Crystalline Solids*, American Elsevier, New York.

de Groot, S. and Mazur, P., 1984, *Non-Equilibrium Thermodynamics,* Dover, New York, pp. 20-29.

Deresiewicz, H., 1957, "Plane Waves in a Thermoelastic Solid," *Journal of the Acoustical Society of America*, Vol. 29, No. 2, pp. 204-209.

DiCarlo, J., 1976, "Anelastic Deformation of Boron Fibers," *Scripta Metallurgica*, Vol. 10, pp. 115-119.

DiCarlo, J. and Maisel, J., 1979, "High Temperature Dynamic Modulus and Damping of Aluminum and Titanium Matrix Composites," in *Advanced Fibers and Composites for Elevated Temperatures* (TMS and ASM), Eds.: I. Ahmad and V. Noton, pp. 55-79.

Eshelby, J., 1949, "Dislocations as a cause of mechanical damping in metals," *Proceedings of the Royal Society, London*, Vol. A197, pp. 396-416.

Gillis, W., 1968, "Damping of Thermoelastic Structures," Technical Memorandum X-53722, George C. Marshall Space Flight Center, Hunstville, Alabama.

Goodman, L., Chang, C., and Robinson, A., 1962, "Thermoelastic Damping," Technical Documentary Report No. ASD-TDR-62-1031, Wright-Patterson Air Force Base, Ohio.

IMSL Libraries, Version 2.0, September, 1991, IMSL, inc., Houston, Texas.

Jones, M., 1975, *Mechanics of Composite Materials*, Hemisphere, New York, pp. 147-173.

Kinra, V. and Milligan, K., 1994, "A Second Law Analysis of Thermoelastic Damping," *ASME Journal of Applied Mechanics*, Vol. 61, No. 1, pp. 71-76.

Kinra, V. and Wolfenden, A., eds., 1992, *M^3D: Mechanics and Mechanisms of Material Damping, ASTM STP 1169*, American Society for Testing and Materials, Philadelphia, Pennsylvania.

Kinra, V., Wren, G., Rawal, S., and Misra, M., 1991, "On the Influence of Ply-Angle on Damping and Modulus of Elasticity of a Metal-Matrix Composite," *Metallurgical Transactions*, Vol. 22A, No.3, pp. 641-651.

Kinra, V. and Wren, G., 1992, "Axial Damping in Metal-Matrix Composites. I. A New Technique for Measuring Phase to 10^{-4} Radians," *SEM Journal of Experimental Mechanics*, Vol. 32 No. 2, pp. 163-171.

Landau, L., and Lifshitz, E., 1986, *Theory of Elasticity*, Pergamon Press, New York, pp. 133-143.

Lee, U., 1985, "Thermoelastic and Electromagnetic Damping Analysis," *AIAA Journal*, Vol. 23, No. 11, 1783-1790

Little, W., 1973, *Elasticity*, Prentice-Hall, Englewood Cliffs, New Jersey, pp. 315-317.

Lücke, K., 1956, "Ultrasonic Attenuation Caused by Thermoelastic Heat Flow," *Journal of Applied Physics*, Vol. 27, No. 12, pp. 1433-1438.

McLachlan, N., 1955, *Bessel Functions for Engineers,* Oxford Univ. Press, New York.

Milligan, K. and Kinra, V., 1993, "On the Damping of a One-Dimensional Inclusion in a Uniaxial Bar," *Mechanics Research Communicaton*, Vol. 20, No. 2, pp. 137-142.

Nowick, A. and Berry, B., 1972, *Anelastic Relaxation in Crystalline Solids*, Academic Press, New York.

Nowinski, J., 1978, *Theory of Thermoelasticity with Applications,* Sijthoff and Noordhoff International Publ. B.V., Alphen Aan Den Rijn, The Netherlands.

Ozisik, M., 1980, *Heat Conduction*, John Wiley and Sons, New York, 1980.

Paris, P. and Sih, G., 1965, "Stress Analysis of Cracks," in *STP Fracture Toughness Testing and its Applicatons*, STP 381, American Society for Testing and Materials, Philadelphia, Pennsylvania. pp. 30-83.

Press, H., et al., 1989, *Numerical Recipes: the Art of Scientific Computing*, Cambridge University Press, Cambridge.

Savage, J., 1966, "Thermoelastic Attenuation of Elastic Waves by Cracks," *Journal of Geophysical Research*, Vol. 71, No. 16, pp. 3929-3938,

Shieh, R., 1971, "Thermoelastic Damping and Its Effect on Flutter of Stressed Panels Situated in a Supersonic Airflow," NASA TND-6448, NASA Langley Research Center, Hampton, Virginia, 1971.

Shieh, R., 1975, "Thermoelastic Vibration and Damping for Circular Timoshenko Beams," *ASME Journal of Applied Mechanics*, Vol. 42, No. 2, pp. 405-410.

Shieh, R., 1979, "Eigensolutions for Coupled Thermoelastic Vibrations of Timoshenko Beams," *ASME Journal of Applied Mechanics*, Vol. 46, pp. 169-174.

Tasi, J., 1963, "Thermoelastic Dissipation in Vibrating Plates," *ASME Journal of Applied Mechanics*, Vol. 30, pp. 562-567.

Tasi, J., and Herrmann, G., 1964, "Thermoelastic Dissipation in High-Frequency Vibrations of Crystal Plates," *Journal of the Acoustical Society of America*, Vol. 36, No. 1, pp. 100-110.

Weiner, J., 1958, "Thermoelastic Dissipation due to High-Speed Dislocations," *Journal of Applied Physics*, Vol. 29, No. 9, pp. 1305-1307.

Westergaard, H., 1939, "Bearing Pressures and Cracks," *ASME Journal of Applied Mechanics*, Vol. 6, pp. A49-A53.

Wolfenden, A. and Wolla, J., 1992, "Dynamic Mechanical Properties," in *Metal Matrix Composites*, Academic Press, New York, pp. 287-328.

Wong, C. and Holcomb, S., 1992, "Damping Studies of Ceramic Reinforced Aluminum," in *M^3D: Mechanics and Mechanisms of Material Damping*, ASTM STP 1169, Eds.: V. Kinra and A. Wolfenden, pp. 76-93.

Wren, G. and Kinra, V., 1988, "An Experimental Technique for Determining a Measure of Structural Damping," *ASTM Journal of Testing and Evaluation*, Vol. 16, No. 1, pp. 77-85.

Wren, G. and Kinra, V., 1992, "Axial Damping in Metal-Matrix Composites. II. A Theoretical Model and its Experimental Verification," *SEM Journal of Experimental Mechanics*, Vol. 32, No.2, pp. 172-178.

Zemansky, M., and Dittman, R., 1981, *Heat and Thermodynamics*, 6th ed., McGraw-Hill, New York, pp. 224-225.

Zener, C., 1937, "Internal Friction in Solids I. Theory of Internal Friction in Reeds," *Physical Review*, Vol. 52, pp. 230-235.

Zener, C., 1938a, "Internal Friction in Solids II. General Theory of Thermoelastic Internal Friction," *Physical Review*, Vol. 53, pp. 90-99.

Zener, C., 1938b, "Internal Friction in Solids III. Experimental Demonstration of Thermoelastic Internal Friction," *Physical Review*, Vol. 53, pp. 100-101.

APPENDIX

To illustrate the physics of elastothermodynamic damping in a simple setting, consider the following quasistatic problem. In analogy to a beam in bending, two identical isotropic homogeneous thermoelastic material elements of unit volume, labeled *A* and *B*, are taken through a series of five processes as shown in the schematics of Figure A1 and listed below. A diathermal interface exists between the two materials which may be turned on and off as desired.

process 1-2: Material *A* initially at a temperature T_o is stressed adiabatically from $\sigma_{kk} = 0$ to $\sigma_{kk} = \sigma$. Material *B*, also initially at a temperature T_o, is stressed adiabatically from $\sigma_{kk} = 0$ to $\sigma_{kk} = -\sigma$.

process 2-3: Materials *A* and *B* transfer heat across the diathermal interface at constant stress until an equilibrium temperature is obtained.

process 3-4: Material *A* is stressed adiabatically from $\sigma_{kk} = \sigma$ to $\sigma_{kk} = 0$. Material *B* is stressed adiabatically from $\sigma_{kk} = -\sigma$ to $\sigma_{kk} = 0$.

process 4-5: Material *A* and *B* transfer heat across the diathermal interface at zero stress until an equilibrium temperature is obtained.

Note that the system *A-B* is adiabatic.

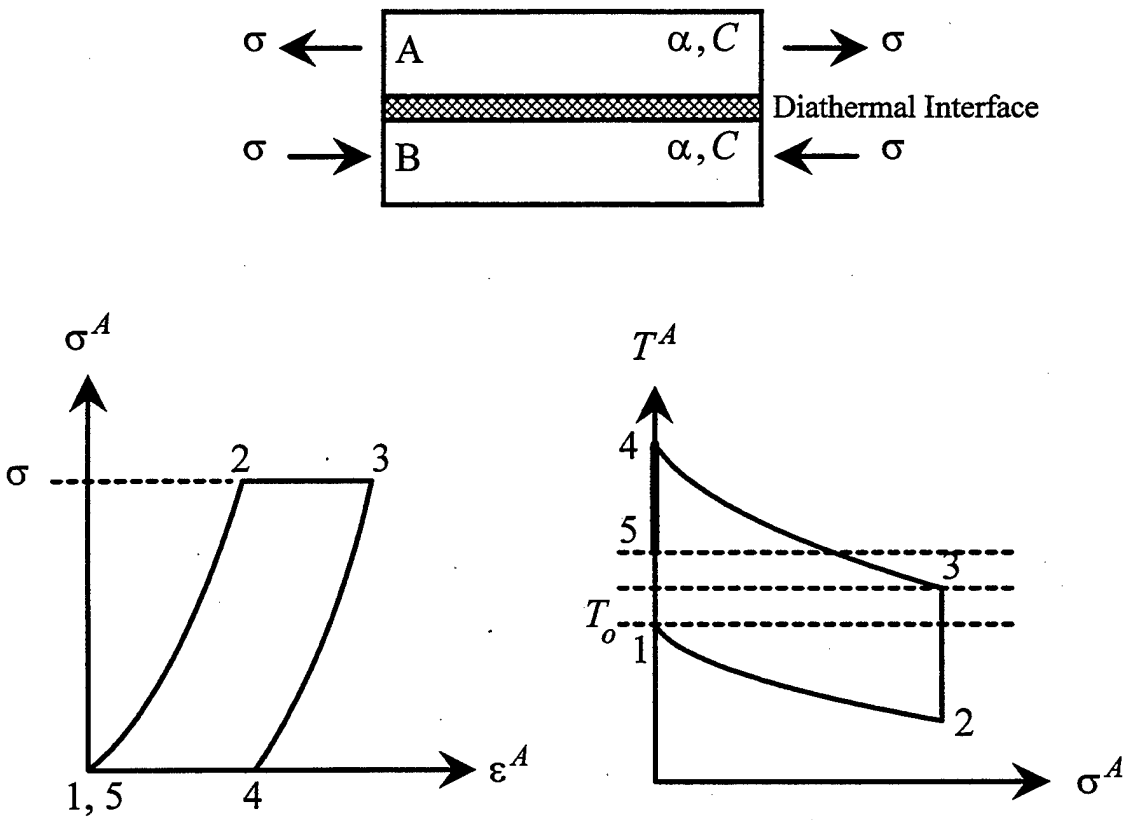

Figure A1. Schematic of the system *A-B* and the five processes for material *A*. (Those of material *B* are similar. The curvatures in the processes (12) and (34) are highly exaggerated.)

SOLUTION USING THE LINEAR ONE-WAY COUPLED THEORY

The elastothermodynamic work lost for this problem is now calculated using linear one-way coupled theory of elastothermodynamic damping, which for this simple example is equivalent to the linearization of Eq. (1),

$$\left(\frac{\partial T}{\partial \sigma_{kk}}\right)_S = -T_o \frac{\alpha}{C} \tag{A1}$$

(Note that Eq. (1) was derived using the first and second laws of thermodynamics. Therefore, it is expected that in using Eq. (A1) these laws will be violated to some extent.) Since the stress is independent of the temperature, these two variables may be separated in Eq. (A1), yielding

$$dT/T_o = -(\alpha/C)d\sigma \tag{A2}$$

where σ represents σ_{kk}. Integrating gives

$$T_{i+1} = T_i - T_o \frac{\alpha}{C}(\sigma_{i+1} - \sigma_i) \tag{A3}$$

where the subscripts denote the process number. Using Eq. (A3) and noting that $T_3^A = T_3^B = \left(T_2^A + T_2^B\right)/2$, and $T_5^A = T_5^B = \left(T_4^A + T_4^B\right)/2$ (the superscripts denote the material), the temperatures of both materials A and B at the completion of each process were calculated and are given in Table A1. Note that the temperature of both materials at the completion of the *stress* cycle (12345) is the same as the temperature at the beginning of the cycle, T_o. Thus, within the linear theory, the system *A-B* has undergone a *thermodynamic* cycle.

Table A1 Process temperatures (using Eq. (A205))

Material *A*	**Material *B***
$T_1 = T_o$	$T_1 = T_o$
$T_2 = T_o - T_o\alpha\sigma/C$	$T_2 = T_o + T_o\alpha\sigma/C$
$T_3 = T_o$	$T_3 = T_o$
$T_4 = T_o + T_o\alpha\sigma/C$	$T_4 = T_o - T_o\alpha\sigma/C$
$T_5 = T_o$	$T_5 = T_o$

The external work performed on a material, W, during the process $i \to i+1$ is given by

$$W_{i,i+1} = \int_i^{i+1} \sigma d\varepsilon = \int_i^{i+1} \sigma\left(d\varepsilon^{\text{mech}} + d\varepsilon^{\text{therm}}\right) = \int_i^{i+1} \sigma \frac{d\sigma}{E} - \sigma\alpha dT \qquad \text{(A4)}$$

where the fact that the mechanical strain $\varepsilon^{\text{mech}} = \sigma/E$, where E is the Young's Modulus, and the thermal strain $\varepsilon^{\text{therm}} = \alpha\left(T_{i+1} - T_i\right)$, has been used. Using Eq. (A4) and the temperatures given in Table A1, the external work performed on materials A and B during each process was calculated and is given in Table A2. The net work performed on the system during the *stress* cycle (12345), ΔW, is the sum of the work done during each process for both materials. Using Table A2, this sum is equal to $\Delta W = 2T_o\alpha^2\sigma^2/C$. (For a numerical example, take steel where $\alpha = 12\text{x}10^{-6}K^{-1}$ and $C = 3.8\text{x}10^6\ J/m^3K$. If $\sigma = 100\,MPa$ and $T_o = 300K$, then $\Delta W = 227J$ for a unit volume.) It is instructive to calculate ΔW using the first law of thermodynamics, instead of using Eq. (A4) explicitly. Taking both materials as our thermodynamic

system, the first law may be written $\Delta U = \Delta W + \Delta Q$. Here, $\Delta Q = 0$; since $T_5^A = T_5^B = T_1^A = T_1^B = T_o$, and at the completion of the stress cycle (12345) both materials are unstressed, it follows that $\Delta U = 0$ as well. Thus, $\Delta W = 0$, contradicting the previous result. Therefore, the linear one-way coupled theory violates the first law of thermodynamics (see the note after Eq. (A1)). This violation is tolerated since the discrepancy between the actual and the approximate ΔW is negligible. (This fact will be exhibited in the next section.)

Table A2 Work performed during each process (linear theory)

Material *A*	**Material *B***
$W_{12} = \frac{\sigma^2}{2E} - T_o \frac{\alpha^2 \sigma^2}{2C}$	$W_{12} = \frac{\sigma^2}{2E} - T_o \frac{\alpha^2 \sigma^2}{2C}$
$W_{23} = T_o \frac{\alpha^2 \sigma^2}{C}$	$W_{23} = T_o \frac{\alpha^2 \sigma^2}{C}$
$W_{34} = -\frac{\sigma^2}{2E} + T_o \frac{\alpha^2 \sigma^2}{2C}$	$W_{34} = -\frac{\sigma^2}{2E} + T_o \frac{\alpha^2 \sigma^2}{2C}$
$W_{45} = 0$	$W_{45} = 0$

Within the linear one-way coupled theory, the work lost may also be calculated using the entropy produced. The entropy change of each material, ΔS, during the process $i \to i+1$ is given by

$$\Delta S_{i,i+1} = C\int_{i}^{i+1}\frac{dT}{T} = C\ln\frac{T_{i+1}}{T_i} \tag{A5}$$

Using the temperatures given in Table A1, these entropies were calculated and are given in Table A3. To first order in the parameter $\alpha\sigma/C$, the total entropy production during the stress cycle (12345) is $\Delta S = 2\alpha^2\sigma^2/C$. Thus, $\Delta S = \Delta W/T_o$ or $\Delta W = T_o\Delta S$. In Section 3.1 this result is proven using the linear one-way coupled theory, for the general problem of a composite material made up of several subregions, each of which may be anisotropic, and whose interfaces may be thermally imperfect, stressed time-harmonically. Even though the system is adiabatic, the quantity $T_o\Delta S$ is viewed as the "heat increment" per *stress* cycle since, as the exact solution will indicate, in reality the temperature of the system at the completion of the stress cycle increases as though a quantity of heat had been transferred to the system.

Table A3 Entropy change during each process (linear theory)

Material *A*	**Material *B***
$\Delta S_{12} = 0$	$\Delta S_{12} = 0$
$\Delta S_{23} = -C\ln(1-\alpha\sigma/C)$	$\Delta S_{23} = -C\ln(1+\alpha\sigma/C)$
$\Delta S_{34} = 0$	$\Delta S_{34} = 0$
$\Delta S_{45} = -C\ln(1+\alpha\sigma/C)$	$\Delta S_{45} = -C\ln(1-\alpha\sigma/C)$

EXACT SOLUTION

For this simple example, the elastothermodynamic work lost may be calculated exactly. Since for this problem, the stress is independent of the temperature, these two variables may be separated in Eq. (1) yielding

$$dT/T = -(\alpha/C)d\sigma \tag{A6}$$

Integrating gives

$$T_{i+1} = T_i e^{-\frac{\alpha}{C}(\sigma_{i+1}-\sigma_i)} \tag{A7}$$

Using Eq. (A7) and noting that $T_3^A = T_3^B = \left(T_2^A + T_2^B\right)/2$, and $T_5^A = T_5^B = \left(T_4^A + T_4^B\right)/2$, the temperatures of both materials A and B at the completion of each process were calculated and are given in Table A4. Note that the temperature of both materials at the completion of the *stress* cycle (12345) is not the same as the temperature at the beginning, T_o, as was the case using the linear theory. Thus the system A-B does not undergo a complete *thermodynamic* cycle. (For the numerical example using steel, the temperature at the completion of the *stress* cycle is $T_5^A = T_5^B = (1.00003)T_o$..)

Using Eq. (A4) and the temperatures given in Table A4, the external work performed on materials A and B during each process was calculated and is given in Table A5. The net work performed on the system during the stress cycle (12345) is equal to $\Delta W = 2CT_o \sinh^2(\alpha\sigma/C)$. Recall the work lost using the linear theory was $\Delta W = 2T_o \alpha^2\sigma^2/C$ which is the first order approximation to the exact work lost. (For the numerical example using steel, the percent difference between these two results is 0.0000034%, thus justifying the use of the linear theory.) As in the linear approximation, since $\Delta Q = 0$, the first law

reduces to $\Delta U = \Delta W$. Since $\Delta U = \left(T_5^A - T_o\right) + \left(T_5^B - T_o\right) = 2\left(T_5^A - T_o\right)$, it is easily shown that the first law is satisfied as expected.

Table A4 Process temperatures (exact, using Eq. (A7))

Material *A*	**Material *B***
$T_1 = T_o$	$T_1 = T_o$
$T_2 = T_o e^{-\alpha\sigma/C}$	$T_2 = T_o e^{\alpha\sigma/C}$
$T_3 = T_o \cosh(\alpha\sigma/C)$	$T_3 = T_o \cosh(\alpha\sigma/C)$
$T_4 = T_3 e^{\alpha\sigma/C}$	$T_4 = T_3 e^{-\alpha\sigma/C}$
$T_5 = T_3 \cosh(\alpha\sigma/C)$	$T_5 = T_3 \cosh(\alpha\sigma/C)$

Table A5 Work performed during each process (exact solution)

Material *A*	**Material *B***
$W_{12} = \frac{\sigma^2}{2E} + T_o\left[(\alpha\sigma + C)e^{-\alpha\sigma/C} - C\right]$	$W_{12} = \frac{\sigma^2}{2E} + T_o\left[(-\alpha\sigma + C)e^{\alpha\sigma/C} - C\right]$
$W_{23} = \sigma\alpha(T_3 - T_2)$	$W_{23} = -\sigma\alpha(T_3 - T_2)$
$W_{34} = -\frac{\sigma^2}{2E} - T_3\left[\alpha\sigma + C\left(1 - e^{\alpha\sigma/C}\right)\right]$	$W_{34} = -\frac{\sigma^2}{2E} - T_3\left[-\alpha\sigma + C\left(1 - e^{-\alpha\sigma/C}\right)\right]$
$W_{45} = 0$	$W_{45} = 0$

Using (A5) and the temperatures given in Table A4, the entropy change for each material was calculated for each process, and is given in Table A6. Unlike in the linear approximation, the elastothermodynamic work lost can not be related to the entropy produced with the formula $\Delta W = T_o \Delta S$, since the total entropy change is $\Delta S = 4C \ln \cosh(\alpha\sigma/C) \neq \Delta W/T_o$.

Table A6 Entropy change during each process (exact solution)

Material *A*	**Material *B***
$\Delta S_{12} = 0$	$\Delta S_{12} = 0$
$\Delta S_{23} = C \ln \cosh(\alpha\sigma/C) + \alpha\sigma$	$\Delta S_{23} = C \ln \cosh(\alpha\sigma/C) - \alpha\sigma$
$\Delta S_{34} = 0$	$\Delta S_{34} = 0$
$\Delta S_{45} = C \ln \cosh(\alpha\sigma/C) - \alpha\sigma$	$\Delta S_{45} = C \ln \cosh(\alpha\sigma/C) + \alpha\sigma$

VITA

Joseph Edward Bishop was born on July 17, 1968, in Gladewater, Texas (pop. 7000) to George and Betty Bishop. He graduated from Gladewater High School in May 1986. He attended Kilgore Junior College for one year and three summers and then transferred to Texas A&M University. He met Roseanne Jackson in April 1989, and they were married eight months later on December 9, 1989. He graduated magna cum laude with a Bachelor of Science in Aerospace Engineering in May 1990. He received a Master of Science degree in Aerospace Engineering in December 1991 from Texas A&M University. He was awarded a National Defense Science and Engineering Graduate Fellowship to pursue a Doctor of Philosophy degree in Aerospace Engineering at Texas A&M University. He plans to start work on a Doctor of Philosophy degree in Mathematics at Michigan State University starting in the Fall of 1995. He may be reached through the following address:

Joseph E. Bishop
1103 Hall Street
Gladewater, Texas 75647